

University of Southern Queensland, Australia



**Tissue Conductivity based Human Head Model Study for
EEG**

A Dissertation Submitted by

Md. Rezaul Bashar

For the Award of Doctor of Philosophy

Abstract

The electroencephalogram (EEG) is a measurement of neuronal activity inside the brain over a period of time by placing electrodes on the scalp surface and is used extensively in clinical practices and brain researches, such as sleep disorders, epileptic seizure, electroconvulsive therapy, transcranial direct current stimulation and transcranial magnetic stimulation for the treatment of the long term memory loss or memory disorders.

The computation of EEG for a given dipolar current source in the brain using a volume conductor model of the head is known as EEG forward problem, which is repeatedly used in EEG source localization. The accuracy of the EEG forward problem depends on head geometry and electrical tissue property, such as conductivity. The accurate head geometry could be obtained from the magnetic resonance imaging; however it is not possible to obtain *in vivo* tissue conductivity. Moreover, different parts of the head have different conductivities even with the same tissue. Not only various head tissues show different conductivities or tissue inhomogeneity, some of them are also anisotropic, such as the skull and white matter (WM) in the brain. The anisotropy ratio is variable due to the fibre structure of the WM and the various thickness of skull hard and soft bones. To our knowledge, previous work has not extensively investigated the impact of various tissue conductivities with the same tissue and various anisotropy ratios on head modelling.

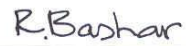
In this dissertation, we investigate the effects of tissue conductivity on EEG in two aspects: inhomogeneous and anisotropic conductivities, and local tissue conductivity. For the first aspect, we propose conductivity models, such as conductivity ratio approximation, statistical conductivity approximation, fractional anisotropy based conductivity approximation, the Monte Carlo method based conductivity approximation and stochastic method based conductivity approximation models. For the second aspect, we propose a local tissue conductivity model where location specific conductivity is used to construct a human head model. We use

spherically and realistically shaped head geometries for the head model construction. We also investigate the sensitivity of inhomogeneous and anisotropic conductivity on EEG computation.

The simulated results based on these conductivity models show that the inhomogeneous and anisotropic tissue properties affect significantly on EEG. Based on our proposed conductivity models, we find an average of 54.19% relative difference measure (RDM) with a minimum of 4.04% and a maximum of 171%, and an average of 1.64 magnification (MAG) values with a minimum of 0.30 and a maximum of 6.95 in comparison with the homogeneous and isotropic conductivity based head model. On the other hand, we find an average of 55.16% RDM with a minimum of 12% and a maximum of 120%, and 1.18 average MAG values with a minimum of 0.22 and a maximum of 2.03 for the local tissue conductivity based head model. We also find 0.003 to 0.42 with an average of 0.1 sensitivity index, which means 10% mean scalp potential variations if we ignore tissue conductivity properties. Therefore, this study concludes that tissue properties are crucial and should be accounted in accurate head modelling.

Declaration

I certify that this dissertation has not been previously submitted for a degree or diploma in any university. To the best of my knowledge and belief, the dissertation contains no material previously published or written by another person except where due reference is made in the text.



(Md Rezaul Bashar)

Date:



(Dr Peng (Paul) Wen)

Associate Supervisor



(Associate Professor Yan Li)

Principal Supervisor

Acknowledgements

I would like to express my gratitude to my principal supervisor A/Prof Yan Li for offering me the opportunity to perform this research under her supervision, support, motivation, encouragement, advice, comments and discussions. I owe much gratitude to my associate supervisor Dr Peng (Paul) Wen for his guidance, continuous support, encouragement, his knowledge and willingness to answer my questions, discussions about current research issues and critically evaluating my work during my whole research period. I would not imagine carrying out this research without his constant support and help.

I would like to thank Dr Guang Bin Liu, Department of Psychology for his support to understanding the most complex organ of the human body, the brain and its function at the beginning of this research. I would also like to thank A/Prof Shahjahan Khan, Department of Mathematics & Computing and Md. Masud Hasan (Sunshine Coast University) for their assistance in the understanding of statistical analysis.

I would like to thank Professor Mark Sutherland, Director of Centre for Systems Biology for the support of my partial international tuition fees and grants to attend conference.

I wish to thank my colleagues in our research group for their discussions and comments during our discussions, especially in the monthly seminars.

I also want to thank the Australian Research Council discovery grant for my scholarship, Department of Mathematics & Computing for my studentship and travel grant to attend international conferences and the higher degrees research office for International research excellence award during my study.

I would like to thank Dr Ian Weber, Learning and Teaching Support Unit, USQ and Lynne A. Higson, West Queensland for their efforts to correct my English.

Last but not least, I offer my gratitude to my wife Mst Asmaul Husna and my lovely son Md Samiul Bashar for their endless support and enduring love.

I would like to dedicate this dissertation to my parents whom I always miss in my foreign life.

Table of Contents

Abstract	i
Declaration	iii
Acknowledgement	iv
Table of Contents	v
List of Figures	x
List of Tables	xv
List of Acronyms	xviii
Notation and Symbols	xx
Publications	xxi
1 Introduction	1
1.1 Electroencephalography and Head Modelling	2
1.2 Significance of Head Modelling	3
1.3 The Originality of this Dissertation	5
1.4 Organization of the Dissertation	6
2 Features of Human Head	8
2.1 Anatomy of Human Head	8
2.1.1 Anatomy of the brain	8
2.1.1.1 Anatomy of the neuron	11
2.2.1.2 Physiology of the neuron	12
2.1.2 Anatomy of the skull	13
2.1.3 Anatomy of the scalp	14
2.2 Generation and Collection of EEG	15
2.3 Electric Features of the Head	17
2.4 Summary	18
3 Human Head Model and Tissue Conductivity	20
3.1 Human Head Modelling	20
3.1.1 Spherical head model	20
3.1.2 Realistic head model	21
3.2 Electrical Conductivity of Head Tissues	23
3.3 Tissue Conductivity used in the Dissertation	26
3.4 Homogeneous Tissue Conductivity	27

3.5 Methods to Determine Inhomogeneous Tissue Conductivity	27
3.5.1 Pseudo conductivity based inhomogeneous conductivity	28
3.5.2 The brain tissue inhomogeneity	28
3.5.3 The skull tissue inhomogeneity	29
3.5.4 The scalp tissue inhomogeneity	29
3.6 Methods to Determine Anisotropic Tissue Conductivity	30
3.6.1 White matter anisotropy	30
3.6.1.1 The Volume constraint	31
3.6.1.2 The Wang's constraint	33
3.6.2 Skull Anisotropy	33
3.7 Inhomogeneous and Anisotropic Tissue Conductivity	35
3.7.1 Conductivity ratio approximation model	36
3.7.2 Statistical conductivity approximation model	36
3.7.3 Fractional anisotropy based inhomogeneous and anisotropic	37
3.7.4 The Monte Carlo method based inhomogeneous and anisotropic	39
3.8 Conclusion and Contribution	41
4 The Forward Problem and its Solution using FEM	42
4.1 Maxwell's and Poisson's Equations	42
4.2 Boundary Conditions	45
4.3 The Current Source or Dipole Model	46
4.4 The EEG Forward Problem	47
4.5 General Algebraic Formulation of the EEG Forward Problem	48
4.6 Electric Potential in a Multi-layer Spherical Model	49
4.7 Numerical Solution of the EEG Forward Problem	51
4.7.1 Direct approach	51
4.7.2 Subtraction approach	52
4.7.3 The finite element method	53
4.7.3.1 Why do we select FEM?	53
4.7.3.2 Formulation of FEM	54
4.8 Summary	57
5 Effects of Tissue Conductivity on Head Modelling	58
5.1 Methodology and Tools	58
5.1.1 A spherical head model construction	58
5.1.2 Used tools	60
5.2 Influence of Anisotropic Conductivity	61
5.2.1 Objective of the study	61

5.2.2 Head model construction	61
5.2.3 Simulation setup	61
5.2.4 Simulation results	63
5.2.5 Conclusion	64
5.3 Influence of Inhomogeneous and Anisotropic Tissue	64
5.3.1 Objective of the study	64
5.3.2 Conductivity ratio approximation model	65
5.3.2.1 Simulation setup	65
5.3.2.2 Simulated results	66
5.3.2.3 Conclusion	68
5.3.3 Statistical conductivity approximation model	68
5.3.3.1 Simulation setup	69
5.3.3.2 Simulation results	70
5.3.3.3 Conclusion	71
5.3.4 Fractional Anisotropy based conductivity model	71
5.3.4.1 Head model construction and simulation	71
5.3.4.2 Simulations and results	71
5.3.4.3 Conclusion	73
5.3.5 The Monte Carlo method based conductivity model	73
5.3.5.1 Simulation	74
5.3.5.2 Simulation results	74
5.3.5.3 Conclusion	75
5.3.6 Effects of conductivity variations on EEG	76
5.3.6.1 Objective of the study	76
5.3.6.2 Head model construction	76
5.3.6.3 Simulation setting and computing	76
5.3.6.4 Conclusion	80
5.3.7 Implementation of inhomogeneous and anisotropic conductivity using stochastic FEM	80
5.3.7.1 Objective of the study	80
5.3.7.3 Simulation setup	81
5.3.7.4 Simulation results	82
5.3.7.5 Conclusion	87
5.4 Conclusion and Contribution	87
6 Advanced study	89
6.1 Local Tissue Conductivity	89
6.1.1 Aims of the study	89
6.1.2 Introduction	89

6.1.3 Local tissue conductivity based head model I	91
6.1.3.1 Spherical head model construction	91
6.1.3.2 Realistic head model construction	93
6.2.3.3 Conductivity assignment	95
6.2.3.4 Simulations	95
6.2.3.5 Simulation results	96
6.1.4 Local tissue conductivity based head model II	101
6.1.4.1 Head models construction	101
6.1.4.2 Simulation and results	102
6.1.4.3 Discussion	103
6.2 EEG Analysis on Alzheimer's Disease Sources	105
6.2.1 Aims of the Study	105
6.2.2 Introduction	105
6.2.3 Methods	106
6.2.3.1 Finite element conductivity	107
6.2.3.2 Source modelling	107
6.2.3.3 Simulation and results	108
6.2.3.4 Discussion	110
6.3 Conclusion	111
7 Sensitivity Analysis	113
7.1 Head Model Construction	113
7.2 Uncertain Conductivity Approximation	113
7.3 Sensitivity Parameter Definition	115
7.4 Implementation and Experimentation	117
7.5 Experimental Results	117
7.5.1 Results in the spherical head models	117
7.5.2 Results in the realistic head model	121
7.6 Discussion and Conclusion	122
8 Conclusion	124
8.1 Main Contributions	124
8.1.1 A series of head model construction on inhomogeneous and anisotropic tissue conductivity	125
8.1.2 Systematically studied the effects of inhomogeneous and anisotropic tissues on EEG computation	126
8.1.3 Local tissue conductivity on head modelling	126
8.1.4 Computation of sensitivity indexes for inhomogeneous and anisotropic conductivity	127

8.2 Future Work	127
8.2.1 The model improvement	128
8.2.2 Segmentation	128
8.3.3 Conductivity	128
8.3 Summary	129

List of Figures

No.	Title	Page
Figure 2.1	Mid sagittal view of the human brain	9
Figure 2.2	The four lobes of the brain	10
Figure 2.3	Internal structure of the brain as seen in coronal section	11
Figure 2.4	Structure of a neuron and information transmission	12
Figure 2.5	Different parts of the skull.	14
Figure 2.6	A cross sectional view of the scalp, skull and brain	15
Figure 2.7	Head muscles	15
Figure 2.8	The 10-20 international electrode system for the placement of electrodes at the head surface	16
Figure 2.9	EEG on referential montage using Advance Source Analysis	17
Figure 3.1	A five-layered spherical head model.	21
Figure 3.2	Head tissue classification from a raw MRI	22
Figure 3.3	Sample FEM tetrahedral mesh with tissue classification	23
Figure 3.4	Anisotropic conductivities of white matter. σ_{long} represents longitudinal and σ_{trans} represents transversal conductivity	30
Figure 3.5	The linear relationship between the eigen values of the diffusion and conductivity ellipsoid. The resulting ellipsoid is identical to the diffusion ellipsoid up to an unknown scaling factor, which can be derived using the volume constraint with the isotropic conductivity sphere of white matter.	32
Figure 3.6	The linear relationship between the eigen values of diffusion tensor and conductivity values for the Wang's constraint	33
Figure 3.7	The anisotropic skull conductivity.	34
Figure 3.8	Different conductivity values of the skull for different anisotropy ratios: (a) WM tissues and (b) skull tissues.	35

Figure 3.9	Fractional anisotropy for WM	38
Figure 3.10	Conductivity ratio Vs fractional anisotropy (FA).	38
Figure 3.11	Volume constrained conductivities produced by Monte Carlo method. Conductivity analysis using histogram: (a) radial conductivities and (b) tangential conductivities	40
Figure 4.1	Boundary between two compartments. σ_1 and σ_2 are conductivities of tissue layer 1 and 2, respectively, and the normal vector \mathbf{e}_n is the interface.	45
Figure 4.2	A dipole model. \mathbf{r}_0 is the location of dipole centre. $+I_0$ is current source and $-I_0$ is the current sink points. \mathbf{d} is distance from source to sink and $I(\mathbf{r})$ is current field at a point \mathbf{r} .	47
Figure 4.3	The angle between vectors pointing to surface position \mathbf{r} and dipole location \mathbf{r}_q is denoted τ . The angle the dipole \mathbf{q} makes with the radial direction at \mathbf{r}_q is denoted α . The angle between the plane formed by \mathbf{r}_q and \mathbf{q} , and the plane formed by \mathbf{r}_q and \mathbf{r} is denoted β	50
Figure 5.1	Spherical head model construction	59
Figure 5.2	(a) Value of conductivity ratio (ξ_{lt}) between longitudinal and transverse conductivity for each WM element generated by CRA, (b) clear view of (a) from 10^2 to 10^3 WM elements, (c) longitudinal (long.) and transverse (trans.) conductivity values for each WM elements based on ξ_{lt} of (a) using Volume constraint, and (d) clear view of (c) from 10^2 to 10^3 WM elements	66
Figure 5.3	(a) Value of ξ_{lt} (conductivity ratio) between longitudinal and transverse conductivity for each WM element generated by SCA, (b) clear view of (a) from 10^2 to 10^3 WM elements, (c) longitudinal and transverse conductivity values for each WM elements based on ξ_{lt} of (a) using	69

	Volume constraint, and (d) clear view of (c) from 10^2 to 10^3 WM elements	
Figure 5.4	Probability density function of Rayleigh distribution.	77
Figure 5.5	Inhomogeneous anisotropic conductivities produced by SCA. (a)–(d) WM elements and (e)–(h) skull elements.	78
Figure 5.6	Effects of inhomogeneous anisotropic WM conductivity on EEG: (a) relative errors (ϵ) values (in percentage) and (b) correlation coefficient (η) values.	83
Figure 5.7	Effects of inhomogeneous anisotropic skull conductivity on EEG: (a) relative errors (ϵ) values (in percentage) and (b) correlation coefficient (η) values.	84
Figure 5.8	Effects of inhomogeneous anisotropic WM and skull conductivities together on EEG: (a) relative errors (ϵ) values (in percentage) and (b) correlation coefficient (η) values.	85
Figure 5.9	Effects of inhomogeneous anisotropic head model on EEG: (a) relative errors (ϵ) values (in percentage) and (b) correlation coefficient (η) values.	86
Figure 5.10	Topographic visualization of the scalp electrode potentials. (a) head model (A) and head model (D): (b) from the parallel Volume constraint, (c) from the parallel Wang's constraint, (d) from the perpendicular Volume constraint and (e) from the perpendicular Wang's constraint conductivity for the first dipole (elevation angles $\pi/5.22$ and azimuth angle $\pi/4$).	87
Figure 6.1	Simplified local tissue conductivity based three-layered spherical head model showing different tissues.	92
Figure 6.2	Local scalp tissue conductivity approximation. The conductivity for scalp (skin) is 0.33 S/m, wet skin (place of electrodes) is 0.1 S/m and fat is 0.04 S/m.	93
Figure 6.3	A realistic head model construction	94

Figure 6.4	RDM and MAG from assigning local conductivity to different layers in a three-layered spherical head model using the somatosensory cortex (SC) and the thalamic dipoles. In the above figures, label <i>Br</i> , <i>Sk</i> and <i>Sc</i> represent brain, skull and scalp, respectively.	97
Figure 6.5	RDM and MAG from assigning local conductivity to different layers in a four-layered spherical head model using the somatosensory cortex and the thalamic dipoles. In the above figures, label <i>Br</i> , <i>Sk</i> and <i>Sc</i> represent the brain, skull and scalp, respectively.	98
Figure 6.6	RDM and MAG from assigning the local conductivity to different layers in the realistic head model for both dipoles.	100
Figure 6.7	The brain is viewed from the outer side and front with the hippocampus and amygdala.	107
Figure 6.8	Location of one of the AD sources in RA by the cross hairs in different views.	108
Figure 6.9	RDM (a) and MAG (b) errors from different brain tissue distortion levels on source to source basis.	109
Figure 6.10	RDM (a) and MAG (b) errors from RA and LA sourced without and with different brain tissue distortion levels to SC sourced normal EEG.	109
Figure 6.11	Contour view of scalp potentials obtained from somatosensory cortex (a) reference model, (b) five percent, (c) ten percent, (d) fifteen percent and (e) twenty percent brain tissue distortions.	110
Figure 6.12	Electrode positions (left ear-Nasion – right ear). Odd number with electrode names indicate left hemisphere, even number with electrode names indicate right hemisphere.	111
Figure 7.1	WM conductivity uncertainty: (a) mean relative errors ($m\varepsilon$) and (b) mean correlation coefficient ($m\eta$) values generated by incorporating WM conductivity uncertainty. <i>RefA</i> and	118

RefB represent the Reference Models A and B, respectively. *long* represents the longitudinal and *trans* represents the transversal conductivities with *V* for Volume constraint and *W* for Wang's constraint.

Figure 7.2 Skull conductivity uncertainty: (a) mean relative errors ($m\varepsilon$) and (b) mean correlation coefficient ($m\eta$) values generated by incorporating skull conductivity uncertainty. *RefA* or *RefB* stands for either reference model A or B. *tan* represents the tangential and *rad* represents the radial conductivities with *V* for Volume constraint and *W* for Wang's constraint. 119

Figure 7.3 The scalp conductivity uncertainty: (a) mean relative errors ($m\varepsilon$) and (b) mean correlation coefficient ($m\eta$) values. *RefA* or *RefB* stands for either reference model A or B. *tan* represents the tangential and *rad* represents the radial conductivities with *V* for Volume constraint and *W* for Wang's constraint. 121

List of Tables

No.	Title	Page
Table 3.1	Skull resistivity (reciprocal of conductivity).	24
Table 3.2	Body tissue conductivity.	25
Table 3.3	Head tissue conductivity.	26
Table 3.4	Head tissue conductivities used in this dissertation.	27
Table 3.5	Homogeneous and isotropic conductivities used in this dissertation.	27
Table 4.1	Comparison among different methods for solving the forward problem.	54
Table 5.1	Average related error (ε) and correlation coefficient (η) values resulted by Models A and B.	63
Table 5.2	Average ε and η values resulted by comparing Models A and C.	63
Table 5.3	Average ε and η values resulted by comparing Models A and D.	64
Table 5.4	RDM and MAG values between reference and computed models for WM.	67
Table 5.5	RDM and MAG values between reference and computed models for skull.	68
Table 5.6	RDM and MAG values between reference and computed models for WM and skull together.	68
Table 5.7	RDM and MAG values using SCA for the WM.	70
Table 5.8	RDM and MAG values using SCA for the skull.	70
Table 5.9	RDM and MAG values using SCA for the WM and skull together.	70
Table 5.10	RDM and MAG values generated by inhomogeneous anisotropic WM conductivities	72

Table 5.11	RDM and MAG values generated by inhomogeneous anisotropic skull conductivities.	73
Table 5.12	RDM and MAG values generated by inhomogeneous anisotropic WM and skull conductivities.	73
Table 5.13	Average RDM and MAG errors for the WM inhomogeneous and anisotropic conductivities for the orthogonal dipole orientations of X, Y and Z.	74
Table 5.14	Average RDM and MAG errors for the skull inhomogeneous and anisotropic conductivities for the orthogonal dipole orientations of X, Y and Z.	75
Table 5.15	Average RDM and MAG errors for the WM and skull inhomogeneous and anisotropic conductivities for the orthogonal dipole orientations of X, Y and Z.	75
Table 5.16	RDM and MAG values produced by longitudinal conductivities.	79
Table 5.17	RDM and MAG values produced by transverse conductivities.	80
Table 5.18	Effects of inhomogeneous scalp tissue conductivity on EEG.	85
Table 6.1	Effects of principal tissue variations assigning local conductivity in three-layered spherical head model.	97
Table 6.2	Effects of element variations assigning local conductivity in four-layered spherical head model.	99
Table 6.3	Effects of element variations assigning local conductivity in realistic head model.	101
Table 6.4	Skull conductivity, width and features at different places.	102
Table 7.1	The uncertain parameter (conductivity) and its ranges used in this study for the head model construction.	115
Table 7.2	Homogeneous conductivity values for different tissue layers for the construction of the reference head models.	116
Table 7.3	Relative error % (ε) values produced by the white matter	119

	conductivity perturbations for different dipole eccentricities.	
Table 7.4	Sensitivity indexes for different conductivities in the spherical head model comparing with the reference model A.	120
Table 7.5	Sensitivity indexes for different conductivities in realistic head model comparing with the reference model A.	122

List of Acronyms

AD- Alzheimer's disease
AP – Action potential
ASA- Advanced source analysis

BEM – Boundary Element Method
BEV –Brain element variation
BTDL- Brain tissue distortion level

CC – Correlation coefficient
CDL – Cortical dipole layer
CRA- Conductivity ratio approximation
CSF – Cerebrospinal Fluid
CT- Computed tomography

DB- Dipole bunch
DT- Diffusion tensor
DT-MRI- Diffusion tensor magnetic resonance imaging

EEG- Electroencephalography

FA- Fractional anisotropy
FE – Finite Element
FDM – Finite Difference Method
FEM – Finite Element Method

GM- Gray matter

LTC-Local tissue conductivity

MAG – Magnification factor
MEG- Magnetoencephalography
MLE- Maximum likelihood estimator
MRI-Magnetic resonance imaging

PDF- probability density function

SC-Somatosensory cortex
SCA- Statistical conductivity approximation

SCEV – Scalp element variation

SEV – Skull element variation

RDM – Relative difference measure

RE- Relative errors

VC- Volume constraint

WC-Wang's constraint

WM- White matter

Notations and Symbols

ρ - Charge density (ρ)

μ - Mean or homogeneous conductivity of a tissue layer

ξ - Anisotropy or conductivity ratio

σ^2 – Variance of conductivity

σ - Conductivity

$\underline{\underline{\sigma}}$ - Conductivity tensor

σ_t , – Transversal conductivity of the white matter, Tangential conductivity of the skull

σ_{trans} – Transversal conductivity of the white matter

σ_{long} – Longitudinal conductivity of the white matter

σ_{rad} – Radial conductivity of the skull

σ_{tan} – Tangential conductivity of the skull

ε -Relative error

η -Correlation coefficient

B - Magnetic field

D - Electric field

E- Electric field

H - Magnetic field

K^+ - Potassium ion

Na^+ – Sodium ion

Cl^- – Chloride ion

m- Maximum likelihood estimator

Publications

1. **Bashar, M. R.**, Li, Y. and Wen, P., *Effects of Local Tissue Conductivity on Spherical and Realistic Head Models*, Australasian Physical & Engineering Sciences in Medicine, Vol 33, No 3, pp. 333-342, 2010.
2. **Bashar, M. R.**, Li, Y. and Wen, P., *Uncertainty and sensitivity analysis for anisotropic inhomogeneous head tissue conductivity in human head modelling*, Australasian Physical & Engineering Sciences in Medicine, Vol 33, No 2, pp. 145-152, 2010.
3. **Bashar, M. R.**, Li, Y. and Wen, P., *Study of EEGs from Somatosensory Cortex and Alzheimer's Disease Sources*, International Journal of Medicine and Medical Sciences, Vol 1, No 2, pp. 62-66, 2010 .
4. **Bashar, M. R.**, Li, Y. and Wen, P., *A systematic study of head tissue inhomogeneity and anisotropy on EEG forward problem computing*, Australasian Physical & Engineering Sciences in Medicine, Vol 33, No 1, pp. 11-21, 2010.
5. **Bashar, M. R.**, Li, Y. and Wen, P., *Effects of Local Tissue Conductivity on Spherical and Realistic Head Models*, Australasian Physical & Engineering Sciences in Medicine, Vol 31, No 2, pp. 122-130, 2008.
6. **Bashar, M. R.**, Li, Y. and Wen, P., *Effects of the Local and Spongiosum Tissue Conductivities on Realistic Head Modelling*, International Conference on Complex Medical Engineering, (CME 2010), 13 -15 July, Gold Coast, Australia, 2010.
7. **Bashar, M. R.**, Li, Y. and Wen, P., *EEG analysis on skull conductivity perturbations using realistic head mode*, International Conference on Rough Set and Knowledge Technology (RSKT2009), 14-16 July, 2009, Gold Coast, Australia.
8. **Bashar, M. R.**, Li, Y. and Wen, P., *A study of white matter and skull inhomogeneous anisotropic tissue conductivities on EEG forward*

- head modelling*, IEEE International Conference on Computer and Information Technology (ICCIT 2008), 24-25 December, 2008, Khulna, Bangladesh.
9. **Bashar, M. R.**, Li, Y. and Wen, P., *Effects of white matter on EEG of multi-layered spherical head models*, IEEE International Conference on Electrical and Computer Engineering (ICECE 2008), 20-22 December, 2008, Bangladesh.
 10. **Bashar, M. R.**, Li, Y. and Wen, P., *Tissue conductivity anisotropy inhomogeneity study in EEG head modelling*, International Conference on Bioinformatics and Computational Biology, 14-17 July, 2008, Las Vegas, Nevada, USA.

CHAPTER 1

INTRODUCTION

Human brain consists of 10^{10} - 10^{11} neurons that are closely interconnected to each other. The brain receives its input from different senses such as sight, sound, touch and taste. These perceived inputs give the brain knowledge of the surrounding environment. It has been recognized that electrical interaction between neurons is responsible for the transmission of information. As information from these senses travels through the brain, it interacts with an enormous number of neurons ($10^3 - 10^5$), and undergoes progressively more complex processing. In this way, knowledge of the environment can be combined with the current 'state of mind' to produce a set of outputs. This output causes movement of the muscles to allow the body to respond appropriately to the environment.

Neuron, the core component of the brain, processes and transmits information by electrochemical signalling. More generally, neurons communicate with each other via a chemical messenger, such as diffusion of Potassium ions (K^+), which are regulated by the electrical state of neurons. When an area of the brain is activated, the electric potential of the neurons within that region is generated (in milliVolt amplitude) and changed over time. This electrical activity in the brain, in turn, produces an electric field that affects the entire body. The electric potentials within this electric field conduct up through the brain tissue, enter the membranes and continue on up through the skull to the scalp. When the electric potentials appear in the scalp, it turns into micro Volts in amplitude. Although small in amplitude, this field can be detected by placing electrodes on the head surface, and recording the electric potential at each electrode. This recording of potentials on the head surface using electrodes is known as an electroencephalogram (EEG). EEG provides a picture of the neuronal activity of the brain over time.

1.1 Electroencephalography and Head Modelling

In order to understand the relationship between EEG and the sources of brain activity, the electrical conduction properties within the head is to be modelled mathematically. An enormous number of studies have been performed in last few decades in developing efficient head modelling techniques [Zhou and Oostendrop 1992, de Munck and Peters, 1993]. Brain researchers have started head modelling from the fundamental concept of a spherical head (single-layered head model) [Marin *et al* 1998, Mosher *et al* 1999, Muravchik *et al* 2001]. Then, they progress it making three-sphere (brain, skull and scalp) head models. Later on, they have added cerebrospinal fluid to the three-layered head model and produced a four-layered model. Finally, they are able to make five-layers to N layers head models [Vanrumste 2002]. As the spherical head model fails to satisfy the actual geometry of a head, researchers have discovered a challenging topic to create a realistic head model. Even more challenges are posed when realistic conductivities are included in the head model construction. Such challenges include: (i) the anatomic construction of accurate head geometries of each compartment of the head, (ii) the specification of material properties (most of which are inhomogeneous and some are anisotropic), (iii) the numerical approximation of the biophysical field equation and (iv) the large-scale nature of computation. Though researchers have developed anatomically accurate head geometries from magnetic resonance imaging (MRI), studied conductivities from diffusion tensor MRIs and implemented piecewise numerical computation with an excessively large computer to construct a more realistic head model, a complete volume conductor model of a human head has not yet been accomplished, especially in terms of conductivity [Vanrumste 2002, von Ellenrieder *et al* 2008]. The structure of the human head is too complex to be represented exactly by an artificial computer model. This thesis attempts to develop new approaches to model a human head using spherical and realistic head geometries based on the head tissue properties (conductivity). It is our hope that these additional concepts may contribute to the successful head modelling, which can be used in both clinical purposes and brain research.

Among the head tissues, most tissues are inhomogeneous and some are anisotropic at a microscopic level. Inhomogeneous means that a tissue has different conductivities in different locations regardless of directions. Anisotropy means the

conductivity is dependent on the directions. These directions are either in the radial or in the tangential. Different tissues have different conductivities; even the same tissues at different places have different conductivities [Hauelsen *et al* 1997, Ramon *et al* 2006a, 2006b]. For example, the white matter (WM), gray matter (GM) and cerebellum of the brain have different conductivities, the presence of the suture line of the skull increases its conductivity in comparison with other non-suture positions, and the subcutaneous fat and muscle in the scalp have different conductivities than the skin. When the electric currents are obstructed by a high resistance obstruction, the currents move in other radial or tangential directions rather than its original direction and cause anisotropy. It happens especially in the WM of the brain when the electric currents move towards the WM from the GM, and in the skull where electric currents move from the brain to the lower hard skull bone, or from the inner soft skull bone to the outer hard bone.

1.2 Significance of Head Modelling

The main purpose of head modelling is the solution of the forward problem to compute the scalp potentials or EEG originated from the brain. The solution of the forward problem is evaluated several times during the solution of the inverse problem for the source analysis purposes. Source analysis examines the best location of the source which best fits the given scalp potentials. Therefore, the head modelling is an essential part of source analysis or source reconstruction procedure. The source analysis is extensively used in different presurgical evaluations, clinical research and applications [He *et al* 1999, Vanrumste 2002, Mosconi *et al* 2006]. The EEG and source localization are also used to determine and research on different mental disorders, such as dementia, autism and epilepsy. EEG has become a popular non-invasive method in all aspects of brain related researches.

In a clinical setting, the EEG is used for the diagnosis of epilepsy. The EEG from an epilepsy patient may have an abnormal amplitude and waveform. For patients with partial epilepsy, a focal group of brain cells is responsible for an epileptic seizure. A neurologist inspects the EEG and the behaviour of the patients at the onset of a seizure to determine the epileptic zone or the source location. Another application area is sleep disorder [Vanrumste 2002, Hallez 2008b]. Different stages of sleep phases are mainly determined by the EEG analysis. EEG of a patient

complaining from sleeplessness or from fatigue can be recorded and abnormalities in the EEG may be found when compared with the EEG obtained from normal sleep. The other application area is the evoked potentials. Evoked potentials can be generated in the EEG by means of stimulating peripheral nerves. These potentials are much smaller in amplitude than the available background EEG. This approach can be applied to test the functioning of the peripheral nerves and the integrity of various central nervous pathways.

Head modelling, or the solution of forward problem has been extensively used in cognitive science for decades. Recently, a new technique of electroconvulsive therapy (ECT) is used to eliminate the cognitive side effects by passing pulses of approximately 1 ampere into the brain in order to provoke an epileptic seizure. ECT stimulates the brain and effects on long-term memory to give rise to concerns surrounding its use. ECT is also used as a treatment for severe major depression, mania and catatonia which have not responded to other treatment.

Beside the ECT, transcranial direct current stimulation (tDCS) and transcranial magnetic stimulation (TMS) are also used to modulate or excite the activity of neurons in the brain. Neurons respond to static electrical fields by altering their firing rates. Firing increases when the positive pole or electrode (anode) is located near the cell body or dendrites and decrease when the field is reversed. Currently tDCS can modulate the function of the spinal cord and of the cerebellum and is being studied for the treatment of a number of conditions including major depression. On the other hand, TMS is a noninvasive method to excite the elementary unit of the nervous system where weak electric currents are induced in the tissue by rapidly changing magnetic fields. This way, brain activity can be triggered with minimal discomfort, and the functionality of the circuitry and connectivity of the brain can be studied. In the clinic, TMS is used to measure activity and function of specific brain circuits in humans. The most robust and widely-accepted use is in measuring the connection between the primary motor cortex and a muscle. This is most useful in stroke, spinal cord injury, multiple sclerosis and motor neuron disease.

Head modelling establishes an accurate insight into the electrical activity of the brain by studying the properties of cerebral and neuronal networks. From the above discussion, it is perceived the importance of head modelling. An accurate head

modelling is the underneath mechanism to analysis and diagnosis different mental disorders, therapies and brain stimulations.

1.3 The Originality of this dissertation

The aim of this dissertation is to construct an accurate head model for the solution of EEG forward problem. It mainly depends on head geometry and tissue conductivity [Vanrumste *et al* 2000, van Uiter *et al* 2004, Ramon *et al* 2006a]. Accurate head geometry is obtained from an MRI [Huiskamp *et al* 1999]. However it is difficult to obtain accurate tissue conductivity as it varies from person to person or even same person in different situations. This dissertation focuses on conductivity modelling for the construction of a human head and to investigate the effects of conductivity on EEG. Several studies [de Munck and Peters 1993, Zhang 1995, Vanrumste *et al* 2000, Baillet *et al* 2001, Mosher *et al* 1999, von Ellenrieder *et al* 2006] implement head model using homogeneous conductivity. As the conductivities of head tissues are inhomogeneous, other studies [Cuffin 1993, Klepfer *et al* 1997, Marin *et al* 1998, Wen 2000, Nicolas *et al* 2004] implement head model using inhomogeneous conductivity. Later on, it is found that a head model is not accurate unless anisotropic conductivity in the WM and skull. Several studies [Marin *et al* 1998, Anwender *et al* 2002, Wolters 2003, Gullmar *et al* 2006, Wolters *et al* 2006, Hallez *et al* 2009] implemented head model using constant or fixed anisotropy ratio. However, the anisotropy ratio varies in different regions of WM and skull due to anatomical structure.

This dissertation investigates the effects of tissue conductivity on EEG in two aspects: (A) inhomogeneous and anisotropic conductivities and (B) local tissue conductivity. For the aspect (A), conductivity models (conductivity ratio approximation, statistical conductivity approximation, fractional anisotropy based conductivity approximation and the Monte Carlo method based conductivity approximation) are proposed based on various anisotropy ratios to overcome the limitations of fixed anisotropy ratio. This dissertation also investigates the effects of local tissue conductivity on EEG implementing conductivity model based on tissue position in the head for approach (B). Besides these, an application of head

modelling to investigate the effects of Alzheimer's disease sourced EEG on somatosensory cortex sourced normal EEG is also discussed.

1.4 Organization of the Dissertation

Chapter 2 gives an introduction of the features of a human head and head modelling. The Chapter starts with a brief introduction to head anatomy and neurophysiological structure and processes behind the neuronal activity generated in the brain. We discuss how brain tissue generates electrical potentials, how it propagates to the scalp and how EEG is measured.

Chapter 3 describes head modelling and the presentation of tissue conductivity. In the head modelling, we describe the spherical and realistic head models. Some question arises in describing tissue conductivity. First, the question, "Why the head tissue conductivities are inhomogeneous and anisotropic?" is explained in this Chapter. Then, "How do we tackle these inhomogeneous and anisotropic conductivities?" is described. We describe different conductivity models to implement inhomogeneous and anisotropic conductivities into a head model.

In Chapter 4, we focus on the forward problem and its solution using a finite element method. In the beginning of this Chapter, we show how the electric potential on the head surface is derived from the neuronal activity using the Maxwell and the Poisson equations. We describe how electric current passes from an inner to the outer surfaces using the Dirichlet and Newman boundary conditions. We provide an algebraic formulation of the EEG forward problem and a series expansion for the solution of the EEG forward problem in a multi-layered spherical head.

In Chapter 5, we discuss our methodology and steps for spherical head model construction, and different tools to perform simulation. Then we attempt to answer the question "Is there any effect of inhomogeneous and anisotropic tissue conductivities on EEG head modelling?" We attempt to answer using the simulated results of our proposed conductivity models, such as conductivity ratio approximation, statistical conductivity approximation, fractional anisotropy based conductivity approximation and the Monte Carlo method based conductivity approximation models. We also study the effects of inhomogeneous and anisotropic conductivities using a stochastic method based conductivity approximation model.

Chapter 6 describes local conductivity study and an EEG analysis on a normal source and Alzheimer's disease (AD) source. Firstly, we discuss the different values of conductivity in a same tissue and the development of local tissue conductivity based head model. In the second part of the Chapter, we discuss the sources of AD and find the differences in EEG obtained from the normal and AD sources.

Chapter 7 focuses on the uncertainty and sensitivity of tissue conductivity in EEG. In the first part of the Chapter, we describe the way to select the uncertain parameter in head modelling and the method to determine the sensitivity indexes. In the second part of the Chapter, we describe its effects on EEG and how much it would affect mean scalp potentials for both a spherical and a realistic head model.

Finally, we summarise our works and findings in Chapter 8. In this dissertation, we have successfully developed a series of inhomogeneous and anisotropic head models, systematically studied the effects of inhomogeneous and anisotropic tissues on EEG computation, investigated the local conductivity problem in realistic head modelling and finally we have studied the computation sensitivity of the inhomogeneous and anisotropic tissues.

CHAPTER 2

FEATURES OF HUMAN HEAD

In order to understand head modelling, the EEG forward problem or EEG source analysis, it is important to know the underlying mechanisms of the EEG, the mechanisms of the neuronal action potentials, excitatory post synaptic potentials and inhibitory post synaptic potential. This Chapter provides a general overview of the background for bioelectricity in the human head, gives details of the assumptions to construct a head model from a computational perspective.

2.1 Anatomy of Human Head

The human head consists of three main tissues, the scalp, skull and the brain. The outer most of the human head is the scalp layer which covers the skull. The most remarkable region of the human head is the skull. The skull is a dome shaped hard bone layer which protects the brain. The brain, the innermost part of the head, is the core of the central nervous system. The gap between the skull and brain is filled with a liquid named the cerebrospinal fluid (CSF).

2.1.1 Anatomy of the brain

The human brain is the centre of the central nervous system. Different regions of the brain are designated for different purposes and functions. For example, the frontal region of the brain processes languages and the posterior (occipital) region processes vision. The main function of the brain is to receive, process and communicate information. This processed information can be sent either to other parts of the brain or other parts of the body. The brain is situated inside the skull and is floated with CSF. CSF protects the brain from damage or injury. It also provides sufficient oxygen and essential substances for the metabolism to sustain the brain tissues and give some protection to shock. Human brain basically consists of three parts [Gray, 2002]: the brain stem, the cerebellum and the forebrain or cerebrum as shown in Figure 2.1 [Purves *et al* 2004].

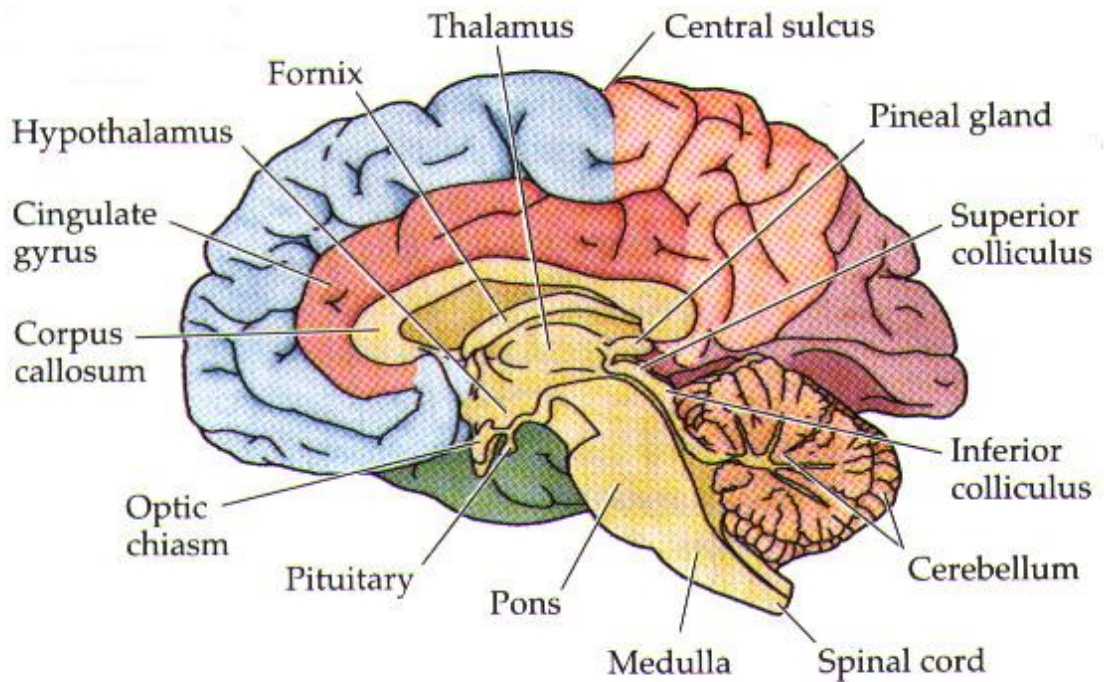


Figure 2.1 Mid sagittal view of the human brain [Mid sagittal view –online]

The brain stem consists of midbrain, pons and medulla. The diencephalon and cerebral hemispheres are collectively known as forebrain, which consists of most of the parts of the brain and is responsible for complex tasks such as muscle movement and language processing. There are two symmetric hemispheres, the left hemisphere and the right hemisphere. Each hemisphere is conventionally divided into four lobes named the frontal, parietal, temporal and occipital lobes as shown in Figure 2.2. The frontal lobe involves the ability to recognize future consequences resulting from current actions, to choose between good and bad actions (or better and best), override and suppress unacceptable social responses, and determine similarities and differences between things or events. Therefore, it is involved in higher mental functions. The parietal lobe integrates sensory information from different modalities, particularly determining spatial sense and navigation. The temporal lobe is involved in auditory processing and the processing of semantics in both speech and vision. The occipital lobe is involved with visual processing.

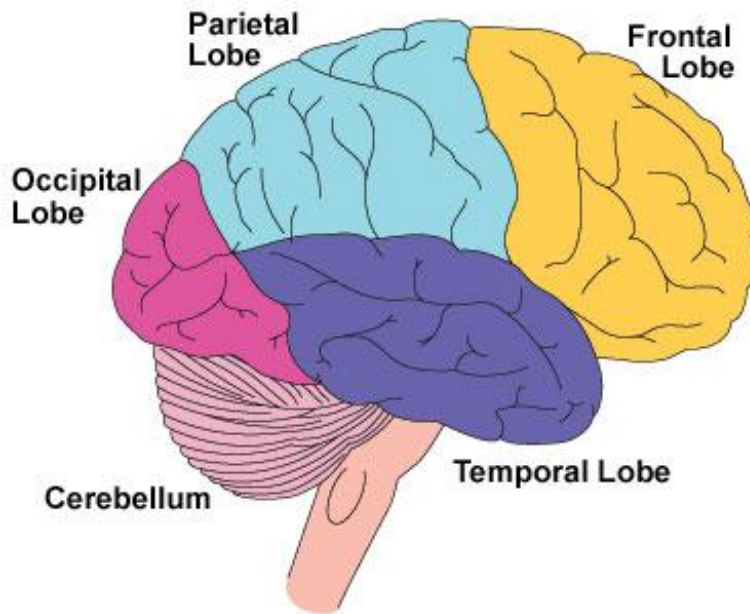


Figure 2.2 The four lobes of the brain [Four lobes-online].

These hemispheres are connected through several commissures with the corpus callosum as the largest fibre bundle. The surface of each hemisphere is 2mm to 4mm thick and called cortex or gray matter. The actual brain activity is generated in the gray matter. The gray matter at the edge of the brain has a folded structure to increase the surface so that the complex connections can be made. It is strongly folded into deep groves or valleys called sulci which are surrounded by the ridges and gyri. The outer layer is also called the cortex or cortical gray matter. In the gray matter, many structures can be identified according to their function in the processing of information. An example of such a structure is the hippocampus which is related to short term memory (Figure 2.3). The hippocampus has a very complicated folded structure. Specific types of epilepsy are related to this structure. In the gray matter nerve cells are the generators of the electro-chemical activity.

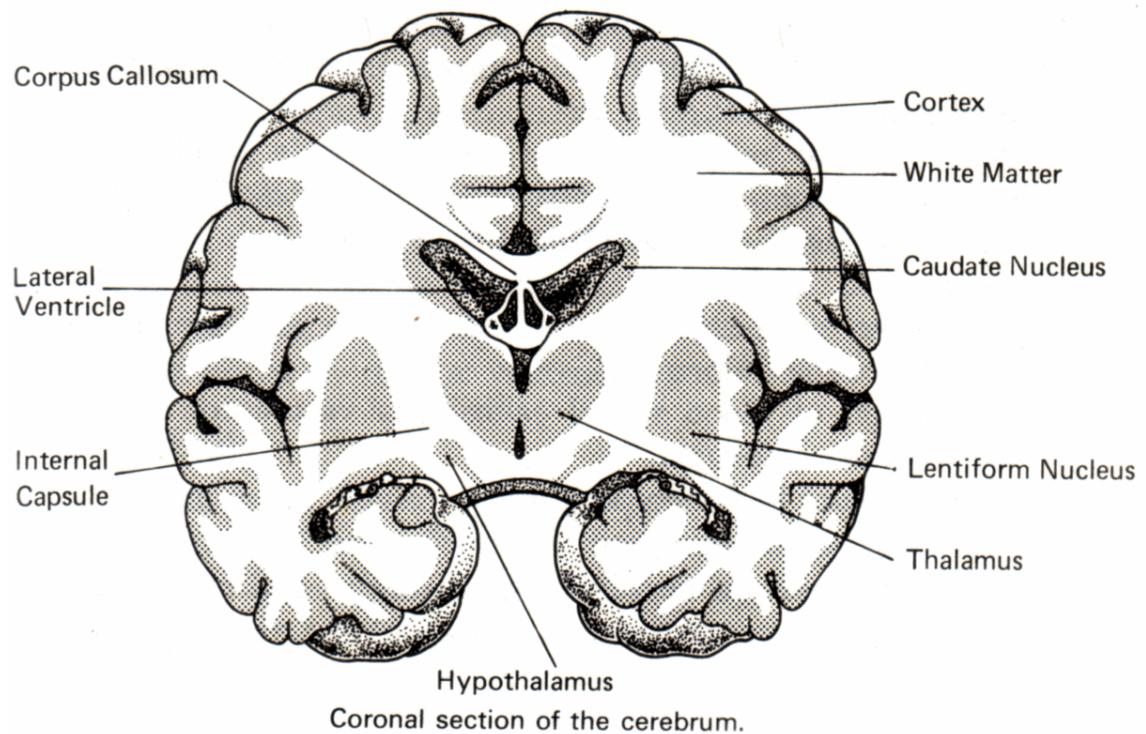


Figure 2.3 Internal structure of the brain as seen in coronal section [Brain structure-online].

The cortex consists of a large number of nerve cells known as pyramidal neurons whereas the underlying white matter is composed of nerve fibers connecting different parts of the brain. The white matter mainly consists of connections from and to different parts of the gray matter. An important connection contained in the white matter is the corpus callosum which connects the right and left hemispheres.

2.1.1.1 Anatomy of the neuron

The human brain consists of about 10^{10} nerve cells or neurons. The shape and size of the neurons vary but they possess the same anatomical structure [Vanrumste 2002]. The neuron consists of a cell body which is also called soma, the dendrites and an axon. In most respects, the structure of neurons is similar to that of other cells [Purves *et al* 2004]. Figure 2.4 shows the structure of a neuron and the signal propagation. The cell body processes the incoming signals and decides if a signal has to be transmitted to the axon or alternatively inhibit the signal. The dendrites originating from the neuronal cell body are specialized in receiving inputs from other nerve cells. The number of inputs that a particular neuron receives depends on the complexity of its dendritic structure ranging from 1 to 10^5 [Purves *et al* 2004]. Receiving inputs by dendrites, the cell body processes the inputs and fires an action

potential (AP) which propagates through the axon. The axon is a unique extension from the soma and is a few hundred micrometers long. The AP is a self-regenerating electrical wave that propagates from its point of initiation at the cell body to the terminus of the axon. The axon's terminus is divided into branches which connect to other neurons or tissues. The information encoded by AP is passed on to the next cell. Therefore, a physiological connection called synapse has to be made [Hallez 2008b]. The synapse is a specialized interface between two nerve cells. Accordingly, axon terminals convey this information to target cells, which include other neurons in the brain, spinal cord, muscles and glands throughout the body. These terminals are called synaptic endings. Each synaptic ending contains secretory organelles called synaptic vesicles. The release of neurotransmitters from synaptic vesicles modifies the electric properties of the target cell (postsynaptic cell). The postsynaptic cells are activated by virtue of neurotransmitters released by the pre-synaptic cells. Further readings on the anatomy of the neuron and the brain can be found in Gray (2002) and Purves *et al* (2004).

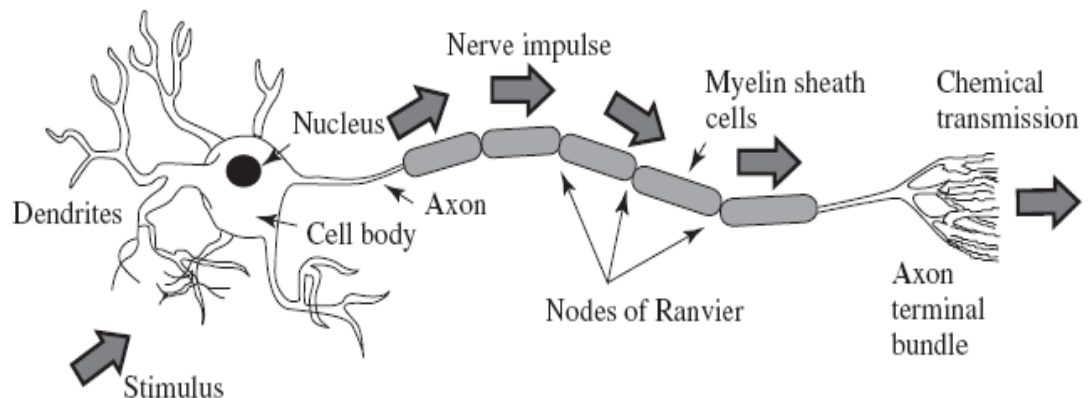


Figure 2.4 Structure of a neuron and information transmission [Sanei and Chambers, 2007].

2.1.1.2 Physiology of the neuron

All cells generate a steady electrochemical potential across their plasma membranes (a membrane potential) because of different ionic concentrations inside and outside the cell. Neurons use minute fluctuations in this potential to receive, conduct and transmit information across other surfaces. The membrane potential of a neuron, known as the resting potential, is similar to that of non-excitable cells. In most neurons it is about 75 mV, inside negative. Such bioelectric potentials result from the selectively permeable nature of the plasma membrane which prevents large

molecules, predominantly with negative charges, from leaving the cell. The cell uses K^+ for this purpose so that there is a high concentration of potassium within the cell.

Any activity which causes a change in the distribution of ions across the plasma membrane inevitably affects the resting potential -75 mV. The entry into neurons of sodium ion (Na^+) or calcium ion (Ca^+) causes depolarization of the cell (0 mV), while an increased chloride influx or increased potassium efflux results in reverse polarization to +40 mV. The reverse polarization actually decreases to be less polarized or repolarization to -75 mV. Then a hyperpolarization due to extracellular environment is happened to -90 mV and depolarization causes to resting potential -75 mV. Once the cell body has a certain threshold voltage it can initiate APs and it will continue to do so. When the AP reaches to the axonal terminals it causes a graded depolarization of the pre-synaptic membrane. As a result, neurotransmitters are released to change the degree of the next neuron or muscle. Further readings on the electrophysiology of a neuron can be found in Bannister (1995) and Gray (2002).

2.1.2 Anatomy of the skull

The skull is the bony structure of the head and is the most impressive region of the human head. It supports the face structure, protects the brain from injury, fixing the distance between two eyes to make an image on the occipital lobe and fixing the position of the ears to help the brain use auditory cues to judge direction and distance. The skull is divided into cranium and mandible. The mandible forms the lower jaw and holds the lower teeth. A skull, except for the mandible, is cranium. We only consider the cranium in this study. Therefore, the skull only means the cranium throughout the study unless specified. The adult human skull contains 22 bones. Among these bones, eight bones are in the neurocranium and fourteen bones are in the splanchnocranium. Bones of the skull are connected together by sutures. A suture is a type of fibrous joint which permits very little movement and contributes to compliance and elasticity of the skull. Figure 2.5 shows different parts of the skull.

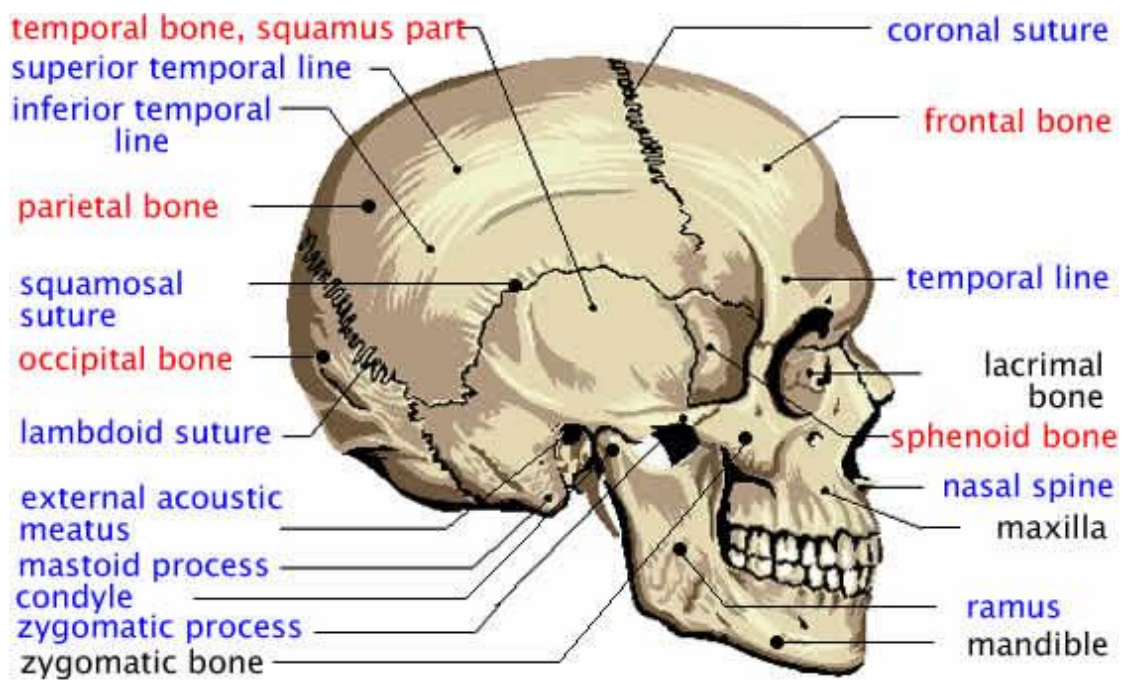


Figure 2.5 Different parts of the skull [Skull parts-online].

2.1.3 Anatomy of the scalp

The scalp is the anatomical boundary covering the head, face and neck. It consists of skin, connective tissue layer, aponeurosis layer, loose areolar connective tissue layer and pericranium layer. The skin is the outermost layer of the scalp from which head hair grows and is supplied extensively with blood vessels. The connective tissue layer is a thin layer of fat and fibrous tissue which lies beneath the skin. The aponeurosis is a layer of dense fibrous tissue which runs from the frontalis muscle anteriorly to the occipitals posteriorly. The loose areolar connective tissue layer makes the separation between the upper three layers and the pericranium. The pericranium is the periosteum of the skull bones. Figure 2.6 shows the cross sectional view of the scalp, skull and brain. Figure 2.7 shows some of the muscles in the human head.

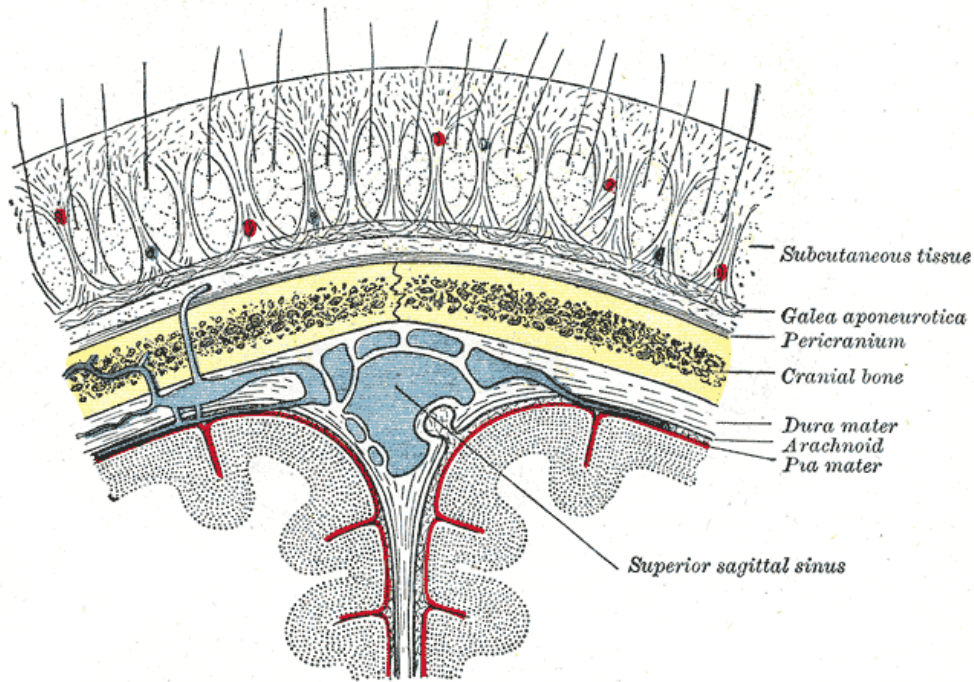


Figure 2.6 A cross sectional view of the scalp, skull and brain [Bannister, 1995].

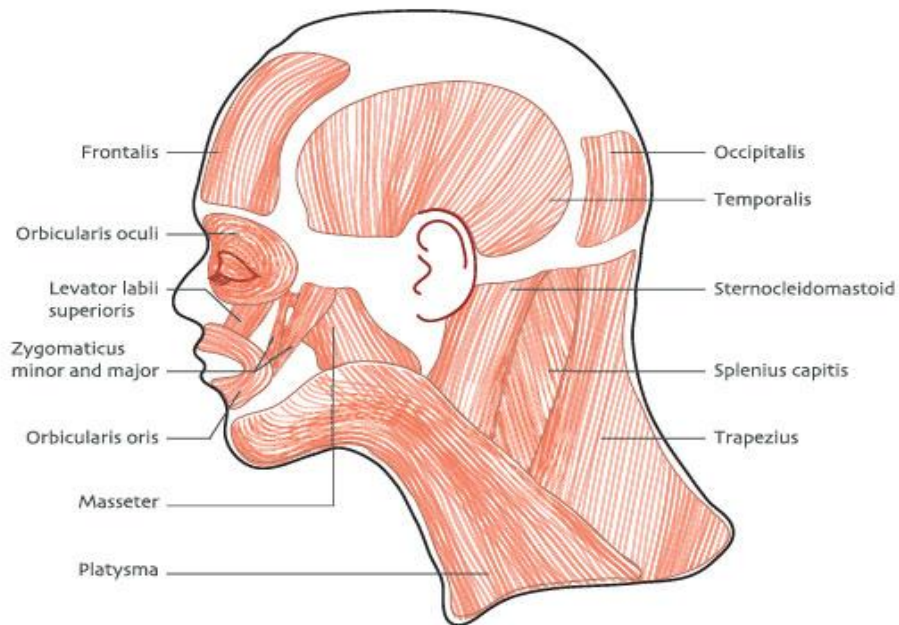


Figure 2.7 Head muscles [Head muscles-online].

2.2 Generation and Collection of EEG

One neuron generates a small amount of electrical activity in the order of femto-Ampere. This small amount cannot be picked up by surface electrodes, as the electrodes are at distance from the neurons. The source is overwhelmed by other electrical activity from neighbouring neuron groups. Consequently, an electrode only

detects summed activities of a large number of neurons which are synchronously active. When a large group of neurons (approximately 1000) is simultaneously active, the electrical activity is large enough to be picked up by the electrodes at the surface, thus generating a meaningful EEG signal [Vanrumste 2002, Hallez *et al* 2007, Hallez 2008b].

The electrical activity of the brain has been measured by electrodes positioning on different places on the head surface (scalp). These electrode positions placed on the scalp need a defacto standard which is unique for research and clinical purposes. The international 10-20 electrode system [Oostenveld and Praamstra 2001, Patel *et al* 2008] is used for measuring the electrical activity shown in Figure 2.8.

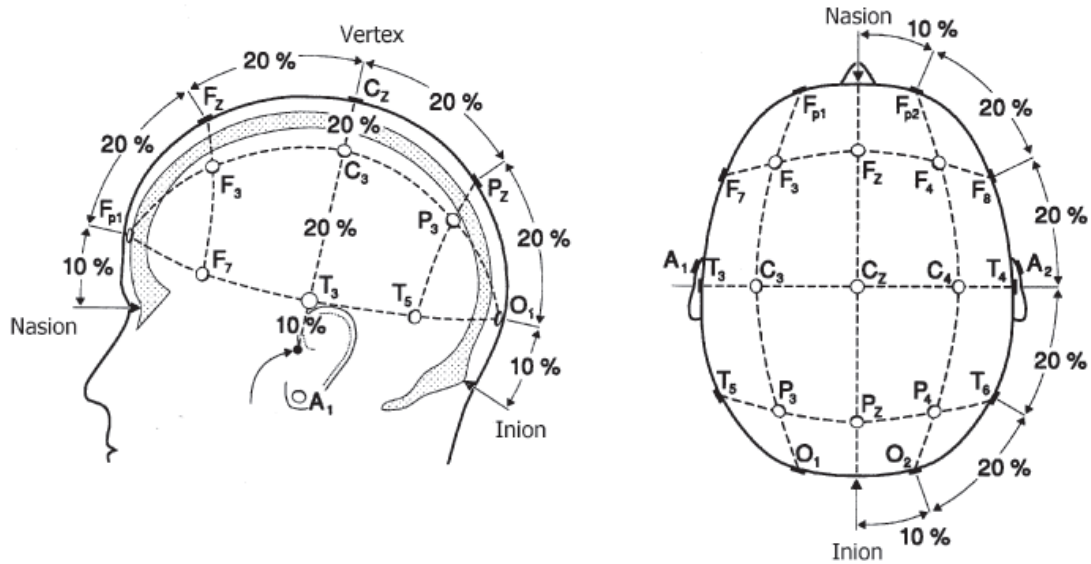


Figure 2.8 : The 10-20 international electrode system for the placement of electrodes at the head surface [Sanei and Chambers, 2007].

There are 27 electrodes in the 10-20 system. However, this number of electrodes is inadequate for clinical purposes to obtain a more accurate EEG. As a result, additional electrodes are placed in the 10-20 system and termed an ‘extension of 10-20 system’. Now, 64 or 128 dipoles are used for these clinical purposes. Additional electrodes can be added to the standard set-up when a clinical or research application demands increased spatial resolution for a particular area of the brain. High-density arrays (typically via cap or net) can contain up to 256 electrodes more-or-less evenly spaced around the scalp. Since an EEG voltage signal represents a difference between the voltages at two electrodes, the display of the EEG may be set up in one of several ways. The representation of the EEG channels is referred to as a montage.

Chapter 2 Features of Human Head

The montages are: bipolar, referential, average reference and Laplacian montages. Figure 2.9 shows an EEG on referential montage.

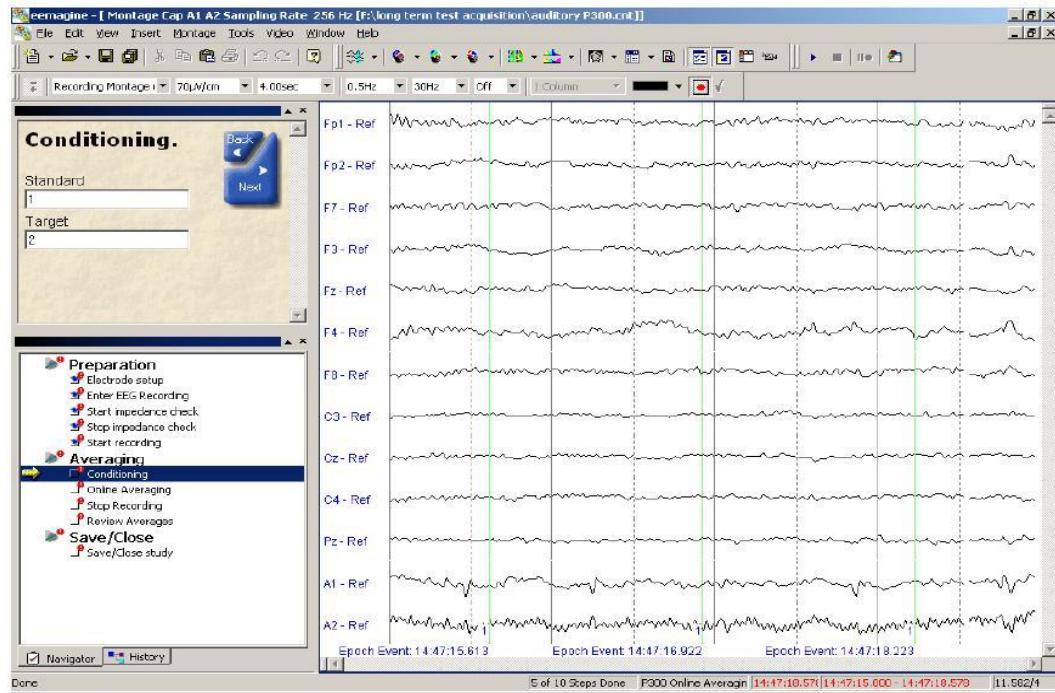


Figure 2.9: EEG on referential montage using Advanced Source Analysis (ASA).

2.3 Electric Features of the Head

It is known [Baillet *et al* 2001, Vanrumste 2002, Hallez *et al* 2007] that the generators of EEG are the synaptic potentials along the apical dendrites of the pyramidal cells which are in the gray matter cortex of the brain. These source currents raise the electric fields within the brain, its surrounding tissues and the head surface. The measured voltages on the scalp surface are related to the electrical activity within the brain via the conductive properties of the intermediary tissues. The general electrical activity at a given point in time is described by the Poisson's equation. Once the boundary condition functions are specified, a unique solution exists. This process is termed the EEG forward problem. To solve this problem, there are three aspects: shape, boundary condition and conductivity which can improve the accuracy of the solution. These aspects are discussed as follows.

The shape of human head is obviously the main parameter that affects the potentials on the scalp surface. This means that the more accurate the head geometry, the more accurate the solution. Much work has been investigated on the effects of

head geometry on the EEG. The boundary condition can also make contributions to the potential distribution. In the boundary condition the entire current passes from inner tissue layer to outer tissue layer but no current passes from the outset layer to the air.

The head tissue conductivity plays a key role in the computation of solving the Poisson's equation. The conductivities of a human head are coarse. At the beginning of head modelling, it is assumed that head tissue layers (scalp, skull and brain) are homogeneous. That means a tissue layer consists of the same tissues with the same conductivity property. Later on, it may be found that the tissue layers are heterogeneous or inhomogeneous, i.e., a tissue layer consists of several tissues. For example, the brain tissue layer consists of GM, WM, cerebellum, blood vessels and other tissues. As each tissue has its individual conductivity, the entire tissue layer becomes inhomogeneous in its conductive nature. Since the role and relative importance of inhomogeneity have been the topics of many different models, many algorithms which can deal with inhomogeneity have been developed. Finally, it is known that some tissues (skull and WM) show direction dependant conductivity either in radial or tangential direction. It is known as anisotropic conductivity. In recent years, there have been several methods and algorithms developed to implement anisotropic head models. Most of the research assumes that the anisotropy ratio (radial:tangential) is constant or homogeneous. However, this ratio is variable or inhomogeneous in different parts of the tissue layer. There is no such head model that incorporates full tissue conductivity. Moreover, location specific conductivity to different head regions (local conductivity) and an alternate solution to assigning accurate conductivity is also an emerging research area.

2.4 Summary

A human head consists of brain, skull and scalp. There are 10^{10} elements or neurons in the brain. A neuron contains a cell body, dendrites and axons. Pyramidal cells are types of neurons consisting of dendrites located close to the cortical surface. The communication between the neighbouring neurons is serviced by neurotransmitters that are released in the synaptic cleft. When an excitatory transmitter is injected in the cleft, a massive influx of positive charge occurs. Then it starts a redistribution of

charge and an extracellular current starts flowing from the cell body. The current flow causes an electric field and also a potential field inside the human head, which extends to the scalp. The electric potentials measured on the scalp are known as EEG.

The anatomy of the human head is too complex. The geometry of different parts of a head is different. For example, the structure of the skull is totally different from the brain or the scalp. Each part of the head consists of several types of tissues, which have different properties and functions. It is important to consider more realistic head geometry and as many tissue properties as possible to compute an accurate EEG.

CHAPTER 3

HUMAN HEAD MODEL AND TISSUE CONDUCTIVITY

An accurate head model requires accurate head geometry and head tissue conductivity. A spherical head model is constructed on a sphere and a realistic head model from magnetic resonance imaging (MRI). An MRI provides accurate head geometry of a particular object other than a sphere. It is difficult to measure accurate conductivity for the head model development as head tissue conductivity varies from place to place. In this Chapter, we introduce spherical and realistic head models based on conductivity modelling of head tissues. Section 3.1 describes the human head modelling. Different tissues of a head have different conductivities. The description of different conductivity values in the skull tissue and other head tissues are described in Section 3.2. Section 3.3 reports the surveyed conductivity values for this dissertation. Section 3.4 describes the homogeneous conductivity values of different head tissues. Tissue inhomogeneity and anisotropy are discussed in Sections 3.5 and 3.6, respectively. Conductivity models to approximate the conductivity values based on inhomogeneous and anisotropic tissue conductivity properties are described in Section 3.7. Finally, Section 3.8 summarizes our contribution to approximate tissue conductivity values for constructing an accurate head model.

3.1 Human Head Modelling

At the beginning of the head model development, a spherical head model is introduced. Later on, it is noticed that the spherical head model is unable to satisfy the real geometry of the human head. Therefore, the realistic head model is introduced to obtain a more accurate head model.

3.1.1 Spherical head model

The simplest head model of a human head consists of a single sphere of homogeneous conductivity. It is noticed that the skull has different conductivity than

the scalp or brain. The scalp, skull and brain conductivity ratio as 1: (1/80): 1 [Geddes and Baker 1967, Rush and Driscoll 1968]. Therefore, a single sphere head model is not sufficient to represent the human head and a three-sphered head model is introduced. In the three-sphered head model, the outer sphere is the scalp, the intermediate sphere is skull and the inner sphere is brain. Later on, the ventricle system filled by CSF is considered, and a four-sphered head model is introduced [Zhou and Oosterom 1992, de Munck and Peters 1993, Vanrumste 2000]. A five-sphered model dividing the brain into the GM and WM is seen in the de Munck and Peters article (1993) and is used in several studies [Hallez *et al* 2005a, 2005b, Bashar *et al* 2008a,b,c,d]. We consider each sphere as a layer. In the five-layered head model, the innermost layer is WM, then GM, CSF, skull and the outer most layer is the scalp. An example of a five-layered head model is shown in Figure 3.1.

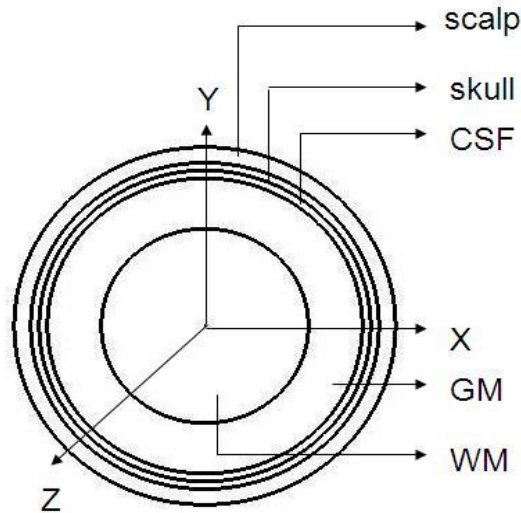


Figure 3.1: A five-layered spherical head model.

3.1.2 Realistic head model

In head model development, none of the spherical models provide a close fit to a real head as spheres are used to represent either a tissue layer or the entire head. As a result, a head model from MRI or Computed tomography (CT) scan becomes popular for a realistic head model development. A realistic head model can be developed as follows.

A realistic head model construction starts with tissue segmentation from raw MRI. Firstly, non-brain tissues are removed from the MRI using skull stripping.

Skull stripping is addressed to identify brain and nonbrain voxels in MRI. It is done for the precaution to avoid voxel identifying critic as the measured signal intensities of brain tissues, such as WM, GM and CSF can overlap with those of other head tissues, such as skin, bone, muscle and fat. It is also a three-step procedure: (a) MRI processing to smooth non-essential gradients using an anisotropic diffusion filter; (b) identifying anatomical boundaries using Marr-Hildreth edge detector; and (c) objects identified by a sequence of mathematical morphological operations. Secondly, the compensation for image nonuniformity is performed. Nonuniformity is compensated due to inhomogeneities in the magnetic fields, magnetic susceptibility variations in the scanned subject and other factors. Signal intensities measured at each voxel in an ideal MRI acquisition system will vary throughout the volume depending only on the tissues presenting at that location. However, MRI shows nonuniform tissue intensities in practice. Therefore, tissue labels cannot be reliably assigned to voxels and it requires nonuniformity compensation, which is performed by spatially slowly varying a multiplicative bias field. The variations of bias fields are estimated by fitting a parametric tissue measurement model to the histograms of small neighbourhoods. Thirdly, each voxel is classified according to its tissue type. Each voxel intensity-normalized MRI is labelled using maximum a posteriori classifier. This classifier combines the partial volume tissue measurement model with a Gibbs prior that models the spatial properties of brain tissue. More details can be found in other studies [Shattuck *et al* 2001, Shattuck and Leahy 2002, Shattuck 2005, Dogdas *et al* 2005]. Figure 3.2 shows the brain tissue segmentation from a raw MRI [Shattuck 2005]. Finally, scalp and skull are modelled by using various threshold operators [Dogdas *et al* 2005, Lee *et al* 2009]. Figure 3.3 shows different tissues segmenting from an MRI. These segmented head tissues are tessellated to be ready to assign conductivities and other forward computing steps.

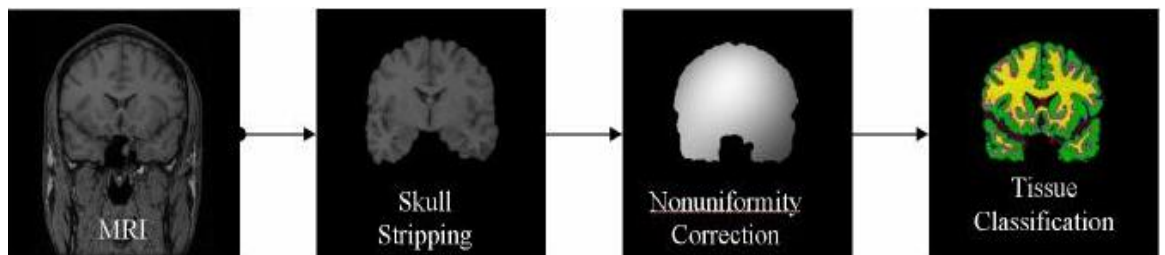


Figure 3.2: Head tissue classification from a raw MRI [BrainSuite2].

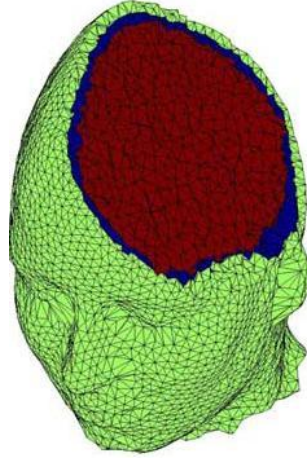


Figure 3.3: Sample FEM tetrahedral mesh with tissue classification using BrainSuite2 [Darvas *et al*, 2004].

3.2 Electric Conductivity of Head Tissues

The conductivity is a material property of a tissue. At a macroscopic level, all tissues are homogenous and isotropic in the 0-100 Hz bandwidth which is relevant for EEG. However, at a microscopic level, the discrete nature of a cell structure says that many tissues are inhomogeneous and anisotropic.

In 1993, Law (1993) studied on a human skull and reported the resistivity (the reciprocal of conductivity) and thickness over the upper surface. His measurements are listed in Table 3.1. From this Table, it is obvious that the conductivity of a skull tissue varies on location. This means that the human skull shows inhomogeneity in conductivity.

In 1996, Gabriel *et al* (1996) studied electrical properties of tissues and reported various tissue conductivities of the human body. These conductivity values are listed in Table 3.2.

Table 3.1: Skull resistivity (reciprocal of conductivity).

Locations	Resistivity (Ohm –cm)	Width (cm)	Distinguishable features
FPZ	6650	0.52	Frontal crest
F3	5620	0.62	
F1	7790	0.45	
FZ	8860	0.50	
F2	6780	0.47	Arachnoid pits
F8	9850	0.37	
T5	8360	0.44	
T3M	21400	0.47	Compact bone
C3M	7310	0.55	
CZ	3940	0.47	Suture line
C4M	6330	0.60	
C4	5670	0.62	
T4M	12700	0.46	Compact bone
T6	7800	0.49	
P3	6580	0.50	
PZ	3540	0.47	Suture line
P4	9020	0.50	
O1	3520	0.62	
OZ	1360	0.68	Suture line
O2	8230	0.50	Suture line

*Skull width and features are at different places [Law 1993]. The letter ‘F’ represents frontal, ‘P’ represents parietal, ‘T’ represents temporal, ‘O’ represents occipital lobes. ‘C’ represents central and ‘Z’ stands for midline identification purposes. The even numbered digits represent the right hemisphere and odd numbered are on the left hemisphere.

In 1997, Haueisen *et al* (1997) also studied the resistivity of different tissues in a human head. His findings are reported in Table 3.3. From these reported values, we also realize that conductivity of different parts of the head are different even in the same tissue. For example, the brain has different tissues, such as GM, WM, cerebellum, etc and the conductivity of these tissues is different.

Table 3.2: Body tissue conductivity.

Tissue	Conductivity (S/m)
Bladder	0.2
Bone -Cancellous	0.07
Bone -Marrow	0.05
Cartilage	0.18
Cerebrospinal Fluid	2.0
Cornea	0.4
Fat	0.04
Gall Bladder Bile	1.4
Heart	0.1
Lens	0.25
Lung -Deflated	0.2
Muscle	0.35
Pancreas	0.22
Small Intestine	0.5
Stomach	0.5
Testis	0.4
Tongue	0.3
Blood	0.7
Bone -Cortical	0.02
Breast	0.06
Cerebellum	0.1
Colon	0.1
Dura	0.5
White matter	0.06
Grey Matter	0.1
Kidney	0.1
Liver	0.07
Lung -Inflated	0.08
Nerve	0.03
Skin -Wet	0.1
Spleen	0.1
Tendon	0.3
Vitreous Humour	1.5
Thyroid	0.5

*Estimation of the conductivity (S/m) of body tissues below 100 Hz at body temperature Gabriel *et al* (1996).

Table 3.3 Head tissue resistivity.

Tissue	Mean resistivity (ohm-cm)	Lower and upper bound (ohm-cm)
Brain white matter	700	300 and 1050 ($\pm 50\%$)
Brain gray matter	300	150 and 450 ($\pm 50\%$)
Spinal cord and cerebellum	650	325 and 975 ($\pm 50\%$)
Cerebrospinal fluid	65	32.5 and 97.5 ($\pm 50\%$)
Hard bone	16,000	8,000 and 50,000
Soft bone	2500	1250 and 3750 ($\pm 50\%$)
Blood	160	80 and 240 ($\pm 50\%$)
Muscle	1000	200 and 1800 ($\pm 50\%$)
Fat	2500	1500 and 5000
Eye	200	100 and 400
Scalp	230	115 and 345 ($\pm 50\%$)
Soft tissue	500	250 and 750 ($\pm 50\%$)
Internal air	50,000	50,000 and 100,000

*Head tissue types, isotropic resistivity in and lower and upper bounds Haueisen *et al* (1997).

Though these studies focused on different aspects, all of them drew the conclusion that human head tissues are inhomogeneous and show considerable conductivity variations.

3.3 Tissue Conductivity used in this Dissertation

From our research, we find that different tissues have different conductivities, even the same tissue shows different conductivities based on its position or location. Different researchers implement their model using different conductivities [Haueisen *et al* 1997, 2002, Ramon *et al* 2006a,b]. To make our model consistent with other researchers' models, we use the conductivities that are reported, implemented or surveyed by other researchers. Table 3.4 shows the conductivity values surveyed for our head modelling in this dissertation [Bashar *et al* 2010d].

Table 3.4 Head tissue conductivities used in this dissertation.

Tissue layer	Tissue	Mean conductivity (S/m)	Reference
Brain	GM	0.33	Wolters (2003)
	WM	0.14	Wolters (2003)
	Blood	0.7	Gabriel <i>et al</i> (1996)
	Cerebellum	0.1	Wen (2000)
	Nerve	0.4	Gabriel <i>et al</i> (1996)
	Liquid brain lesion	1.2	Vatta <i>et al</i> (2002)
	Calcified brain	0.0044	Vatta <i>et al</i> (2002)
CSF	CSF	1.0	Gabriel (1996)
Skull	Compact bone	0.006	Haueisen <i>et al</i> 1997
	Cancellous bone	0.07	Haueisen <i>et al</i> 1997
	Dura matter	0.5	Gabriel <i>et al</i> (1996)
	Suture lines	0.04	Law (1993)
	Air in sinus cavity	6×10^{-5}	Awada <i>et al</i> (1996)
Scalp	Scalp	0.33	Wolters (2003)
	Wet skin	0.1	Gabriel <i>et al</i> (1996)
	Fat	0.04	Awada <i>et al</i> (1998)

3.4 Homogeneous Tissue Conductivity

Facing up to the above facts and challenges, the estimation of tissue conductivity becomes a tough problem. The homogeneous and isotropic conductivities for different head models are listed in Table 3.5 [Bashar *et al* 2008a,b,c,d, 2010a,b,c,d,e]. In this dissertation, we use homogeneous and isotropic conductivities as ‘homogeneous conductivity’ everywhere unless otherwise specified.

Table 3.5 Homogeneous and isotropic conductivities used in this dissertation.

Head model	Brain (S/m)		CSF (S/m)	Skull (S/m)	Scalp (S/m)
4-layer	0.33		1.0	0.0042	0.33
5-layer	GM	WM	1.0	0.0042	0.33
	0.33	0.14			
Realistic	0.33		1.0	0.0042	0.33

3.5 Methods to Determine Inhomogeneous Tissue Conductivity

In Section 3.2, we have identified the inhomogeneous property of different tissue conductivity and have reported conductivity values for different head tissues. This

Section describes different methods of inhomogeneous tissue conductivity approximations.

3.5.1 Pseudo conductivity based inhomogeneous conductivity generation

First, we create a vector whose entries are chosen from Gaussian distribution with mean zero and variance one. Afterwards, the mean and variance are transferred to mean conductivity and the given variance with the following procedure. Let \mathbf{X} be a vector with mean μ and variance σ^2 , and a new vector $\hat{\mathbf{X}}$ can be defined as [Wen 2000]:

$$\hat{\mathbf{X}} = \kappa_1 \mathbf{X} + \kappa_2 \quad \dots\dots\dots (3.1)$$

where κ_1 and κ_2 are parameters. The mean $\hat{\mu}$ and variance $\hat{\sigma}^2$ of the new vector $\hat{\mathbf{X}}$ are given by

$$\hat{\mu} = \kappa_1 \mu + \kappa_2 \quad \dots\dots\dots (3.2)$$

$$\hat{\sigma}^2 = \kappa_1 \sigma^2 \quad \dots\dots\dots (3.3)$$

Given the mean $\hat{\mu}$ and variance $\hat{\sigma}^2$, κ_1 and κ_2 can be determined, and finally the conductivity ranges can be decided.

3.5.2 The brain tissue inhomogeneity

In the case of the brain, the majority of the brain is WM and GM. The brain has a homogeneous mean conductivity (μ) 0.33 S/m [Geddes and Baker 1967]. We assume the conductivity of WM as 0.14 S/m [Wolters 2003] and GM as 0.33 S/m [Wolters 2003]; the conductivity of other tissues are as 0.1 S/m for cerebellum [Gabriel *et al* 1996], 0.7 S/m for blood [Haueisen *et al* 1997] and 0.35 S/m for nerve [Awada *et al* 1998]. We also assume that each of WM and GM accounts for 35% of the brain, cerebellum contains 10% and the blood and nerve contain the remaining 10%. Based on these assumptions and conductivity values, we can determine the variance (σ^2) as:

$$\sigma^2 = E[(x - \mu)^2] = \sum_{i=1}^{\infty} (x_i - \mu)^2 f(x_i) \quad \dots\dots\dots (3.4)$$

$$\begin{aligned} &= 0.35 * (0.33 - 0.33)^2 + 0.35 * (0.14 - 0.33)^2 + 0.1 * (0.1 - 0.33)^2 \\ &+ 0.03 * (0.7 - 0.33)^2 + 0.03 * (0.35 - 0.33)^2 \\ &= 0.0220 \end{aligned}$$

Therefore, $\sigma = 0.1485 \approx 15\%$, that is the standard deviation (SD), 15% of the mean conductivity. Substituting the values of μ and σ^2 into Equations (3.1) to (3.3) we generate inhomogeneous conductivity for the brain.

3.5.3 The skull tissue inhomogeneity

In the generation of the skull tissue inhomogeneous conductivity, we assume different conductivity values at different parts of the skull. Law (1993) measured the skull conductivity at 20 different places or regions shown in Table 3.1. We assume that these regions are same in size (i.e. each region is 5% of the entire the skull). We also assume that the mean skull conductivity (μ) is 0.0180 S/m (from Table 3.1). We have converted resistivity in ohm-cm to conductivity S/m by $100/\text{resistivity}$. Therefore, using Equation (3.4) we obtain

$$\begin{aligned} \sigma^2 &= E[(x - \mu)^2] = \sum_{i=1}^{\infty} (x_i - \mu)^2 f(x_i) \\ &= 0.05 * (100 / 6650 - 0.0180)^2 + 0.05 * (100 / 5260 - 0.0180)^2 + \\ &..... + +0.05 * (100 / 8230 - 0.0180)^2 \\ &= 0.00019 \end{aligned}$$

Therefore, $\sigma = 0.0141 \approx 1\%$, that is the SD, 1% of the mean conductivity. Substituting the values of μ and σ^2 into Equations (3.1) to (3.3), we generate inhomogeneous conductivity for the skull.

3.5.4 The scalp tissue inhomogeneity

The scalp consists of five tissue layers, such as the skin, fat and muscle. We find only the conductivity values of the skin, fat and muscle. We assume that these tissues contain the same region of the scalp or the same width of scalp tissue layer. The mean conductivity of the scalp (μ) is 0.33 S/m [Gedds and Baker 1967, Baillet *et al* 2001, Hallez *et al* 2009, Gullmar *et al* 2010]. Therefore, using Equations (3.1) to (3.3) and conductivity values reported in Table 3.3, we obtain the variance of the scalp tissue layer as $\sigma = 0.22210$, which also generates a 22% standard deviation.

3.6 Methods to Determine Anisotropic Tissue Conductivity

It is widely known that the WM and the skull are anisotropic because of their anatomical structure.

3.6.1 White matter anisotropy

Some important structures in the white matter consist of nerve bundles which are aligned in parallel to each other [Hallez 2008a, b]. The corpus callosum and anterior commissure connect the left and right hemispheres of the brain. The structure of the corpus callosum and anterior commissure consists of many parallel nerve bundles. Therefore, it becomes highly anisotropic. The internal capsule is another example of such a structure, which connects the nerve fibers coming from the centre of the brain to regions in the cortical gray matter. The nerve bundles consist of nerve fibres or axons (in Figure 3.4). Water and ionized particles can move more easily along the nerve bundle than perpendicular to the nerve bundle. The direction of a nerve bundle can be estimated by a diffusion tensor magnetic resonance imaging (DT-MRI) [Basser 1994]. It is assumed that the conductivity is the highest in the direction in which the water diffuses most easily [Tuch 2001]. Different studies [Hallez *et al* 2005a, Haueisen *et al* 2002] have shown that anisotropic conducting compartments should be incorporated in volume conductor models of the head whenever possible.

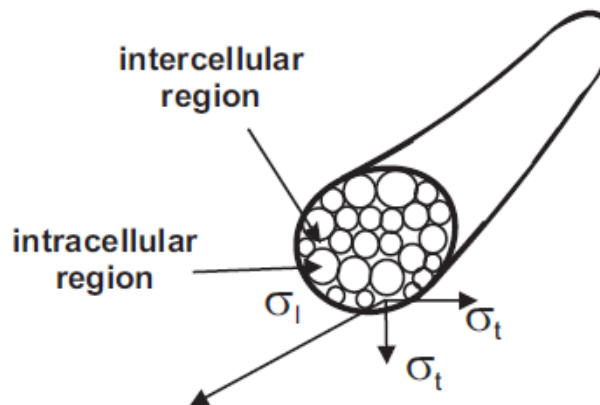


Figure 3.4 Anisotropic conductivities of white matter. σ_l represents longitudinal and σ_t represents transversal conductivity [Hallez *et al* 2005a].

When a tissue is assumed to be anisotropic, conductivity is defined either in longitudinal (parallel) or in transversal (perpendicular) direction [Sadleir and

Argibay, 2007]. The longitudinal conductivity is modelled as ten times higher than the transversal conductivity [Marin *et al* 1998, Wolters 2003, Hallez *et al* 2005a]. It can be expressed as:

$$\sigma_{long} = \xi \cdot \sigma_{trans} \dots\dots\dots (3.5)$$

where σ_{long} is the longitudinal, σ_{trans} is the transversal conductivities and ξ is the conductivity or anisotropy ratio between longitudinal and transversal. To construct an anisotropic model, it is important to ensure that the total amount of conductivity between isotropic and anisotropic medium is the same. In isotropic conductivity, the conductivity in each direction is the same and can be represented by a sphere. An anisotropic conductivity is represented by conductivity tensor which is usually derived from DT-MRI. In anisotropic conductivity, the conductivity in each direction is not same and represented by an ellipsoid. Therefore, the volume of sphere derived from the isotropic conductivity and the volume of the ellipsoid derived from the anisotropic conductivity tensor would be same. This is represented by Volume constraint [Wolters 2003, Gullmar *et al* 2006, Wolters *et al* 2006, Li *et al* 2007, Hallez *et al* 2008b, Bashar *et al* 2008b, Lee *et al* 2009] which is proposed by Wolters (2003). Moreover, in a fluid system with two types of non-uniformly distributed molecules, the molecule concentrations change with time until both concentrations have the same value throughout the system. As a result, it is essential to restrict these longitudinal and transversal conductivities. The conductivity of two directions would be same of the square of the isotropic conductivity which is represented by Wang's constraint [Wang *et al* 2001, Wolters 2003, Wolters *et al* 2006, Bashar *et al* 2008b, 2010a,c] proposed by Wang *et al* (2001).

3.6.1.1 Volume constraint

Tissue anisotropic conductivity is commonly derived from a DT-MRI. Diffusion is the transportation of water molecules, while conductivity is the transportation of charged particles. DT-MRI does not measure conductivity tensor directly but rather infers from the diffusion tensors which describe the movement of both water molecules and electrically charged particles (ions). To implement conductivity tensor, we assume that the same structural features that result in anisotropic mobility of water molecules also result in anisotropic conductivity. This assumption can be expressed as the eigen vectors of the conductivity tensor, similar to those from water

diffusion tensor. However, there are some problems for the conductivity tensor reconstruction process as addressed by Zhao *et al* (2005). One problem is the volume of tissues which varies due to several factors, such as age, diseases, environmental factors, and personal constitutions [Muravchik and Nehorai 2001, Haueisen *et al* 1997]. To overcome this obstacle, Wolters (2003) proposed Volume constraint (VC), which restricts the volume of the isotropic conducting sphere to the volume of the anisotropic conducting ellipsoid as constants. The VC is defined as [Wolters 2003, Hallez *et al* 2009, Gullmar *et al* 2010]:

$$\frac{4}{3}\pi\sigma_{long} \cdot (\sigma_{trans})^2 = \frac{4}{3}\pi\sigma_{iso}^3 \dots\dots\dots (3.6)$$

where σ_{iso} is the isotropic and homogeneous WM conductivity. Using Equations (3.5) and (3.6), we solve σ_{long} and σ_{trans} . Solving these Equations, we compute Volume constrained longitudinal (σ_{long}^{Vol}) and transversal (σ_{trans}^{Vol}) conductivities, and obtain $\sigma_{long}^{Vol} = 0.65$ S/m and $\sigma_{trans}^{Vol} = 0.065$ S/m with $\sigma_{iso} = 0.14$ S/m. Figure 3.5 shows the relationship of the eigen values (λ_i) of diffusion to the conductivity values (σ_i) for the VC.

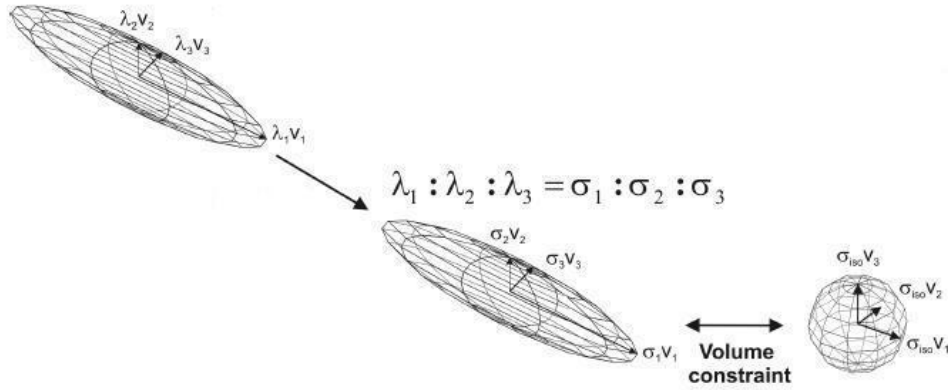


Figure 3.5: The linear relationship between the eigen values of the diffusion and conductivity ellipsoid. The resulting ellipsoid is identical to the diffusion ellipsoid up to an unknown scaling factor, which can be derived using the volume constraint with the isotropic conductivity sphere of white matter [Hallez 2008b].

3.6.1.2 Wang's constraint

Another problem for the conductivity tensor reconstruction process is the movement of water molecules (direction). Water molecules usually move in a direction towards the high conductivity. In white matter the diffusion of water molecules in the direction of perpendicular to fiber, is slower than parallel. To stay constant for these molecules Wang *et al* (2001) proposed a constraint method. Wang's constraint (WC) is defined as, the product of longitudinal and transverse conductivities stay constant and is equal to the square of the isotropic conductivity. It is represented as [Wang *et al* 2001, Wolters 2003, Wolters *et al* 2006, Bashar *et al* 2008a, 2010a, 2010c]:

$$\sigma_{long} \cdot \sigma_{trans} = \sigma_{iso}^2 \quad \dots\dots\dots (3.7)$$

Figure 3.6 shows relationship between the eigen values of diffusion tensor and conductivity values for the Wang's constraint.

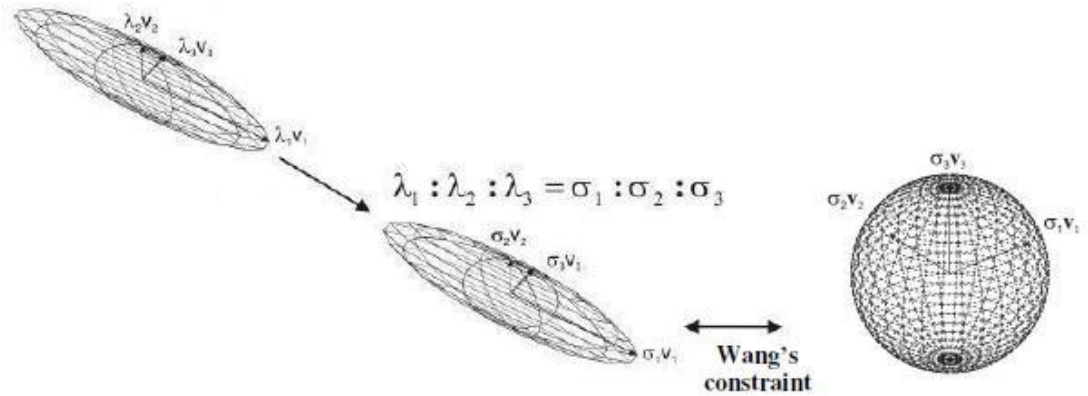


Figure 3.6 The linear relationship between the eigen values of diffusion tensor and conductivity values for the Wang's constraint.

3.6.2 Skull anisotropy

The skull is a hard bone layer between the brain and the outside to protect the brain from outside injury. The hard structure acts as a low conductive medium due to the high resistance of the hard bone. It has a layered structure (Figure 3.7), which consists of 3 layers: a spongiform or soft bone layer between two hard bone layers. Blood, Water, and also ionized particles can move easily through the spongiform layer, but not through the hard layers [Geddes and Baker 1967, Wolters 2003].

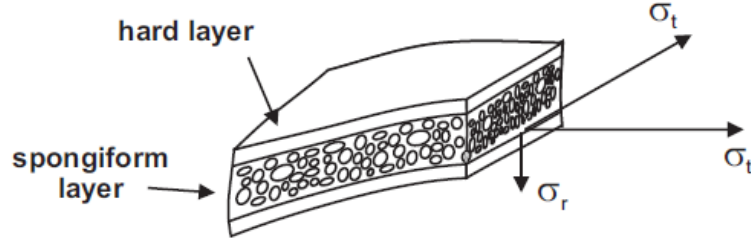


Figure 3.7: The anisotropic skull conductivity. σ_t represents tangential and σ_r represents radial conductivity [Hallez *et al* 2005a].

At the skull the conductivity tangential to the surface is 10 times the conductivity perpendicular to the surface [Anwandwer *et al* 2002, Wolters 2003, Nicolas *et al* 2004]. To model the skull anisotropy we model the tangential conductivity as ten times higher than the radial conductivity

$$\sigma_{tgl} = \xi \cdot \sigma_{rdl} \dots\dots\dots (3.8)$$

where σ_{tgl} and σ_{rdl} present tangential and radial conductivities [Sadleir and Argibay 2007], respectively, and $\xi = 10$.

Similar to the WM, the VC for the skull is defined as [Wolters 2003, Hallez *et al* 2008a,b]:

$$\frac{4}{3} \pi \sigma_{rdl} \cdot (\sigma_{tgl})^2 = \frac{4}{3} \pi \sigma_{Skull}^3 \dots\dots\dots (3.9)$$

where σ_{Skull} is the skull isotropic conductivity with $\sigma_{Skull} = 0.0042$ S/m. Using Equations (3.8) and (3.9), we solve σ_{rdl} and σ_{tgl} . Solving these Equations, we compute Volume constrained radial (σ_{rdl}^{Vol}) and tangential (σ_{tgl}^{Vol}) conductivities, and obtain $\sigma_{rdl}^{Vol} = 0.0009$ S/m and $\sigma_{tgl}^{Vol} = 0.009$ S/m, respectively. Similarly, the WC for the skull is defined as [Wang *et al* 2001, Wolters 2003, Wolters *et al* 2006, Bashar *et al* 2008a]:

$$\sigma_{rdl} \cdot \sigma_{tgl} = \sigma_{Skull}^2 \dots\dots\dots (3.10)$$

Using Equations (3.8) and (3.10), we solve σ_{rdl} and σ_{tgl} for WC. Solving these Equations, we compute Wang's constrained radial (σ_{rdl}^{Wang}) and tangential (σ_{tgl}^{Wang}) conductivities, and obtain $\sigma_{rdl}^{Wang} = 0.0001$ S/m and $\sigma_{tgl}^{Wang} = 0.001$ S/m, respectively.

From the above discussion, it is obvious that the WM and the skull are anisotropic in conductivity. We consider the longitudinal conductivity of the WM

and tangential conductivity of the skull as parallel conductivity. On the other hand, the transversal conductivity of the WM and the radial conductivity of the skull are considered as perpendicular conductivity throughout this dissertation.

3.7 Inhomogeneous and Anisotropic Tissue Conductivity Approximation

From Equation (3.5) we can have the anisotropy ratio ξ as:

$$\xi = \frac{\sigma_{long}}{\sigma_{trans}} \dots\dots\dots (3.11)$$

Several studies [Wolters 2003, Wolters *et al* 2006, Gullmar *et al* 2006] assume ξ as a constant with the value of 10 to implement anisotropic conductivity for both the WM and skull. In reality, ξ varies from 1 to 10 [Wolters 2003, Wolters *et al* 2006, Gullmar *et al* 2006, Li *et al* 2007] which can be expressed as [Bashar *et al* 2008b]:

$$\sigma_{long} : \sigma_{trans} = \xi : 1 \text{ where } \xi = 1 \text{ to } 10 \dots\dots\dots (3.12)$$

As the value of ξ varies, the conductivity is also changed. Figure 3.8 shows different conductivity values due to changing ξ for the WM and the skull tissue layers using Volume and Wang's constraints.

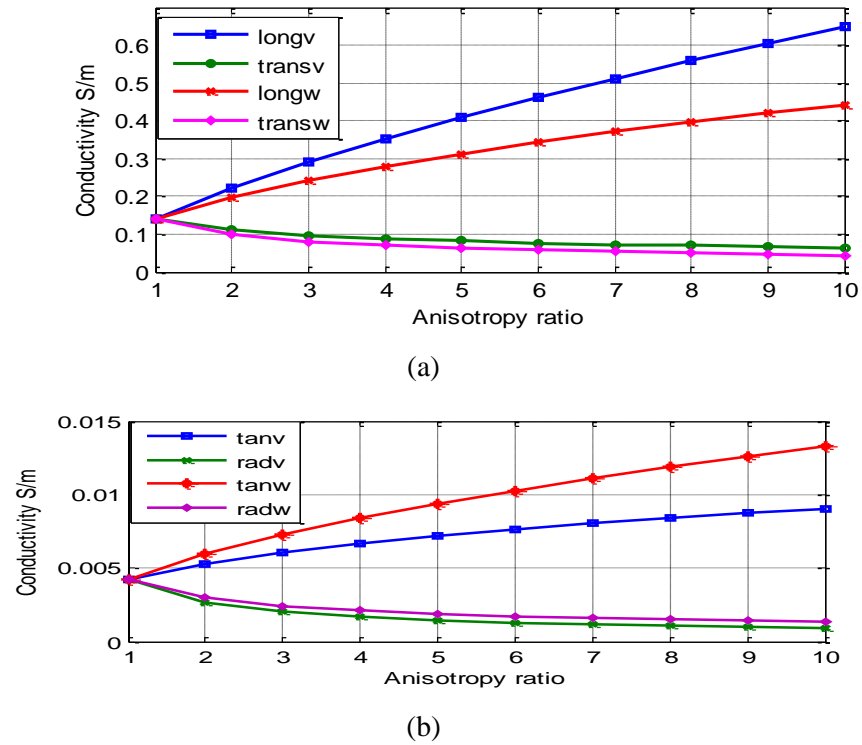


Figure 3.8: Different conductivity values of the skull for different anisotropy ratios:

(a) WM tissues and (b) skull tissues.

To determine the inhomogeneous and anisotropic conductivities, we propose different conductivity models. These models are described in the subsequent sections.

3.7.1 Conductivity ratio approximation model

In the conductivity ratio approximation (CRA) model, firstly, we generate a vector σ_{ξ} with all possible anisotropy ratios from 1 to 10. Secondly, we select the anisotropy ratio ξ using random selection where $\xi \in \sigma_{\xi}$. Based on this anisotropy ratio ξ we determine the longitudinal and transverse inhomogeneous conductivities by means of Equations (3.5) to (3.7) for the WM. Using Equations (3.8) to (3.10), we determine the tangential and radial conductivities for the skull. However, we only select those whose values satisfy $\sigma_{long} \geq \sigma_{trans}$ or $\sigma_{tgl} \geq \sigma_{rdl}$. For example, if ξ is 2, then the longitudinal and transverse conductivities are 0.222 S/m and 0.111 S/m, respectively.

3.7.2 Statistical conductivity approximation model

Shimony *et al* (1999) measured diffusion anisotropy in 12 regions of interest in human white and gray matters. They showed that the shape of diffusion ellipsoids are strongly prolate (“cigar-shaped”), whereas they found gray matter as closely isotropic. Gullmar *et al* (2006) used prolate ellipsoids to represent conductivity tensor and found that Rayleigh distribution fits the mean and variance of their experimental results which produces a prolate shape. Hallez *et al* (2008a, 2008b) mentioned that an ellipsoid can present anisotropy tensor. Therefore, we assume that Rayleigh distribution can generate random numbers that fit the inhomogeneous anisotropic conductivities and define as statistical conductivity approximation (SCA) model. The probability density function of Rayleigh distribution is defined as [Rayleigh distribution]

$$f(x, m) = \frac{x}{m^2} e^{\left(\frac{-x^2}{2m^2}\right)} ; \quad \mathbf{x} \in [0, \infty) \quad \dots\dots\dots (3.13)$$

where \mathbf{x} is a vector of random variables and m is the maximum likelihood estimator (MLE) of Rayleigh distribution.

The mean, variance and cumulative density function (cdf) of Rayleigh distribution are as:

$$mean = m\sqrt{\frac{\pi}{2}} \dots\dots\dots (3.14)$$

$$var = \frac{4-\pi}{2}m^2 \dots\dots\dots (3.15)$$

$$cdf = 1 - e^{\frac{-x^2}{2m^2}} \dots\dots\dots (3.16)$$

We select the inverse transform method for random number generation [Rodney *et al* 1988]. The following algorithm generates the random numbers which meet Rayleigh distribution. Firstly, we determine \mathbf{X} = random number generated from uniform distribution. We set the mean or homogeneous conductivities according to Table 3.5. Then, we determine m based on the Equation (3.14). Finally, we determine the random numbers according to Rayleigh distribution by applying the *cdf* defined in the Equation (3.16). We treat these random numbers as longitudinal inhomogeneous conductivities. Based on these conductivities, we determine the transverse inhomogeneous conductivities by using either Volume or Wang's constraint where $\sigma_{long} \geq \sigma_{trans}$. Using the same algorithm, we can determine the conductivity values for the skull tissues.

3.7.3 Fractional anisotropy based inhomogeneous and anisotropic conductivities model

Fractional anisotropy (FA) is a technique to measure the extent of the anisotropy property for each voxel (element). Let us suppose that λ_1 , λ_2 , and λ_3 ($\lambda_1 \geq \lambda_2 \geq \lambda_3$) are the three eigenvalues of diffusion tensor matrix and λ is the average eigen value. Then FA is defined as [Li *et al* 2006]:

$$FA = \frac{\sqrt{3}}{\sqrt{2}} \frac{\sqrt{(\lambda_1 - \lambda)^2 + (\lambda_2 - \lambda)^2 + (\lambda_3 - \lambda)^2}}{\sqrt{\lambda_1^2 + \lambda_2^2 + \lambda_3^2}} \dots\dots\dots (3.17)$$

The FA is in the range from 0 to 1 [Li *et al* 2006]. A fully anisotropic tissue has a factor FA=1, and an isotropic tissue has a factor FA=0. Figure 3.9 shows FA for the WM.

To implement inhomogeneous anisotropy, Li *et al* (2007) proposed threshold controlled FA using step and linear functions. For the homogeneous anisotropic model, all elements share the same conductivity ratio (R_{lt}) between longitudinal and transversal conductivities. However, R_{lt} varies for inhomogeneous anisotropy. R_{lt} reflects the extent of the anisotropy property as the FA does, so we set R_{lt} as a variable of FA. By implementing the Equation (3.17) we establish the relation between FA and R_{lt} as shown in Figure 3.10. Though the values of FA lie between 0 and 1 [Li *et al* 2006], however, we find the values of FA ranging from 0 to 0.9. Considering Figure 3.10 and based on literature [Li *et al* 2007], we define the multi-steps function stated in Equation (3.18) as [Bashar *et al* 2008d]:

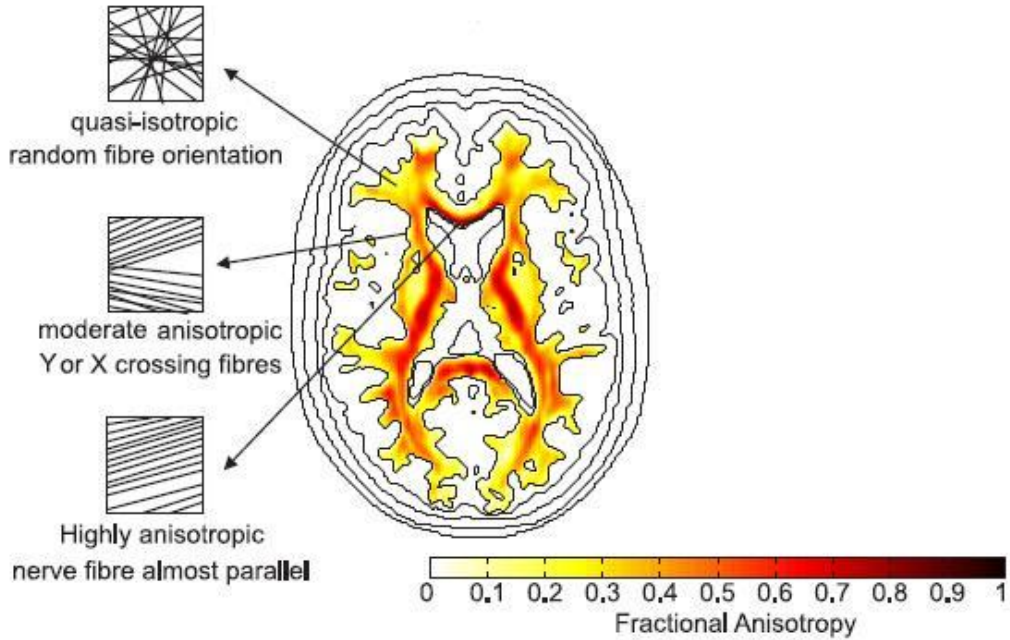


Figure 3.9: Fractional anisotropy for WM [Hallez *et al* 2008b].

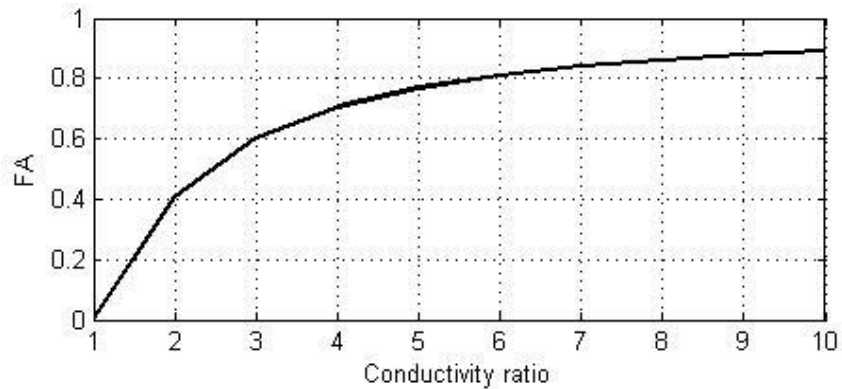


Figure 3.10: Conductivity ratio Vs fractional anisotropy (FA).

$$R_{lt} = \begin{cases} 10, & FA > 0.8 \\ 6, & FA > 0.7 \\ 4, & FA > 0.4 \\ 2, & otherwise \end{cases} \dots\dots\dots (3.18)$$

Using R_{lt} , we generate longitudinal and transversal inhomogeneous conductivities for Volume and Wang's constrained WM and skull tissue layers.

3.7.4 The Monte Carlo method based inhomogeneous and anisotropic conductivities model

To construct different radial and tangential conductivities shown in Figure 3.8, we implement the Monte Carlo Method [Wittwer 2004] using the following steps: (A) generate a set of conductivity values σ_i using

$$\sigma_i = \mu + randn() * SD$$

where μ and SD are the mean and standard deviation of restricted conductivities, respectively. $randn()$ generates a random number from Normal distribution with $\mu = 0$ and $SD = 1$, (B) determine the conductivity values, (C) Prepare histogram to visualise the conductivity values and finally, (D) Create a conductivity model $y = f(\mathbf{x}, \boldsymbol{\sigma})$, where \mathbf{x} is head elements and $\boldsymbol{\sigma}$ is the values of conductivity for those elements.

In Step 2, we use $\mu = \sum_{\xi=1}^{10} \sigma_{cond}$, in which σ_{cond} is restricted conductivity,

and $SD = \sqrt{\frac{1}{P} \sum_{\xi=1}^P (\sigma_{cond(\xi)} - \mu)^2}$, in which $P=10$. For instance, Volume constrained radial conductivity of the skull ranges between 0.0009 S/m and 0.0042 S/m shown in Figure 3.8.

For the illustration of this conductivity model, we provide an example of the approximation of inhomogeneous anisotropic skull conductivities. The generated random numbers for the skull are shown in Figure 3.11. We have generated these random numbers for 15 executions and selected the best execution, which best satisfies the conductivity ranges. As generated random numbers are out of range for certain anisotropic conductivity values as shown in Figure 3.8, we implement

conductivity frontier constraint to select the conductivity values from these generated random numbers within the given range. For instance, the radial conductivity values of Volume constrained skull lie in the range of 0.0009 S/m to 0.0042 S/m. However, the generated random numbers are between -0.0028 and 0.0060, therefore we implement frontier constraint to select the conductivity values between the given ranges as $\sigma_{rdl}^{Vol} = random[0.0009 \ 0.0042]$ (shown between two vertical lines in Figure 3.11). Applying this constraint, we ensure that our computed conductivity values satisfy Volume constrained conductivities, and it is also ensured that heterogeneous anisotropic conductivity remains mean homogeneous isotropic conductivity constant. For example, if radial conductivity of a skull element is 0.015 S/m, its tangential conductivity is 0.0317 S/m, which is in agreement with Equation (3.9). The mean value of radial conductivity is 0.098 S/m and 0.035 S/m is for tangential conductivity. As a result, it produces mean conductivity, which is close to the homogeneous isotropic conductivity.

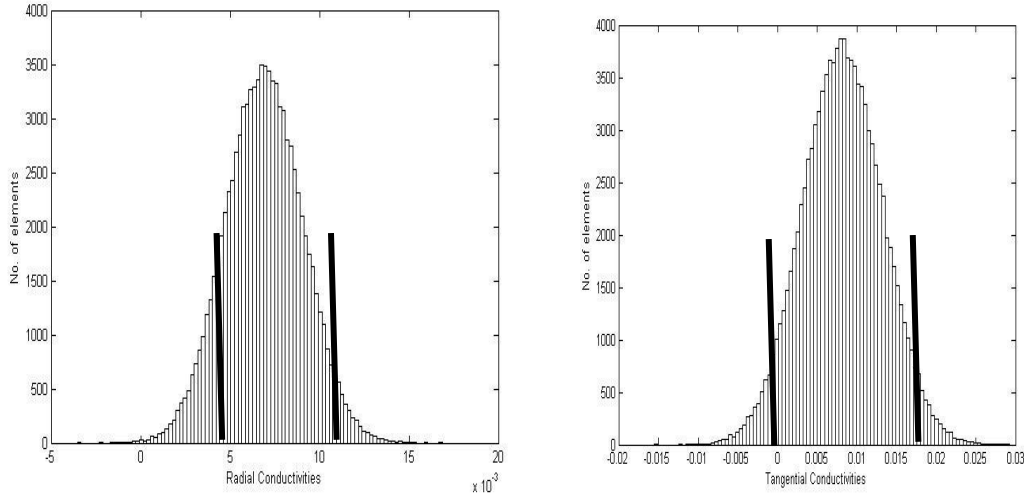


Figure 3.11: Volume constrained conductivities produced by Monte Carlo method. Conductivity analysis using histogram: (a) radial conductivities and (b) tangential conductivities.

In a similar way, we implement the inhomogeneous and anisotropic conductivities for both the WM and skull layers. To construct a full inhomogeneous and anisotropic conductivities profile of a human head, we implement the WM and skull inhomogeneous and anisotropic properties with the scalp inhomogeneity in addition.

3.8 Conclusion and Contribution

In this Chapter, we introduce head tissue conductivity in human head modelling. Firstly, we investigate the conductivity (homogeneous) values of different head tissues and find that the same tissues at different places have different conductivity values. This conductivity property makes a human head an inhomogeneous medium. To approximate inhomogeneous tissue conductivity, we use pseudo conductivity [Wen 2000] based on Normal distribution. Secondly, we introduce the conductivity anisotropy of the WM and skull tissues. Anisotropic conductivity is direction based and parallel conductivity is higher than the perpendicular conductivity due to the cell or nerve structure and organization. Some studies implement tissue anisotropy considering a fixed anisotropy ratio [Wolters 2003, Wolters *et al* 2006, Gullmar *et al* 2006, Hallez *et al* 2008a, Gullmar *et al* 2010]. However, the anisotropy ratio is variable, such as in the corpus callosum, anterior commissure and internal capsule in WM. We also find that the FA is variable [Hallez 2008b] which causes a variable anisotropy ratio [Li *et al* 2007, Bashar *et al* 2008d]. In order to implement a variable anisotropy ratio, we propose conductivity ratio approximation [Bashar *et al* 2008b], statistical conductivity approximation [Bashar *et al* 2008b], FA based conductivity approximation [Bashar *et al* 2008d] and Monte Carlo method based conductivity approximation models. To make the conductivity consistent between the homogeneous and anisotropic tissues, we use Volume and Wang's constraints [Wolters 2003, Wang *et al* 2001]. Finally, we combine the concepts of tissue inhomogeneity and anisotropy properties to approximate a full accounting of the conductivity values of the entire head tissues.

CHAPTER 4

THE FORWARD PROBLEM AND ITS SOLUTION USING FEM

In this Chapter, we derive the differential equations together with the boundary conditions to describe the EEG forward problem. The EEG forward problem describes the relationship between the primary currents in the brain, which are directly driven by the neuronal process and the measured potentials at the head surface. We model the head as a volume conductor to solve the EEG forward problem.

There are many methods for solving the forward problem. Among these methods, de Munck and Peters (1993) introduced an analytic solution for an anisotropic spherical head model. Most other researchers are interested in the numerical approximation techniques, such as boundary element method (BEM), finite element method (FEM) and finite difference method (FDM), etc. Among these numerical methods, we prefer FEM because it is able to treat realistic, heterogeneous and anisotropic electric properties to implement an accurate forward computation [Marin *et al* 1998, Wolters 2003, Wolters *et al* 2006]. In this Chapter, firstly we present the physical model based on Maxwell's equations, the mathematical formulation for the primary current sources, and the description of the EEG forward problem. Secondly, we present a series expansion formula for the potential distribution of a dipolar current source in a multi-layered spherical head model. Thirdly, we present the EEG forward problem. Finally, we show the solution of the EEG forward problem using the FEM.

4.1 Maxwell's and Poisson's Equations

Activation of individual neurons inside the brain gives rise to the flow of electric current in the brain. The electric current then passes to the CSF, skull bones, muscles, subcutaneous fat and the scalp. The flow of current establishes an electric potential field over the head and this potential can be measured using the head surface mounted electrodes. The rules covering this succession of events are known

as Maxwell's equations. The Maxwell equations are the electromagnetic connections which connect time-varying electric and magnetic fields so that when there are bioelectric fields there are always biomagnetic fields, and vice versa [Malmivuo and Plonsey 1995]. These equations dictate the behaviour of electromagnetic fields in any type of medium. These equations are as follows [Nunez and Srinivasan 2006].

The first kind of spatial rate of change (*divergence*) of electric field (**D**) is proportional to charge density (ρ) and defined as:

$$\nabla \cdot \mathbf{D} = \rho \quad (4.1)$$

The second kind of spatial rate of change (*curl*) of electric field (**E**) is proportional to time rate of change of magnetic field **B** and defined as:

$$\nabla \times \mathbf{E} = -\frac{\partial \mathbf{B}}{\partial t} \quad (4.2)$$

The first kind of spatial rate of change of **B** is zero and defined as:

$$\nabla \cdot \mathbf{B} = 0 \quad (4.3)$$

The second kind of spatial rate of change of magnetic field (**H**) is proportional to the current density (**J**) plus the time rate of **D** and defined as:

$$\nabla \times \mathbf{H} = \mathbf{J} + \frac{\partial \mathbf{D}}{\partial t} \quad (4.4)$$

As biological tissue can be treated as an electrolyte, these equations for a liner homogeneous material can be expressed as:

$$\mathbf{D} = \epsilon \mathbf{E} \quad (4.5)$$

$$\mathbf{B} = \mu \mathbf{H} \quad (4.6)$$

where ϵ is electric permeability and μ is magnetic permeability. We assume that μ is constant over the whole volume and equal to the permeability of vacuum [Wolters 2003]. Therefore, the Maxwell equations are reduced to

$$\nabla \cdot \mathbf{D} = \rho \quad (4.7)$$

$$\nabla \times \mathbf{E} = 0 \quad (4.8)$$

$$\nabla \cdot \mathbf{B} = 0 \quad (4.9)$$

$$\nabla \times \mathbf{B} = \mu \mathbf{J} \quad (4.10)$$

and the electric field can be expressed as a negative gradient of a scalar potential (Φ),

$$\mathbf{E} = -\nabla \Phi \quad (4.11)$$

The current density is generally divided into two parts, the primary current **J_p** and the return current **J_r**. The **J_r** can be represented according to the Ohm Law as

$$\mathbf{J}_r = \sigma \mathbf{E} \dots\dots\dots (4.12)$$

where σ is the conductivity. Then, the current density becomes

$$\mathbf{J} = \mathbf{J}_p + \mathbf{J}_r = \mathbf{J}_p + \sigma \mathbf{E} \dots\dots\dots (4.13)$$

The \mathbf{J} is a three dimensional position-dependent vector field, where the direction of the vector indicates the direction of motion of the charges. At one moment in time, an active electric source triggers all the fields. Hence, no time delay effects are introduced. All fields and currents behave as if they were stationary at each instance in time and these conditions are known as Quasi-static conditions. However, they are not static because the neural activity changes with time. These changes are slow compared to the propagation effects. These quasi-static conditions result in the decoupling of the electric and magnetic components, and allow us to view the electric components only. In equation form, it can be defined as:

$$\nabla \cdot \mathbf{J} = 0 \dots\dots\dots (4.14)$$

Substituting Equation (4.13) to (4.14) we get,

$$\begin{aligned} \nabla \cdot (\mathbf{J}_p + \mathbf{J}_r) &= 0 \\ \nabla \cdot \mathbf{J}_r &= -\nabla \cdot \mathbf{J}_p \dots\dots\dots (4.15) \end{aligned}$$

Substituting Equation (4.12) to (4.15) we get,

$$\nabla \cdot \sigma \mathbf{E} = -\nabla \cdot \mathbf{J}_p \dots\dots\dots (4.16)$$

Substituting Equation (4.11) to (4.16) we get,

$$\nabla \cdot \sigma (-\nabla \Phi) = -\nabla \cdot \mathbf{J}_p \dots\dots\dots (4.17)$$

$$\nabla \cdot (\sigma \nabla \Phi) = \nabla \cdot \mathbf{J}_p \dots\dots\dots (4.18)$$

It is to be noted that $-\nabla \cdot \mathbf{J}_p$ is merely the source density inside the domain. If we denote $-\nabla \cdot \mathbf{J}_p$ as the current per unit volume \mathbf{I}_v , then we obtain at Poisson's equation- a mathematical description of a typical bioelectric volume conductor problem

$$\nabla \cdot (\sigma \nabla \Phi) = -\mathbf{I}_v \dots\dots\dots (4.19)$$

Here, \mathbf{I}_v is defined within the solution domain Ω . For the special case of a region of the head containing no current sources or sinks, then the Equation (4.19) simplifies to the Laplace equation as:

$$\nabla \cdot (\sigma \nabla \Phi) = 0 \dots\dots\dots (4.20)$$

Either the Poisson or the Laplace equation is used to formulate the most bioelectric volume conductor models. Then, the fundamental problem becomes

finding a technique that will accurately represent the domain, and will also allow the solutions of Equation (4.19) or (4.20). The associated boundary conditions depend on what type of problem is going to be solved.

4.2 Boundary Conditions

The boundary condition expresses the way to represent the potential or current that passes from one tissue layer or compartment to its neighbouring tissue layer or compartment. There are two boundary conditions at the interface between two tissue layers. Figure 4.1 describes the boundary condition in a sphere.

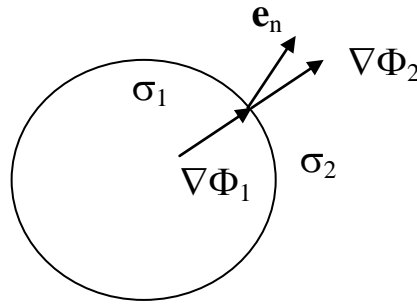


Figure 4.1: Boundary between two compartments. σ_1 and σ_2 are conductivities of tissue layer 1 and 2, respectively, and the normal vector \mathbf{e}_n is the interface.

In the first condition, all current leaving a tissue layer with conductivity σ_1 through the interface must enter the other tissue layer with conductivity σ_2 . This process can be stated as [Vanrumste 2002]:

$$\mathbf{J}_1 \cdot \mathbf{e}_n = \mathbf{J}_2 \cdot \mathbf{e}_n \dots\dots\dots (4.21)$$

where \mathbf{e}_n is the normal component on the interface. Equation (4.21) can be stated using Equations (4.11) and (4.12) as

$$(\sigma_1 \nabla \Phi_1) \cdot \mathbf{e}_n = (\sigma_2 \nabla \Phi_2) \cdot \mathbf{e}_n \dots\dots\dots (4.22)$$

However, no current would be passed from the outer tissue layer of the head to the air. Therefore the current density at the surface of the head is:

$$\mathbf{J}_1 \cdot \mathbf{e}_n = 0 \dots\dots\dots (4.23)$$

$$(\sigma_1 \nabla \Phi_1) \cdot \mathbf{e}_n = 0 \dots\dots\dots (4.24)$$

Equation (4.23) is known as Neumann boundary condition and Equation (4.24) is known as the homogeneous Neumann boundary condition [Vanrumste 2002].

In the second boundary condition, the potential after crossing the interface is continuous. It is stated as:

$$\Phi_1 = \Phi_2 \quad (4.25)$$

This equation is known as the Dirichlet boundary condition. In the Dirichlet boundary condition, there is no interface with air and is used for inner tissue layer interfaces.

4.3 The Current Source or Dipole Model

The primary currents are due to the movements of ions within the dendrites of the large pyramidal cells of activated regions in the cortex. The stimulus induced activation of a large number of excitatory synapses of a whole pattern of neurons leads to negative current monopoles under the brain surface. It also leads to positive monopoles quite closely underneath [Wolters 2003]. Current source (+ I_0) and current sink (- I_0) are used to represent an active pyramidal cell at microscopic level [Hallez 2008b]. They can be modelled as a current dipole shown in Figure 4.2. The position parameter \mathbf{r} of the dipole is typically chosen half way between the two monopoles.

A common concept of modelling the primary current distribution \mathbf{J}_p on the right hand side of Equation (4.18) is the mathematical current dipole. The mathematical dipole is an adequate model for the synchronous polarization of a cortical surface [de Munck *et al* 1988, Wolters 2003]. It is stated as [Yan *et al* 1991, Baillet *et al* 2001, Wolters 2003, von Christine 2008, Lanfer 2007]:

$$\mathbf{J}_p(\mathbf{r}) = \mathbf{M} \cdot \partial(\mathbf{r}_1 - \mathbf{r}_2), \quad (4.26)$$

where \mathbf{M} is dipole moment, ∂ is Dirac delta function, \mathbf{r}_1 is the position of the source monopole and \mathbf{r}_2 is the sink monopole. The ∂ is a very strong inhomogeneity that leads to problems in numerical calculations using the mathematical current dipole as source model [von Christine 2008]. These inhomogeneity problems are solved using several models, such as direct method, subtraction method, etc (discussed in Section 4.8).

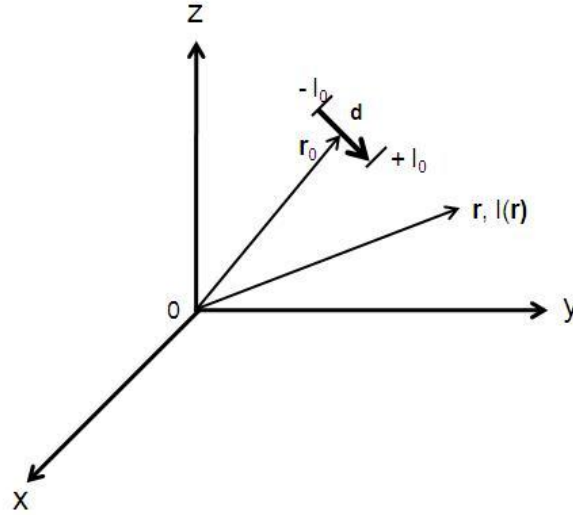


Figure 4.2: A dipole model. \mathbf{r}_0 is the location of dipole centre. $+I_0$ is current source and $-I_0$ is the current sink points. \mathbf{d} is distance from source to sink and $I(\mathbf{r})$ is current field at a point \mathbf{r} .

4.4 The EEG Forward Problem

The solution of the EEG forward problem yields electric potentials on the head surface caused by neuronal depolarization and repolarization in the brain, which can be represented by a current dipole. The forward problem is solved by means of a quasi-static approximation of the Maxwell equation or the Poisson equation (4.19) as:

$$\nabla \cdot (\sigma \nabla \Phi) = -\mathbf{I}_v \text{ in } \Omega \dots\dots\dots (4.27)$$

which describes the potential distribution in the head domain Ω due to a primary current in the brain. A Dirichlet boundary condition is applied in inner boundary surfaces Γ_I as:

$$\Phi_0 = \Phi_1 \text{ on } \Gamma_I \dots\dots\dots (4.28)$$

A Neumann boundary condition needs to be applied at the outer surface, Γ_o , where the medium is contacted with the air as:

$$\sigma \nabla \Phi \cdot \mathbf{n} = 0 \text{ on } \Gamma_o \dots\dots\dots (4.29)$$

where \mathbf{n} is the outward unit normal.

Furthermore, the value of the electric potential must be set to a specific value at one reference point:

$$\Phi(ref) \equiv 0$$

A forward solution determines the electric potentials for a volume conductor with known boundary condition and a given current source configuration. This forward problem has been solved by an analytic method and also approximated by numerical methods, such as the BEM, FEM and FDM.

4.5 General Algebraic Formulation of the EEG Forward Problem

Let us consider that \mathbf{r} is observation point, \mathbf{q} is dipole moment and \mathbf{r}_q is dipole source. A dipole magnitude $q \equiv \|\mathbf{q}\|$ from its orientation $\Phi = q/\|\mathbf{q}\|$ which will be represented in the spherical coordinate as $\Phi = \{\theta, \phi\}$. Let $p(\mathbf{r})$ denote scalp electric potential generated by a dipole [Baillet *et al* 2001]:

$$p(\mathbf{r}) = a(\mathbf{r}, \mathbf{r}_q, \Phi)q, \dots\dots\dots (4.30)$$

where $a(\mathbf{r}, \mathbf{r}_q, \Phi)$ is formed as the solution of the forward problem for a dipole with unit magnitude and orientation Φ . Therefore, scalp electric potentials $\mathbf{p}(\mathbf{r})$ at N sensors are obtained:

$$\mathbf{p} = \begin{bmatrix} p(\mathbf{r}_1) \\ p(\mathbf{r}_2) \\ \vdots \\ p(\mathbf{r}_N) \end{bmatrix} = a \begin{bmatrix} a(\mathbf{r}_1, \mathbf{r}_q, \Phi) \\ a(\mathbf{r}_2, \mathbf{r}_q, \Phi) \\ \vdots \\ a(\mathbf{r}_N, \mathbf{r}_q, \Phi) \end{bmatrix} q \dots\dots\dots (4.31)$$

For the simultaneous activation of multiple dipoles ($i=1$ to M) located at \mathbf{r}_{qi} with moment Φ_i and \mathbf{q}_i magnitude, we can obtain scalp electric potentials as:

$$\mathbf{p} = \begin{bmatrix} p(\mathbf{r}_1) \\ p(\mathbf{r}_2) \\ \vdots \\ p(\mathbf{r}_N) \end{bmatrix} = a \begin{bmatrix} a(\mathbf{r}_1, \mathbf{r}_{q1}, \Phi_1) & \dots & a(\mathbf{r}_1, \mathbf{r}_{qM}, \Phi_M) \\ \vdots & \ddots & \vdots \\ a(\mathbf{r}_N, \mathbf{r}_{q1}, \Phi_1) & \dots & a(\mathbf{r}_N, \mathbf{r}_{qM}, \Phi_M) \end{bmatrix} \begin{bmatrix} q_1 \\ q_2 \\ \vdots \\ q_M \end{bmatrix} \dots\dots\dots (4.32)$$

$$= A(\{\mathbf{r}_{qi}, \Phi_i\})\mathbf{S}^T,$$

where $A(\{\mathbf{r}_{qi}, \Phi_i\})$ is the gain matrix and \mathbf{S} is the generalized matrix of the source amplitude. Each column of the matrix A relates a dipole to the array of sensor measurements and also is known as forward field. For the M sources and T discrete time samples, Equation (4.32) can be represented as:

$$\mathbf{P} = \begin{bmatrix} p(\mathbf{r}_1, 1) & \dots & p(\mathbf{r}_1, T) \\ \vdots & \ddots & \vdots \\ p(\mathbf{r}_s, 1) & \dots & p(\mathbf{r}_s, T) \end{bmatrix} \begin{bmatrix} \mathbf{s}_1^T \\ \mathbf{s}_2^T \\ \vdots \\ \mathbf{s}_M^T \end{bmatrix} \dots \dots \dots (4.33)$$

$$= A(\{\mathbf{r}_i, \Phi_i\}) \mathbf{S}^T,$$

The corresponding time series for each dipole is the columns of the time series matrix \mathbf{S} .

4.6 Electric Potential in a Multi-layer Spherical Model

At the beginning of the mathematical solution of the forward problem, a single-layered spherical head model is considered to obtain the EEG. In this head model the entire conducting volume is modelled as a sphere of a constant homogeneous conductivity σ . Brody *et al* (1973) reviewed earlier formulations and represented a generalized expression for this single-sphered model as:

$$\Phi = \frac{\mathbf{q}}{4\pi\sigma} \cdot \left[\frac{\mathbf{e}_r + \mathbf{e}_R}{rR(1 + \mathbf{e}_r \cdot \mathbf{e}_r)} + \frac{2\mathbf{e}_R}{R^2} \right], \dots \dots \dots (4.34)$$

where r is the distance from the centre of the sphere to the observation point, R is the distance from the dipole position to the observation point, and \mathbf{e}_r and \mathbf{e}_R are unit vectors to the observation point from the centre and dipole location, respectively. However, it was noticed that the single-layered model is too unrealistic due to the variational conductivity of the skull rather than the scalp and brain. Therefore, a refinement of the single-sphered model was required and a three-layered spherical model was introduced.

In the three-layered spherical model, the outer sphere represents the scalp, the intermediate layer represents the skull and the inner sphere represents the brain. Rush and Driscoll (1968) reviewed some of the early solutions to single and homogeneous spheres, then presented the solutions for both anisotropic and multi sphere models. Berg-Scherg (1994) used a single-sphere model to approximate a three- (four-) layered model. In a four-layered model, an additional CSF layer is assumed between the skull and the brain. Zhang (1995) reviewed the solutions using different fast computation methods than the Berg-Scherg approximation. Mosher *et al* (1999) derived the solution of the forward problem according to the derivation of Zhang.

Here we present the form of the solution by Zhang (1995) and Mosher with reference to the geometry in Figure 4.3.

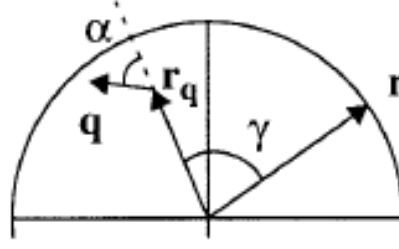


Figure 4.3: The angle between vectors pointing to surface position \mathbf{r} and dipole location \mathbf{r}_q is denoted τ . The angle the dipole \mathbf{q} makes with the radial direction at \mathbf{r}_q is denoted α . The angle between the plane formed by \mathbf{r}_q and \mathbf{q} , and the plane formed by \mathbf{r}_q and \mathbf{r} is denoted β [Zhang 1995, Mosher *et al* 1999].

The multi-shell case of M spherical shells requires the evaluation of an infinite series. The infinite series presentation by Zhang (1995) is as:

$$v^M(\mathbf{r}; \mathbf{r}_q, \mathbf{q}) = \frac{q}{4\pi\sigma_M r^2} \sum_{i=1}^{\infty} \frac{2n+1}{n} \left(\frac{r_q}{r} \right)^{n-1} \cdot \dots \dots \dots (4.35)$$

$$f_n \left(n \cos \alpha P_n(\cos \tau) + \cos \beta \sin \alpha \cdot P_n^1(\cos \tau) \right),$$

where P_n is Legendre polynomial and P_n^1 is associated Legendre polynomial and

$$f_n = \frac{n}{nm_{22} + (1+n)m_{21}}.$$

The coefficients m_{22} and m_{21} are found in the following equation as:

$$\begin{bmatrix} m_{11} & m_{12} \\ m_{21} & m_{22} \end{bmatrix} = \frac{1}{(2n+1)^{M-1}} \prod_{k=1}^{M-1} \begin{bmatrix} n + \frac{(n+1)\sigma_k}{\sigma_{k+1}} & (n+1) \left(\frac{\sigma_k}{\sigma_{k+1}} - 1 \right) \left(\frac{r_q}{r_k} \right)^{2n+1} \\ n \left(\frac{\sigma_k}{\sigma_{k+1}} - 1 \right) \left(\frac{r_k}{r_q} \right)^{2n+1} & (n+1) + \frac{n\sigma_k}{\sigma_{k+1}} \end{bmatrix}, \quad (4.36)$$

where the conductivities are arranged from the innermost sphere to the outer most, $\sigma_1, \dots, \sigma_M$, corresponding to the radii of the spheres $r_1 < r_2 < \dots < r_M$. More details are found in Zhang (1995).

The signed dipole intensity can be represented by its radial component $q_r = q \cos \alpha$ and tangential component $q_t = q \sin \alpha$. The potential can then be expressed as the sum of the two potentials [Mosher *et al* 1999]

$$v^1(\mathbf{r}; \mathbf{r}_q, \mathbf{q}) = v_r^1(\mathbf{r}; \mathbf{r}_q, \mathbf{q}) + v_t^1(\mathbf{r}; \mathbf{r}_q, \mathbf{q}), \dots\dots\dots (4.37)$$

where

$$v_r^1(\mathbf{r}; \mathbf{r}_q, \mathbf{q}) = \left(\frac{q_r}{4\pi\sigma} \right) \left(\frac{2(r \cos \tau - r_q)}{d^3} + \frac{1}{r_q d} - \frac{1}{r r_q} \right)$$

And

$$v_t^1(\mathbf{r}; \mathbf{r}_q, \mathbf{q}) = \left(\frac{q_t}{4\pi\sigma} \right) \cos \beta \sin \tau \left(\frac{2r}{d^3} + \frac{d+r}{r d(r - r_q \cos \tau + d)} \right)$$

However, it is becoming more apparent that the actual geometry of the head with the varying thickness and curvatures of the skull affects the solution [Chauveau *et al* 2003, Cuffin 1993]. So-called realistic head modelling is becoming much more common in conjunction with the BEM, FEM or FDM. However, the computational requirements for a realistic head model are higher than those for a multi-layer sphere.

4.7 Numerical Solution of the EEG Forward Problem

In order to solve the EEG forward problem, the Poisson equation must be solved to compute the unknown potentials on a head surface. For a current source or dipole, the solution for the potentials has a singularity at the dipole position. This singularity poses numerical difficulties for the solution of the FEM. Moreover, the solution of the mathematical dipole using the Dirac delta function also leads inhomogeneity (discussed in Section 4.3). These difficulties can be solved in a variety of ways which can be categorized into two distinct methods: direct approach and subtraction approach.

4.7.1 Direct approach

The direct approach is used to solve the forward problem by directly implementing the dipole source as a current source and sink positions infinitesimally close to each other. The direct method consists of solving Poisson's equation (4.27) with the Neumann boundary conditions (4.29) and a fixed referential potential [Wolters 2003]. The direct approach is easy to implement and can provide a more accurate solution when the conductive media is inhomogeneous [Awada *et al* 1997].

4.7.2 Subtraction approach

The subtraction approach is to solve for the difference between the desired potential and a potential due to a dipole in an infinite homogeneous medium that corresponds to the medium at the dipole location. This approach treats the mathematical dipole singularity and is usually used when the region's conductive media is homogeneous [Awada *et al* 1997]. This approach splits the total potential Φ [Wolters 2003, von Christine 2008] and conductivity σ into two parts, the singularity ($\Phi^\infty, \sigma^\infty$) and the correction (Φ^{cor}, σ^{cor}) as :

$$\Phi = \Phi^\infty + \Phi^{cor} \dots\dots\dots (4.38)$$

$$\sigma = \sigma^\infty + \sigma^{cor} \dots\dots\dots (4.39)$$

The singularity potential Φ^∞ is the solution for a dipole in an unbounded homogeneous conductor with constant conductivity σ^∞ . Therefore, the solution of the Poisson's equation

$$\Delta \Phi^\infty = \frac{\nabla \cdot \mathbf{J}_p}{\sigma^\infty} \dots\dots\dots (4.40)$$

can be expressed at any observation point (\mathbf{x}) and source position (\mathbf{x}_0) as:

$$\Phi^\infty(\mathbf{x}) = \frac{1}{4\pi\sigma^\infty} \frac{(\mathbf{M}, (\mathbf{x} - \mathbf{x}_0))}{|\mathbf{x} - \mathbf{x}_0|^3} \dots\dots\dots (4.41)$$

For a homogeneous and anisotropic conductivity, Equation (4.41) becomes

$$\Phi^\infty(\mathbf{x}) = \frac{1}{4\pi\sqrt{\det \sigma^\infty}} \frac{(\mathbf{M}, (\sigma^\infty)^{-1}(\mathbf{x} - \mathbf{x}_0))}{\left((\sigma^\infty)^{-1}(\mathbf{x} - \mathbf{x}_0), \mathbf{x} - \mathbf{x}_0\right)^{3/2}} \dots\dots\dots (4.42)$$

As Φ^∞ describes the potential in an unbound volume conductor, Φ^{cor} has to be computed to correct the potential with the accurate volume conductor. Substituting Equations (4.38) and (4.39) into Equation (4.18) and using Equation (4.40) we obtain

$$\nabla \cdot (\sigma \nabla \Phi^{cor}) = -\nabla \cdot (\sigma^{cor} \nabla \Phi^\infty) \text{ in } \Omega \dots\dots\dots (4.43)$$

with the Neumann boundary conditions

$$(\sigma \nabla \Phi^{cor}) \cdot \mathbf{n} = -(\sigma^{cor} \nabla \Phi^\infty) \cdot \mathbf{n} \text{ on } \Gamma_0 \dots\dots\dots (4.44)$$

The right-hand side of Equations (4.43) and (4.44) is now singularity-free because of the homogeneity condition:

$$\sigma^{cor} = \sigma^\infty - \sigma = 0 \text{ in } \Omega. \dots\dots\dots (4.45)$$

When solving Equations (4.43) and (4.44) towards Φ^{cor} , the unknown scalar potential Φ can be calculated using the Equation (4.17) or (4.18).

4.7.3 The Finite Element Method

There are many methods, such as BEM, FEM and FDM to solve the forward problem. In this dissertation, we choose the FEM. A relevant question is why we select the FEM.

4.7.3.1 Why do we select FEM?

The BEM, FEM and FDM are three popular approximation methods for solving the forward problem. As discussed earlier that some tissues, such as the skull and the WM are anisotropic. BEM can process only the isotropic. The conductivity of the head tissue is not homogeneous as the conductivity at different places of the head tissue is different, even in the same tissue. BEM is also unable to process the tissue inhomogeneity. It only calculates the solution of the forward problem on the boundaries between the homogeneous isotropic conducting regions. On the other hand, FEM and FDM are able to process anisotropic and inhomogeneous conductivity by calculating the entire volume. As a result, FEM and FDM lead to a larger number of computational points than the BEM.

To determine the potential at an arbitrary point, BEM reapplies the Barnard formula and numerical integration [Vanrumste 2002]. FEM and FDM determine the potential using interpolation of computational points in its vicinity. BEM has limited computational efficiency for solving the forward problem due to the cost of matrix inversion. It becomes a severe problem for the inverse problem, where a large number of forward evaluations are required. As BEM solves the inversion of the system matrix directly, it does not require any iterative solver. The FEM or FDM solves the forward problem using the inversion to a sparse matrix with the help of iterative solvers to speed up its execution. BEM yields smaller errors and consumes less computation time but requires more memory [Wang *et al* 2010]. A summary of the comparison among the BEM, FEM and FDM models is reported in Table 4.1.

Table 4.1: Comparison among different methods for solving the forward problem.

	BEM	FEM	FDM
Anisotropy	no	yes	yes
Inhomogeneity	no	yes	yes
Positional computational points	surface	volume	volume
Free choice computational points	yes	yes	no
System matrix	full	sparse	sparse
Solvers	direct	iterative	iterative
Number of regions	small	large	large
Errors	smaller	larger	larger
Memory	more	less	less
Computation	less	more	more

Finally, we choose the FEM, as it is able to treat arbitrary complex head geometries and inhomogeneous and anisotropic conductivities. Now, FEM is widely used in different research fields including fluid dynamics, heat transfer problems or in structural engineering. FEMs have also been developed by various research groups for the electromagnetic field simulations [Baillet et al 2001 and 2004, Wolters 2003, Wen 2000]. From now on, the focus will be on the FEM method in this dissertation.

4.7.3.2 Formulation of FEM

For the solution of the forward problem using FEM, the basic Poisson's equation is transformed into a variational formulation, which is then discretized using a Galerkin approach.

We use the Galerkin approach [Kwon and Bang 2000] to Poisson Equation (4.27) with the boundary conditions in Equations (4.28) and (4.29). We then multiply the Poisson equation with a test function ψ and integrate over the volume Ω representing the entire head. We obtain

$$\int_{\Omega} \psi \nabla \cdot (\sigma \nabla \Phi) d\Omega = - \int_{\Omega} \psi I_v d\Omega \dots\dots\dots (4.46)$$

Applying Greens' first identity for:

$$\int_{\Omega} \nabla \psi \cdot (\sigma \cdot \nabla \Phi) d\Omega = \int_{\partial\Omega} \Psi (\sigma \cdot \nabla \Phi) d\Omega - \int_{\Omega} \nabla \psi \cdot (\sigma \cdot \nabla \Phi) d\Omega \dots (4.47)$$

in combination with the boundary conditions to Equation (4.46), we obtain the 'weak formulation' of the forward problem as:

$$\int_{\Omega} \nabla \Psi \cdot (\sigma \cdot \nabla \Phi) d\Omega = - \int_{\Omega} \Psi I_v d\Omega \dots\dots\dots (4.48)$$

The entire volume conductor is discretized into small regions called elements and the process is known as tessellation. We tessellate the whole domain $\Gamma(\Omega)$ into N sets of tetrahedral elements. N denotes indexes of the mesh nodes for the finite element (FE) computation. In Equation (4.48), I_v represents the source configuration. Solving this equation for an ideal dipole would result in a singularity at the position of the dipole. We use the direct approach to solve this singularity problem.

For solving the forward problem using the FEM, we choose the electric potential appropriate test functions in the elements and low order polynomials. We assume the tetrahedral elements as

$$\Phi_e = c_1 + c_2x + c_3y + c_4z, \dots\dots\dots (4.49)$$

where c_i are the tetrahedral vertex, and x, y and z are coordinates. As the electric potential is continuous throughout the head domain, its approximation has to be continuous from one element to another. This continuity condition can be defined using local form function or interpolating basis function for an element $\Psi_k^e(x)$ as:

$$\Phi_e(x) = \sum_{k=1}^n u_k \Psi_k^e(x), \dots\dots\dots (4.50)$$

where $\Phi_e(x)$ is unknown element potential, n is the number of nodes in an element, u_k is node variables. This relation has to be fulfilled for every value combination of node variables, so that $\Psi_k^e(x)$ meets the Lagrange condition, $\Psi_k^e(x_i) = \delta_{ik}$ where x_i is a node of the element [von Christine 2008, Lanfer 2007]. Then the nodes of all elements are numbered consecutively and formed global form or basis function Ψ_k , which is composed of the local form function containing 1 at node k . Therefore, the global form function is only non-zero in the elements to which the node k belongs. Now, the unknown electric potential in the whole domain can be written as:

$$\Phi = \sum_{k=1}^N u_k \Psi_k \dots\dots\dots (4.51)$$

We then substitute Equation (4.51) to the quasi-static Equation (4.18). In general, the solution of an arbitrary choice of node variables will not be exact, therefore a residuum R remains:

$$R = \sum_{k=1}^N u_k \nabla \cdot (\sigma \nabla \Psi_k) - \nabla \cdot \mathbf{J}_p \dots\dots\dots (4.52)$$

Applying the method of weighted residuals, this R is weighted with the weighting function w_j . We choose the u_k in such a way that the integral of the weighted residuum over the whole domain vanishes:

$$\int_{\Omega} d\Omega R w_j = 0. \quad (4.53)$$

Following Galerkin's method, we choose w_j equal to the basis function ψ_j such that $w_j = \psi_j$. Substituting this into Equation (4.52) and applying integration by parts we obtain

$$\sum_{i=1}^N u_k \int_{\Omega} d\Omega \sigma \nabla \psi_k \cdot \nabla \psi_j + \int_{\Omega} d\Omega \nabla \cdot \mathbf{J}_p = 0. \quad (4.54)$$

The occurring surface integral is zero because of the boundary conditions. If we assume $u_k = \Phi$, $\int_{\Omega} d\Omega \sigma \nabla \psi_k \cdot \nabla \psi_j = \mathbf{K}$ and $\int_{\Omega} d\Omega \nabla \cdot \mathbf{J}_p = -\mathbf{I}$, we can express

Equation (4.54) as

$$\mathbf{K}\Phi = \mathbf{I}. \quad (4.55)$$

Equation (4.55) produces N equations in N unknown $\Phi = [\Phi_1, \dots, \Phi_N]^T \in \mathbb{R}^{N \times 1}$. Due to the local support of the basis function, each equation consists of only a linear combination of Φ_k and its adjacent computational points. Hence the system matrix $\mathbf{K} \in \mathbb{R}^{N \times N}$ is sparse. $\mathbf{I} \in \mathbb{R}^{N \times 1}$ is the source term obtained by integration of the right hand side of Equation (4.48). The integrand of \mathbf{K} is only non-zero for neighbouring nodes (where i and k are nodes of the same finite element). Therefore, this one row of \mathbf{K} only has as many non-zero entries as a node has neighbours; as a consequence, \mathbf{K} is sparsely populated with non-zero entries. Thus, FEM formulation leads to system equations in which unknowns are the potentials in each node. The elements of \mathbf{K} and \mathbf{I} depend on the geometry of a head model. As \mathbf{K} is sparse, symmetric and positive definite, it requires an iterative solver to accelerate the rate of convergence of iterative solvers. We use preconditioned conjugate gradient as an iterative solver.

The conjugate gradient (CG) method is an iterative method for the numerical solution of a particular system of linear equations, namely those whose matrix is symmetric and positive-definite. The CG method can be applied to the sparse systems that are too large to be handled by direct methods such as the Cholesky decomposition. Solving linear systems resulting from the finite elements shows the limits of the CG. Indeed, the spectral condition number of such matrices is too high. The technique of the preconditioned CG method consists of introducing a matrix \mathbf{C}

subsidiary. Let $\hat{\Phi}$ be the exact solution of this system. It happens sometimes that the spectral condition number $\kappa(\mathbf{K})$ is too high. Preconditionment consists of introducing regular matrix C and solving the system:

$$C^{-1}(\mathbf{K}\hat{\Phi}) = C^{-1}\mathbf{I} \Leftrightarrow \mathbf{K}\hat{\Phi} = \mathbf{I} \dots\dots\dots (4.56)$$

such that the new spectral condition number is smaller for a judicious choice of the matrix C .

4.8 Summary

In this Chapter, we introduce the forward problem and its solution. At the beginning of this Chapter, we describe a mathematical formulation for the primary current source model with the equivalent current source and current sink. For this source configuration, we derive the Poisson equation and its boundary conditions. Poisson's equation connects the electrical source with the potential fields it generates. The EEG forward problem is to solve the Poisson equation, i.e. it calculates the potential for a given source configuration. The generalised algebraic formulation of the forward problem is also shown. We show the potential calculation for a multi-layered spherical head model and also show how the potential passes from one surface to the neighbouring surface by means of the boundary conductions. We then discuss how the forward problem is solved using the FEM. As the FEM requires an iterative solver, the preconditioned conjugate gradient method is also discussed as an iterative solver.

In the next Chapter, we shall discuss and analyze the effects of obtained EEGs from different conductivity based head spherical models.

CHAPTER 5

EFFECTS OF TISSUE CONDUCTIVITY ON HEAD MODELLING

In this Chapter, we investigate EEGs from our proposed different conductivity models. At the beginning, we introduce our methodology and implementation tools to carry out head model construction. Further, we construct a series of human head models using inhomogeneous and anisotropic conductivities. We show the effects of inhomogeneous and anisotropic tissue conductivities on EEG based on our proposed CRA, SCA, FA based and the Monte Carlo based conductivity models. We also implement a head model using a stochastic method to study the effects of inhomogeneous and anisotropic conductivities on EEG. All these models are constructed based on a five-layered spherical head model frame.

5.1 Methodology and Tools

5.1.1 Spherical head model construction

We construct a spherical head model using the following steps: (A) making spheres; (B) performing mesh generation and labelling the mesh elements into surfaces; (C) assigning or allocating conductivity; (D) placing sources; (E) putting electrodes or sensors on the upper sphere; (F) solving the forward problem using FEM and finally (G) storing the computed scalp potentials for each electrode. Figure 5.1 shows the diagram of a spherical head model construction.

In the first step, we make multiple spheres according to the head model structure, such as 3-spheres, 4-spheres and 5-spheres. We perform mesh generation to create tetrahedrons for piecewise FEM elements in the second step. Mesh generation is performed as follows: (a) creating the surfaces of the spheres, (b) generating the vertices of the tetrahedral elements, (c) performing the Delaunay triangulation to confirm no vertex resides inside the circumstances of any tetrahedra and (d) each tetrahedron is labelled to any compartment which it belongs. We mesh these spheres using the Tetgen® package (Si 2004).

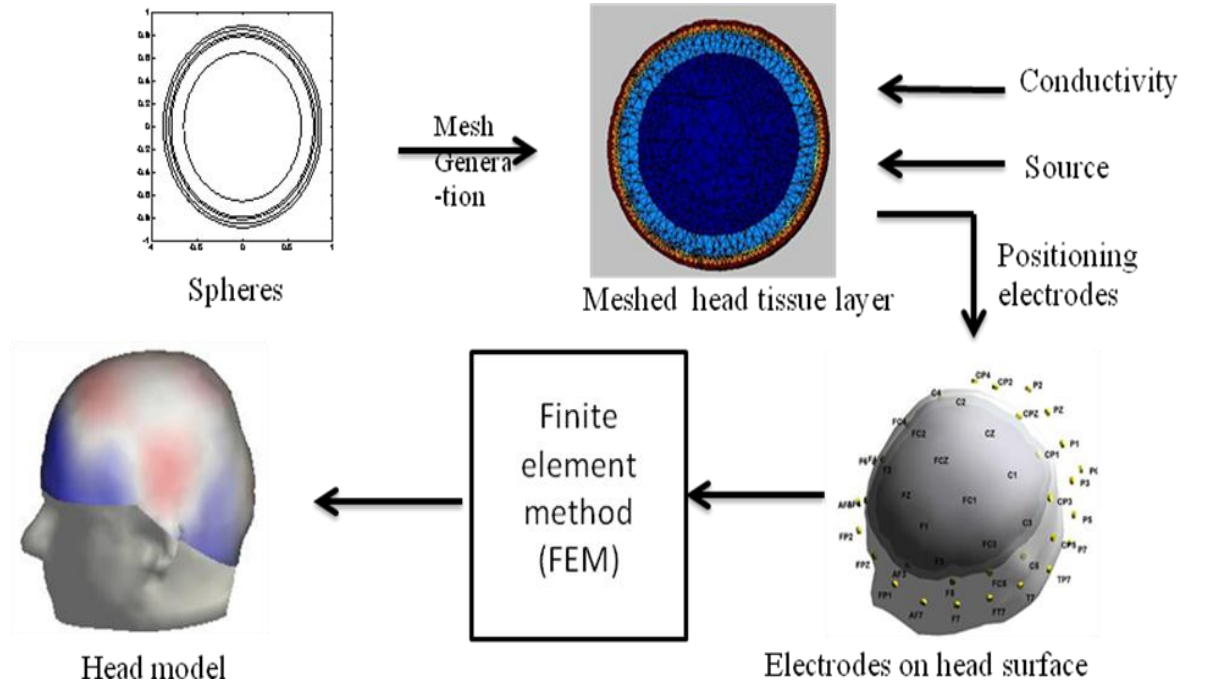


Figure 5.1: Spherical head model construction.

The third step, conductivity allocation, is the most important and the main focus component of this dissertation. We assign either homogeneous isotropic, homogeneous anisotropic or inhomogeneous anisotropic conductivities produced from our proposed conductivity models to each tetrahedron for the computation of the EEG forward problem. We use a scalar value for the homogeneous isotropic conductivity and conductivity tensor for anisotropic conductivity. In the fourth step, we put source(s) inside the GM of the brain. We implement equivalent current dipole configuration [Yan *et al* 1991, Baillet *et al* 2001] to the surface of the cortex (radial direction) with 1 μ A amplitude. We assume that the dipole is in the axial, coronal and sagittal planes. A dipole can be decomposed into three orthogonal dipoles along the main axes. We, therefore, consider the three orthogonal orientations. These orientations are X orientation (along left-right), Y orientation (along back-front) and Z orientation (along bottom-top). We choose the orientations for the dipole indicated by an azimuth angle $\theta \in [-\pi, \pi]$ and an elevation angel $\varphi \in [-\pi/2, \pi/2]$. In the fifth step, we put electrodes on the upper surface of the scalp sphere. We use 64 electrodes to compute the scalp potential excluding a reference electrode. We consider referential montage to compute the potentials. We obtain these electrode positions from the online package Brainstorm2. We align and register the tessellated head

surfaces based on these electrode positions. In the sixth step, we perform the forward computation using FEM tool of Brainstorm2 [Brainstorm] to compute the potentials on the scalp (EEG). Finally, we get the computed scalp potentials from N points where electrodes are located on the upper head surface and save them as EEGs.

5.1.2 Used tools

We mainly use Brainstorm2 [Brainstorm], BrainSuite2 [Shattuck 2005] and advanced source analysis (ASA) [ASA] in our work.

Brainstorm is a free Matlab application dedicated to Magnetoencephalography (MEG) and EEG data visualization, processing and cortical source estimation. The intention of the developer is to make a comprehensive set of tools available to the scientific community involved in MEG/EEG experimental research. It is widely used in this purpose for more than five years is validated and used by physicians and researchers. [Sylvain *et al* 2004, Darvas *et al* 2004, Pantazis *et al* 2005]. Brainstorm was recently updated to Brainstorm3. However, we use the FEM tool of Brainstorm2. We also use the Tetgen® package for mesh generation which is combined with the FEM tool of Brainstorm2.

BrainSuite is an MRI tool designed for identifying tissue types and surfaces in an MRI of the human head. It requires minimal user interaction with the goal of completing the entire process of extracting a topologically spherical cortical surface from a raw magnetic resonance volume. We use Brainsuite2 as it has been written to be compatible with Brainstorm software for the analysis of MEG and EEG data.

Advanced source analysis ASA is a software package designed for functional brain imaging based on EEG/MEG measurements. Our laboratory purchased the ASA from its developer ANT Corporation, in Netherlands. The visualization of the computed EEGs to observe the scalp potentials are presented using ASA. We perform the EEG visualization by adopting and feeding our computed EEGs to ASA.

5.2 Influence of Anisotropic Conductivity

5.2.1 Objective of the study

In the case of the electric fields computation, there are two important aspects: the geometry of the head and the conductivities assigned to each region of the geometry. This Section investigates the influence of head tissue anisotropy on the head modelling for the solution of the EEG forward problem.

5.2.2 Head model construction

We implement a five-layered spherical head model with 8.8cm, 8.5cm, 8.1cm, 7.9cm and 6.5cm radii for the scalp, skull, CSF, GM and WM, respectively. We perform the tessellation and find approximately 315K elements from 54K nodes. Labelling of tetrahedra provides 52519 elements for the scalp, 67403 elements for the skull, 78846 elements for the CSF, 66665 elements for the GM and 50489 elements for the WM. We place six fixed dipoles at a point starting from 2mm outer of WM to 2mm below the cortex surface inside the GM with the elevation angles $\pi/5.22$, $\pi/4.67$, $\pi/4.0$, $\pi/3.86$, $\pi/3.83$ and $\pi/3.77$ radians with fixed azimuth angle $\pi/4$. We construct the following head models:

Model A: head model using homogeneous isotropic conductivity.

Model B: head model using anisotropic WM conductivity.

Model C: head model using anisotropic skull conductivity.

Model D: head model using WM + skull conductivity.

5.2.3 Simulation setup

When a tissue is assumed to be anisotropic, conductivity is defined either in the radial or in the tangential direction [Sadleir and Argibay 2007]. We model the longitudinal or tangential conductivity as ten times higher than the transverse or radial conductivity. It can be stated as:

$$\sigma_{tgl} = 10 \cdot \sigma_{rdl} \dots\dots\dots (5.1)$$

where σ_{tgl} and σ_{rdl} present the tangential and the radial conductivities, respectively. For the implementation of anisotropy, we consider conductivity tensor. For example, we assume the conductivity tensor for WM as [Wolters 2003, Hallez *et al* 2005a, Gullmar *et al* 2006, Wolters *et al* 2006]:

$$\underline{\underline{\sigma}} = \mathbf{S} \begin{pmatrix} \sigma_{long} & 0 & 0 \\ 0 & \sigma_{trans} & 0 \\ 0 & 0 & \sigma_{trans} \end{pmatrix} \mathbf{S}^{-1}, \dots\dots\dots (5.2)$$

where \mathbf{S} is orthogonal matrix of unit length eigenvectors, σ_{long} is the parallel (longitudinal) eigen values, and σ_{trans} is the perpendicular (transverse) eigen values. Developing the Models B to D, we implement the VC and WC using anisotropic conductivity model.

The EEG computed from model A is defined as a reference model throughout this study unless otherwise specified. EEGs obtained from other models are considered as computed models, which are compared to reference EEG. We implement these head models using an Intel® dual core 2.0 Ghz processor. A single computation for the FEM in this research takes approximately three hours CPU time.

To quantify the differences between the reference and computed models, we use two measurements. The first measurement is relative error (ε) and is defined as [Klepfer *et al* 1997, Li *et al* 2007]:

$$\varepsilon = \sqrt{\frac{\|\mathbf{V}_{ref} - \mathbf{V}_{comp}\|_2}{\|\mathbf{V}_{ref}\|_2}} \dots\dots\dots (5.3)$$

where \mathbf{V}_{ref} and \mathbf{V}_{comp} are reference and computed EEGs, respectively, and $\|\mathbf{x}\|_2$ is norm defined as $\|\mathbf{x}\|_2 = \sqrt{\sum_{i=1}^N x_i^2}$, N is the number of electrodes. ε is always positive and the best value is 0.

Another measurement is correlation coefficient (η) and is defined as [Klepfer *et al* 1997, Li *et al* 2007]:

$$\eta = \frac{\mathbf{V}_{ref} \cdot \mathbf{V}_{comp}}{\|\mathbf{V}_{ref}\|_2 \|\mathbf{V}_{comp}\|_2} \dots\dots\dots (5.4)$$

where η is always positive and $\eta=1$ when $\mathbf{V}_{ref} = \mathbf{V}_{comp}$.

5.2.4 Simulation results

We compute the scalp potentials assigning $\sigma_{long} : \sigma_{trans} = 10$ in WM tissue. Table 5.1 shows average ε and η values resulted by the comparison between Model A and Model B. All of the results are away from the ideal ε and η values, 0 and 1, respectively. From these results, we find that there are some significant changes on EEG produced by homogeneous and anisotropic conductivities based models for both constraints from homogeneous isotropic or reference model.

Table 5.1 Average related error (ε) and correlation coefficient (η) values resulted by comparing Models A and B.

Constraint	Conductivity		X orientation	Y orientation	Z orientation
Volume	Longitudinal	ε	42%	43%	64%
		η	0.9664	0.98	0.5426
	Transverse	ε	39%	21%	1.51%
		η	0.9481	0.97	0.43
Wang	Longitudinal	ε	44%	48%	62%
		η	0.9643	0.9821	0.5664
	Transverse	ε	31%	22%	50%
		η	0.9443	0.9704	0.8409

We also develop another model assigning the anisotropic skull conductivity ratio as $\sigma_{igl} : \sigma_{rdl} = 10$ (Model C). Table 5.2 shows average ε and η values resulting from this model. From these results, we also understand the effects of skull homogeneous anisotropic conductivities on EEG.

Table 5.2. Average ε and η values resulted by comparing Models A and C.

Constraint	Conductivity	Error	X orientation	Y orientation	Z orientation
Volume	Tangential	ε	16%	27%	75%
		η	0.1984	0.2451	0.5725
	Radial	ε	49%	58%	53%
		η	0.7601	0.8268	0.6491
Wang	Tangential	ε	20%	25%	57%
		η	0.9768	0.9852	0.8162
	Radial	ε	29%	43%	31%
		η	0.9382	0.9575	0.8672

Similar to Tables 5.1 and 5.2, Table 5.3 shows the combined WM and skull anisotropy on EEG. We also find their combined effects are also significant.

Table 5.3. Average ε and η values resulted by comparing Models A and D.

Constraint	Conductivity	Error	X orientation	Y orientation	Z orientation
Volume	Parallel	ε	43%	54%	57%
		η	0.7523	0.7829	0.5342
	Perpendicular	ε	15%	26%	68%
		η	0.2784	0.2551	0.6325
Wang	Parallel	ε	27%	45%	36%
		η	0.9282	0.9675	0.8922
	Perpendicular	ε	18%	23%	58%
		η	0.982	0.9852	0.852

5.2.5 Conclusion

From the above simulated results, we understand that there are significant effects of tissue anisotropy on EEG. Different models show different relative error or correlation coefficient values, these values are different from the ideal values. Similar anisotropy study by different researchers also shows substantial differences on obtained EEG from anisotropic conductivity to the isotropic conductivity. When combined anisotropic conductivities (WM and skull) are assigned, considerable change is noticed in comparison with single tissue layered anisotropy. This means that relative errors or correlation coefficient values are not additive when more than one tissue layers are combined.

5.3 Influence of Inhomogeneous and Anisotropic Tissue Conductivities

5.3.1 Objective of the study

In medical applications, the head modelling is suggested to be anisotropic though isotropic head modelling is still in use [Juan-Felipe *et al* 2007]. Several studies [Marin *et al* 1998, Wolters 2003, Hallez *et al* 2008a, Gullmar *et al* 2010] implement anisotropic models using a constant anisotropy ratio; however, it is established that the anisotropy ratio is not constant and varies in the range of 1 to 10. Therefore, a complete head model requires a full implementation of variable anisotropic or inhomogeneous anisotropic conductivity. We propose to implement an inhomogeneous and anisotropic conductivities model and to simulate different head models on our proposed conductivity models.

5.3.2 Conductivity ratio approximation model

5.3.2.1 Simulation setup

We use the same head geometry, segmentation and tessellation described in Section 5.2.2. We model a human head based on inhomogeneous anisotropic conductivities generated using conductivity ratio approximation (CRA) model. CRA generates the anisotropy ratio randomly between 1 and 10 for each element. Based on this ratio, the longitudinal and transverse conductivities are determined by applying Volume and Wang's constraints. In the case of the homogeneous anisotropic model, ξ_{lt} (conductivity ratio between longitudinal and transverse conductivities) is constant. For example, Wolters *et al* (2006) and Gullmar *et al* (2006) used 1, 2, 5 or 10 for the value of ξ_{lt} . However, for the inhomogeneous anisotropic case, ξ_{lt} can be 1 to 10. CRA generates different values for ξ_{lt} for WM as shown in Figure 5.2(a). Figure 5.2(c) shows the WM longitudinal and transverse conductivities for VC from the values of ξ_{lt} shown in Figure 5.2(a). In a similar way, we generate inhomogeneous conductivities for skull using both constraints.

We place a dipole at 2mm below the cortex surface inside the GM with the azimuth and elevation orientations $\pi/4$ and $\pi/5$, respectively, and consider X orthogonal dipole orientation only.

Finally, we apply relative difference measure (RDM) and magnification (MAG) techniques to analyze the results. RDM and MAG are introduced by Meijis *et al* (1989) as:

$$RDM = \sqrt{\sum_{i=1}^N \left(\frac{\varphi_{comp}}{\sqrt{\sum_{i=1}^N \varphi_{comp}^2}} - \frac{\varphi_{ref}}{\sqrt{\sum_{i=1}^N \varphi_{ref}^2}} \right)^2} \dots\dots\dots (5.5)$$

$$MAG = \sqrt{\frac{\sum_{i=1}^N \varphi_{comp}^2}{\sum_{i=1}^N \varphi_{ref}^2}} \dots\dots\dots (5.6)$$

where φ_{comp} is computed scalp potentials from the CRA based head model, φ_{ref} is reference scalp potentials obtained from the homogeneous isotropic head model and N is the number of electrodes.

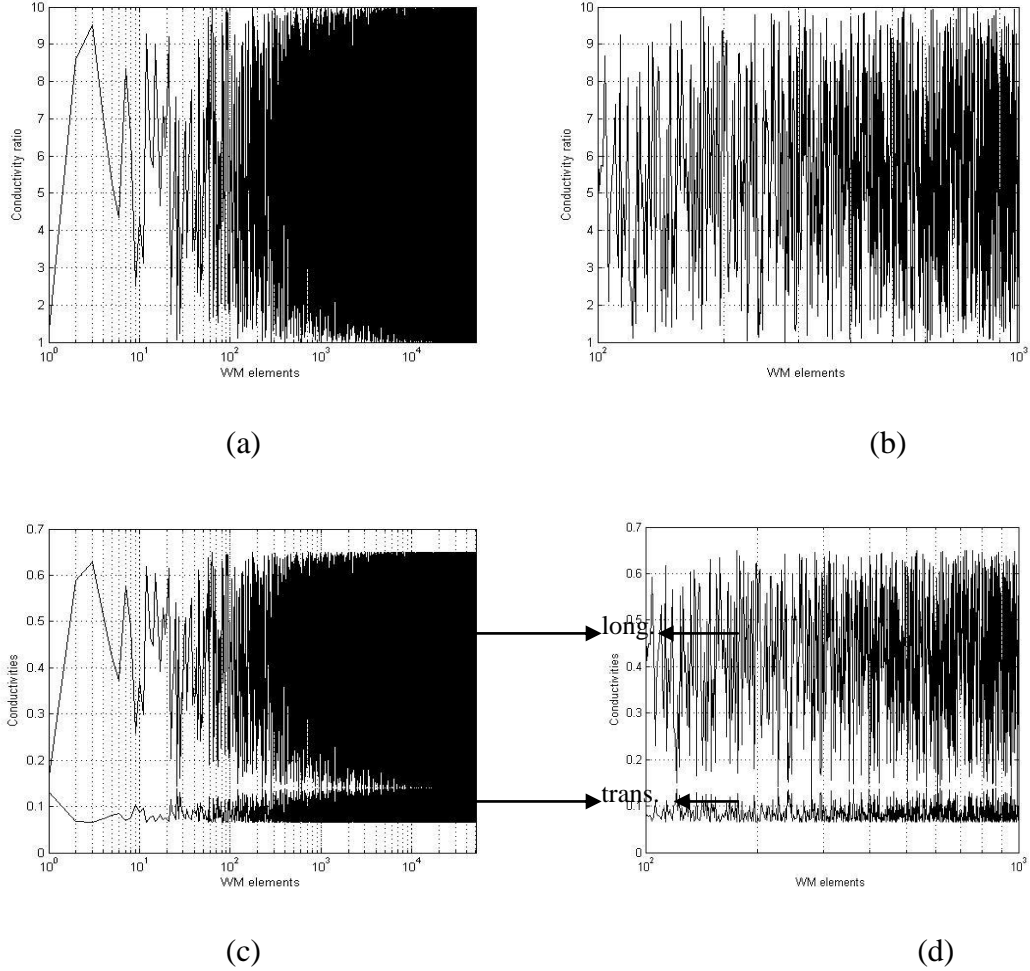


Figure 5.2: (a) Value of conductivity ratio (ξ_{lt}) between longitudinal and transverse conductivity for each WM element generated by CRA, (b) clear view of (a) from 10^2 to 10^3 WM elements, (c) longitudinal (long.) and transverse (trans.) conductivity values for each WM elements based on ξ_{lt} of (a) using VC, and (d) clear view of (c) from 10^2 to 10^3 WM elements [Bashar *et al* 2008b].

5.3.2.2 Simulated results

Table 5.4 presents the RDM and MAG values produced by the CRA technique. For all the cases, RDM and MAG values are far from the ideal values, 0 and 1, respectively. This indicates a strong effect of WM inhomogeneous anisotropy on EEG. While we implement inhomogeneous anisotropy, different conductivities rather than homogeneous isotropy are assigned. Therefore, electrical potentials vary

from the reference model. Volume constrained σ_{long} and Wang's constrained σ_{trans} are more affected by inhomogeneous anisotropy. We find that the Volume constrained σ_{long} has higher values and Wang's constrained σ_{trans} has lower values. These two conductivity values are far away from the homogeneous isotropic conductivity (0.14 S/m). For instance, when $\xi_{lt} = 10$, the value of σ_{long} and σ_{trans} are 0.65 S/m and 0.044 S/m for Volume and Wang's constraints, respectively. In comparison with the homogeneous anisotropic model, inhomogeneous anisotropic models produce less MAG error. In our experiment, we consider $\xi_{lt} = 10$ for the homogeneous anisotropic model. As our inhomogeneous anisotropic model is generated by different conductivity ratios (1 to 10) shown in Figure 5.2(a), it therefore produces greater magnitudes than the reference model. As a result, it becomes closer to homogeneous anisotropic model. Here, the MAG is 1.58 between reference and homogeneous anisotropic models. The longitudinal conductivities for both constraints are more affected by homogeneous isotropy than homogeneous anisotropy (comparing columns 5 and 6 with columns 3 and 4 for longitudinal conductivities). However, transverse conductivities are more affected by homogeneous anisotropy than homogeneous isotropy as shown in rows 4 and 5 in Table 5.4.

Table 5.4: RDM and MAG values between reference and computed models for WM.

	Conductivity	homo_iso vs inho_aniso		homo_aniso vs inho_aniso	
		RDM	MAG	RDM	MAG
Volume constraint	Longitudinal	27.60%	1.4384	6.47%	0.9023
	Transverse	28.21%	0.9104	42.06%	0.9518
Wang's constraint	Longitudinal	19.16%	1.2637	6.11%	0.79
	Transverse	32.90%	0.8923	45.15%	0.9329

* homogeneous isotropic (homo_iso) and inhomogeneous anisotropic (inho_aniso) models, and homogeneous anisotropic(homo_aniso) and inho_aniso models for the WM calculated by either VC or WC conductivities.

By a similar approach, we obtain different RDM and MAG values for inhomogeneous and anisotropic skull and combined WM and skull conductivity models reported in Table 5.5 and Table 5.6, respectively. Analyzing these results, it is also apparent that the effects of inhomogeneous and anisotropic conductivities show some significant effects on EEG.

Table 5.5: RDM and MAG values between reference and computed models for skull.

	Conductivity	homo_iso vs inho_aniso		homo_aniso vs inho_aniso	
		RDM	MAG	RDM	MAG
Volume constraint	Tangential	32.15%	1.4931	12.41%	0.8615
	Radial	38.11%	0.8204	49.22%	0.9314
Wang's constraint	Tangential	22.16%	1.337	13.11%	0.754
	Radial	33.92%	0.8422	47.12%	0.9128

* homogeneous isotropic (homo_iso) and inhomogeneous anisotropic (inho_aniso) models, and homogeneous anisotropic (homo_aniso) and inho_aniso models for the skull calculated by either VC or WC conductivities.

Table 5.6: RDM and MAG values between reference and computed models for WM and skull together.

	Conductivity	homo_iso vs inho_aniso		homo_aniso vs inho_aniso	
		RDM	MAG	RDM	MAG
Volume constraint	Parallel	29.40%	1.3381	8.42%	0.9129
	Perpendicular	27.25%	0.9304	43.02%	0.9181
Wang's constraint	Parallel	17.12%	1.3637	7.15%	0.719
	Perpendicular	33.10%	0.8721	41.12%	0.9222

* homogeneous isotropic (homo_iso) and inhomogeneous anisotropic (inho_aniso) models, and homogeneous anisotropic (homo_aniso) and inho_aniso models for the WM and skull calculated by either VC or WC conductivities.

5.3.2.3 Conclusion

In this study, we apply the conductivity ratio approximation model to assign the different conductivity ratios for the construction of the inhomogeneous anisotropic head model. The preliminary results show that EEG is affected by the inhomogeneous anisotropic conductivities in the both models generated by the Volume and Wang's constraints.

5.3.3 Statistical conductivity approximation model

This subsection also shows the effects of inhomogeneous and anisotropic tissue conductivities on EEG forward computation with a statistical conductivity approximation (SCA) model. The SCA determines the random numbers using Rayleigh distribution, which we consider as longitudinal (tangential) conductivities. Later on, we generate transverse (radial) conductivities according to Volume and Wang's constraints.

5.3.3.1 Simulation setup

Figure 5.3 shows the conductivity ratio (Figure 5.3(a)) and conductivities for Volume constrained WM using SCA (Figure 5.3(c)).

Based on the same head geometry, source configuration and position, and electrode positions stated in Section 5.2.2, we compute the EEG forward solution. We also model a homogeneous, an isotropic, and an inhomogeneous anisotropic conductivities based head. We analyze the obtained EEGs using the RDM and MAG mentioned in Equations (5.5) and (5.6), respectively.

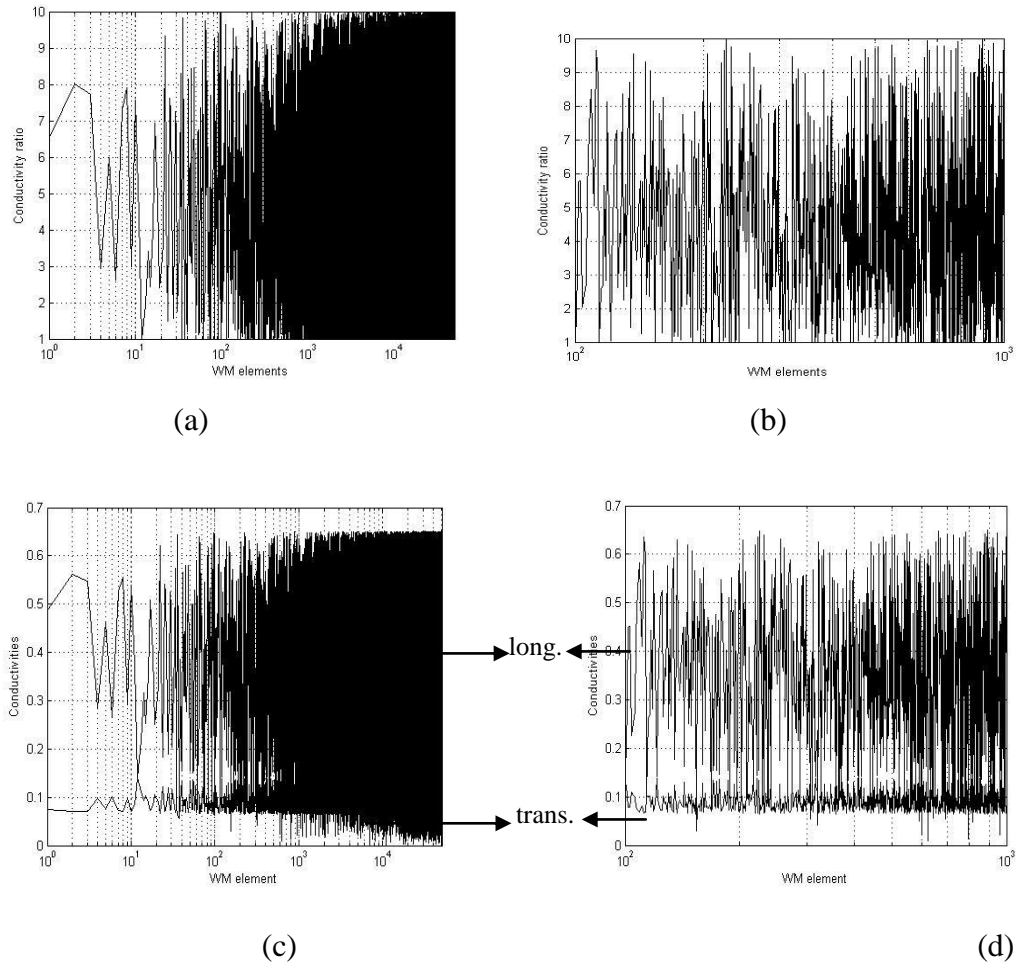


Figure 5.3: (a) Value of ξ_{lt} (conductivity ratio) between longitudinal and transverse conductivity for each WM element generated by SCA, (b) clear view of (a) from 10^2 to 10^3 WM elements, (c) longitudinal and transverse conductivity values for each WM elements based on ξ_{lt} of (a) using Volume constraint, and (d) clear view of (c) from 10^2 to 10^3 WM elements (Bashar *et al* 2008b).

5.3.3.2 Simulation results

Table 5.7 presents the RDM and MAG values produced by the SCA conductivity model for WM. The RDM values are between 5.09% to 36.44% and MAG values are in the range of 0.82 to 1.30. For all the cases, RDM and MAG values are far from the ideal values 0 and 1, respectively. These results indicate that the effects of WM inhomogeneous anisotropy on EEG are significant. Similarly, Table 5.8 represents the RDM and MAG values obtained from the inhomogeneous and anisotropic skull conductivity model while Table 5.9 is from combined model of WM and skull conductivities. From Tables 5.7, 5.8 and 5.9 we find that skull is more affected by inhomogeneous and anisotropic conductivities. Analyzing these results, it is apparent that inhomogeneous and anisotropic tissue conductivities have significant effects on EEG.

Table 5.7: RDM and MAG values using SCA for the WM.

Constraint	Conductivity	homo_iso vs inho_aniso		homo_aniso vs inho_aniso	
		RDM	MAG	RDM	MAG
Volume	Longitudinal	19.91%	1.3056	5.09%	0.8235
	Transverse	24.55%	0.9458	39.38%	0.9888
Wang	Longitudinal	15.24%	1.2402	5.67%	0.9133
	Transverse	18.61%	0.8471	36.44%	0.8856

*RDM and MAG values between homogeneous isotropic (homo_iso) and inhomogeneous anisotropic (inho_aniso), and homogeneous anisotropic (homo_aniso) and inho_aniso models using SCA for the WM computed by either Volume or Wang's constraint conductivities (Bashar, 2008b).

Table 5.8: RDM and MAG values using SCA for the skull.

Constraint	Conductivity	homo_iso vs inho_aniso		homo_aniso vs inho_aniso	
		RDM	MAG	RDM	MAG
Volume	Tangential	22.41%	1.335	12.09%	0.8213
	Radial	26.59%	0.9381	42.31%	0.968
Wang	Tangential	17.42%	1.3104	9.25%	0.8991
	Radial	19.17%	0.8144	39.36%	0.8450

Table 5.9: RDM and MAG values using SCA for the WM and skull together.

Constraint	Conductivity	homo_iso vs inho_aniso		homo_aniso vs inho_aniso	
		RDM	MAG	RDM	MAG
Volume	Parallel	25.32%	1.532	14.44%	0.8111
	Perpendicular	28.51%	0.9211	45.36%	0.9362
Wang	Parallel	19.11%	1.4510	12.21%	0.8594
	Perpendicular	21.14%	0.7142	43.12%	0.8125

5.3.3.3 Conclusion

In this Section we have studied the effects of tissue inhomogeneity and anisotropy on EEG using SCA model. Though SCA is based on statistical assumptions of different conductivities within the given ranges for VC and WC, the simulated results confirm that tissue inhomogeneity and anisotropy have significant effects on EEG.

5.3.4 Fractional anisotropy based conductivity model

Fractional anisotropy (FA) is used to measure the anisotropy property for each voxel. FA varies between 0 and 1 to represent anisotropy. With the changing of FA values, the conductivity or anisotropy ratio also varies. Li *et al* (2007) proposed two levels of conductivity ratios. We suppose that only two levels are not sufficient and propose four different levels of conductivity ratios. Based on these ratios, we determine the radial and tangential conductivities. We also investigate the effects of inhomogeneous anisotropic conductivities on EEG forward computation using FA based conductivity model.

5.3.4.1 Head model construction and simulation

We implement a five-layered spherical head model with 9.2cm, 8.4cm, 8.0cm, 7.6cm and 5.0cm radii for the scalp, skull, CSF, GM and WM, respectively. The mesh generation produces 112K tetrahedral elements from 19K nodes where 19397 elements for scalp, 24563 for skull, 21379 for CSF, 20674 for GM and 26841 elements for the WM. For the homogeneous isotropic model, we assign the mean conductivity to each tissue layer. However, we assign the conductivities produced by multi-steps FA function to individual elements of WM and skull having other tissue layers isotropic for the implementation of an inhomogeneous anisotropic head model. We assume the dipole located in axial, coronal and sagittal planes with the azimuth angle $\pi/4$ and elevation angle $\pi/5$ having the $1\mu\text{A}$ magnitude. Finally, we apply RDM and MAG techniques to analyze the results.

5.3.4.2 Simulations and results

To study the influence of inhomogeneous anisotropic WM and skull tissue conductivities, we carry out four independent experiments. Firstly, we compute an EEG from the reference model. Secondly, we compute an EEG from FA based

conductivity model where inhomogeneous anisotropic conductivities are assigned to WM while other tissue layers are homogeneous and isotropic. Thirdly, we measure an EEG by assigning inhomogeneous anisotropic conductivities to skull while other layers are homogeneous and isotropic. Finally, we compute EEG by assigning the WM and skull inhomogeneous anisotropic conductivities together keeping other layers homogeneous and isotropic.

Table 5.10 shows the RDM and MAG errors caused by the inhomogeneous anisotropic WM conductivities generated using the Volume constraint. We find that the RDM (1.59% ~ 18.87%) and MAG (0.95 ~ 1.12) values are far from their ideal values, 0 and 1, respectively. These results indicate that WM inhomogeneous anisotropy affects the scalp EEG strongly. The longitudinal inhomogeneous conductivities produce fewer errors than those of transversal conductivities. Therefore, WM transversal inhomogeneous conductivities effects are more on EEG than longitudinal inhomogeneous conductivity.

Table 5.10: RDM and MAG values generated by inhomogeneous anisotropic WM conductivities

Conductivity	Dipole orientation	RDM	MAG
Longitudinal	X	4.04%	1.02
	Y	5.91%	1.12
	Z	4.21%	1.03
Transversal	X	18.87%	1.07
	Y	1.59%	0.97
	Z	7.3%	0.95

Table 5.11 presents the RDM and MAG errors due to inhomogeneous and anisotropic skull conductivities. Here, we find the RDM values ranging from 4.37% to 17.19% and MAG values are between 0.84 and 1.11. Therefore, the effects of inhomogeneous anisotropic skull tissue conductivities on EEG are significant. Radial inhomogeneous conductivities produce more errors than tangential inhomogeneous conductivities. These results are consistent with other studies [Wen 2000, Wolters 2003, Wolters *et al* 2006].

Table 5.12 shows the RDM and MAG errors generated by combining the inhomogeneous anisotropic WM and skull tissue conductivities. The parallel conductivities produce 1.23% to 5.9% RDM and 0.95 to 1.01 MAG errors while the perpendicular conductivities produce 7.03% to 20.39% RDM and 1.04 to 1.09 MAG

errors. Therefore, it is significant that the combination of inhomogeneous anisotropic WM and skull conductivities have some combined effects on EEG.

Table 5.11: RDM and MAG values generated by inhomogeneous anisotropic skull conductivities

Conductivity	Dipole	RDM	MAG
Radial	X	17.19%	0.89
	Y	7.93%	0.84
	Z	7.17%	0.96
Tangential	X	8.18%	1.09
	Y	4.37%	1.11
	Z	4.64%	1.03

Table 5.12: RDM and MAG values generated by inhomogeneous anisotropic WM and skull conductivities.

Conductivity	Dipole orientation	RDM	MAG
Parallel	X	5.9%	0.95
	Y	1.23%	1.01
	Z	4.48%	0.99
Perpendicular	X	20.39%	1.09
	Y	8.96%	1.08
	Z	7.03%	1.04

5.3.4.3 Conclusion

We have investigated the influence of WM and skull inhomogeneous anisotropic tissue conductivities using FA on EEG forward computing using a spherical head model. We have implemented the multi-steps FA to generate anisotropic conductivity and various anisotropy ratios to generate inhomogeneity. From our simulated results, we find that there are significant effects of WM and skull inhomogeneous anisotropic tissue conductivities either solely or combined on EEG. We also find that inhomogeneous and anisotropic conductivities produce fewer errors than the homogeneous isotropic conductivity.

5.3.5 The Monte Carlo method based conductivity model

This subsection shows the effects of inhomogeneous and anisotropic tissue conductivities generated using the Monte Carlo method based conductivity model on EEG forward computation.

5.3.5.1 Simulation

We carry out this simulation, based on the head geometry, segmentation, tessellation and electrode positions are similar to other head model frames described in 5.2.2. We construct a heterogeneous anisotropic head models by assigning the Monte Carlo method based conductivity model. This model generates inhomogeneous and anisotropic conductivities using mean, standard deviation and Normal distribution based random numbers. These random numbers are selected using the Volume and Wang's constraint and are considered as inhomogeneous and anisotropic conductivities. We place 104 dipoles inside the brain. We analyze the obtained EEGs by means of the RDM and MAG values.

5.3.5.2 Simulation results

Table 5.13 shows the RDM and MAG values produced by WM inhomogeneous anisotropic conductivities. These errors are between the homogeneous isotropic (reference head model) and the heterogeneous anisotropic model. Incorporating inhomogeneous anisotropic WM conductivities, we find substantial RDM and MAG errors, which are different from their ideal values. Therefore, these results also demonstrate that the effects of inhomogeneous anisotropic WM conductivity on EEG are significant.

Table 5.13: Average RDM and MAG errors for the WM inhomogeneous and anisotropic conductivities for the orthogonal dipole orientations of X, Y and Z.

Constraint	Conductivity	Error (avg)	X	Y	Z
Volume	Tangential	RDM	128%	123%	128%
		MAG	2.29	0.30	0.25
	Radial	RDM	143%	102%	94%
		MAG	4.88	1.06	1.24
Wang	Tangential	RDM	143%	92%	92%
		MAG	1.79	0.69	0.64
	Radial	RDM	109%	65%	76%
		MAG	4.33	1.30	0.92

Table 5.14 shows the resulting average RDM and MAG errors from the skull inhomogeneous anisotropy conductivities. This conductivity model leads to the highest average RDM errors of 145%, 169%, and 171% for X, Y and Z orientations,

respectively. The lowest average errors for these orientations are 119%, 49% and 59%, respectively. On the other hand, the highest average MAG errors are 6.95, 1.75 and 1.95 while the lowest average MAG errors are 1.94, 0.27 and 0.18 for different orientations, respectively. In comparison with Volume and Wang's constraints, we observe that the Volume constraint produces larger errors than Wang's constraint. In most of the cases, the MAG values produced by different radial conductivities are larger than those by different tangential conductivities. Similarly, Table 5.15 shows the average RDM and MAG values from combined WM and skull inhomogeneous anisotropic conductivities. From Tables 5.14 and 5.15, we understand the effects of inhomogeneous and anisotropic conductivities on EEG are non-negligible.

Table 5.14: Average RDM and MAG errors for the skull inhomogeneous and anisotropic conductivities for the orthogonal dipole orientations of X, Y and Z.

Constraint	Conductivity	Error (avg)	X	Y	Z
Volume	Tangential	RDM	124%	169%	171%
		MAG	2.76	0.36	0.18
	Radial	RDM	145%	73%	89%
		MAG	6.95	1.75	1.95
Wang	Tangential	RDM	119%	131%	124%
		MAG	1.96	0.27	0.24
	Radial	RDM	125%	49%	59%
		MAG	1.94	1.2	0.62

Table 5.15: Average RDM and MAG errors for the WM and skull inhomogeneous and anisotropic conductivities for the orthogonal dipole orientations of X, Y and Z.

Constraint	Conductivity	Error (avg)	X	Y	Z
Volume	Tangential	RDM	132%	158%	164%
		MAG	2.61	0.49	0.48
	Radial	RDM	129%	63%	93%
		MAG	5.98	1.44	1.91
Wang	Tangential	RDM	128%	111%	117%
		MAG	1.39	0.46	0.33
	Radial	RDM	108%	38%	43%
		MAG	1.34	1.02	0.81

5.3.5.3 Conclusion

In this study, we investigate the effects of inhomogeneous anisotropic conductivities on the scalp potentials. We develop different head models by assigning the inhomogeneous and anisotropic conductivities to WM, skull, and both the WM and the skull while other tissue layers are homogeneous and isotropic. We then compute

a forward computation for 104 dipoles using the finite element method. This study shows that including inhomogeneous anisotropic conductivity results in the maximum of 171% RDM and the maximum of 0.24 MAG values when comparing with the homogeneous isotropic model.

5.3.6 Effects of conductivity variations on EEG

5.3.6.1 Objective of the study

Conductivity varies from person to person or in different situations. More clearly, conductivity depends on blood cells, especially red cells or blood circulation. It is found that conductivity usually varies in $\pm 50\%$ of its mean value [Hauelsen *et al* 1997]. In this study, we investigate the effects of conductivity variation ranging from 10% to 100% mean anisotropic conductivity on EEG.

5.3.6.2 Head model construction

We also implement a different head model (Bashar 2008a) with the radii of 9.2cm for scalp, 8.4cm for skull, 8.0cm for CSF, 7.6cm for GM and 3.0cm for WM. The mesh generation produces 93K tetrahedral elements from 16K nodes. There are 24845, 27510, 23775, 16322 and 588 elements for different tissue layers, respectively. For the inhomogeneous anisotropic case, inhomogeneous anisotropic conductivities are assigned to individual elements. We perform a forward computation for a fixed current source with the azimuth angle $\pi/4$ and elevation angle $\pi/5$. Then RDM and MAG values are computed to analyze the results. We conduct these computations using an Intel® dual core 2.0 Ghz processor. It takes approximately 18 minutes to carry out each computation.

5.3.6.3 Simulation setting and computing

Shimony (1999) showed that the shape of diffusion ellipsoids are strongly prolate (“cigar –shaped”) whereas they found gray matter as closely isotropic. It is also found that the PDF of Rayleigh distribution follows the cigar shape. Therefore, we assume the conductivities of the elements follow Rayleigh distribution:

$$f(\sigma, m) = \frac{x}{m^2} e^{\left(\frac{-\sigma^2}{2m^2}\right)}, \quad \dots\dots\dots (5.7)$$

where σ is conductivity and m is maximum likelihood estimator. The curve of PDF depends on m which measures the spread of the distribution as shown in Figure 5.4.

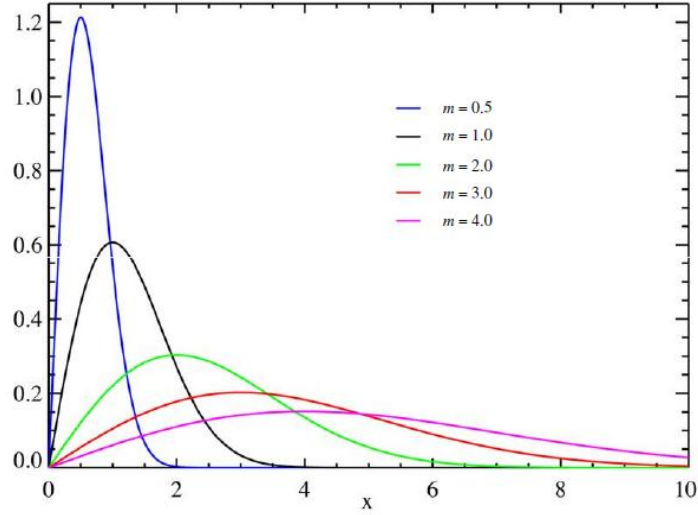
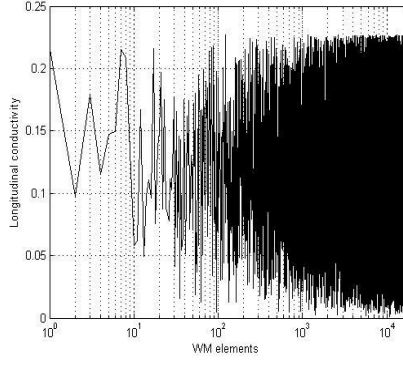


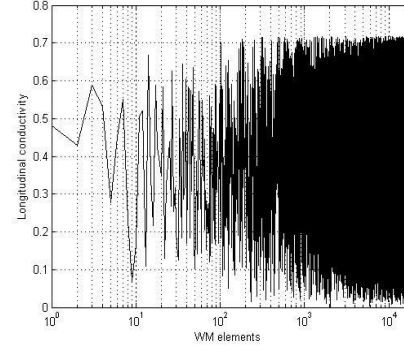
Figure 5.4: Probability density function of Rayleigh distribution [Rayleigh distribution

For the smaller values of m , the curve produces the highest peak and sharp slopes. Thus, it means that the conductivities of the elements within the tissue are centred on the mean. For larger values of m the curve produces less peak and spread slopes. Therefore, changing m corresponds to exploring the inhomogeneity. In this study, we assume that $m=0$ expresses the conductivities of the elements within a tissue centred on the mean value for homogeneous isotropic model. Alternatively, increasing the value of m , the conductivities of the elements are more widely spread for inhomogeneous anisotropic model.

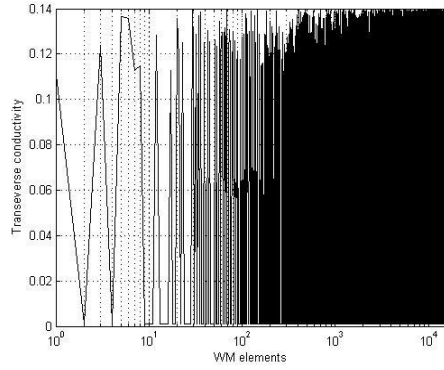
Based on our assumption in Equation (5.7), a set of random data can be derived for a tissue type, from the limited data available in the literature [Bashar *et al* 2008a]. Then, we determine the anisotropic inhomogeneous conductivity values for WM and skull elements by using the SCA technique. Based on the SCA method and varying m from 10% to 100%, we determine different inhomogeneous anisotropic conductivities. Figure 5.5 plots anisotropic conductivity values for the WM and skull when $m=0.1 \times \text{mean}$ and $m=1.0 \times \text{mean}$.



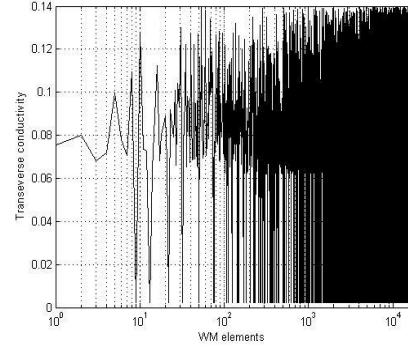
(a) longitudinal conductivity ($m = 0.1 \times \text{mean}$)



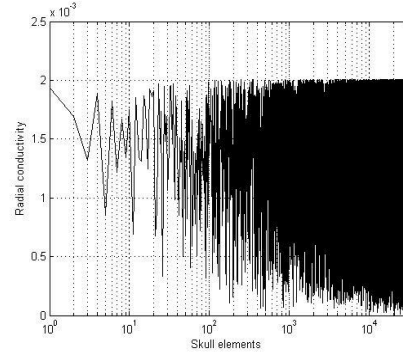
(b) longitudinal conductivity ($m = 0.1 \times \text{mean}$)



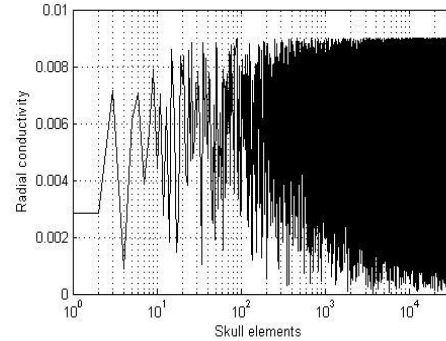
(c) transverse conductivity ($m = 0.1 \times \text{mean}$)



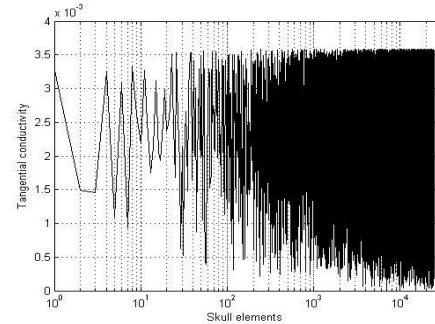
(d) transverse conductivity ($m = 1.0 \times \text{mean}$)



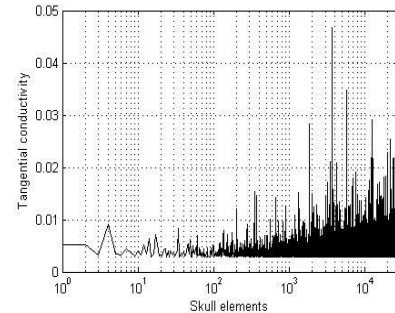
(e) radial conductivity ($m = 0.1 \times \text{mean}$)



(f) radial conductivity ($m = 1.0 \times \text{mean}$)



(g) tangential conductivity ($m = 0.1 \times \text{mean}$)



(h) tangential conductivity ($m = 1.0 \times \text{mean}$)

Figure 5.5: Inhomogeneous anisotropic conductivities produced by SCA. (a)–(d) WM elements and (e)–(h) skull elements.

For this study, we carry out two types of experiments. Firstly, we compute the scalp electric potentials using tissue mean conductivity for isotropic

homogeneous case. Secondly, we calculate the electric potentials using the conductivities produced by SCA with varying m for inhomogeneous anisotropic case. Table 5.16 shows the RDM and MAG values for longitudinal conductivities. The RDM and MAG measurements show the effects of changes in inhomogeneity. For all the cases, The RDM and MAG values are away from their ideal values. As a result, we find that there are certain effects of anisotropic inhomogeneity on isotropic homogeneity. When m is increased from $0.1 \times \text{mean}$ to $1.0 \times \text{mean}$, the RDM values are about 7.5% and MAG values are between 1.40 and 2.49, increasing gradually. When $m < 0.5 \times \text{mean}$ the MAG values are less than 2; however, it increases more than 2 for $m > 0.5 \times \text{mean}$. Thus, we find that the local variations in the conductivity within elements have certain effects on electrical potential distribution. For skull elements, RDM (3.8 % and 2.2%) and MAG (0.9266 and 0.9483) values of $0.1 \times \text{mean}$ and $0.2 \times \text{mean}$ for skull elements differ from ideal values; however, the other RDM and MAG values are very close to ideal values. Thus, we observe that there is a very low effect of skull anisotropy inhomogeneity on EEG in this simulation. Finally, we find the combination of WM and skull anisotropy inhomogeneity has similar effects like WM anisotropy inhomogeneity on EEG.

Table 5.17 shows the RDM and MAG measurements for various values m produced by transverse conductivities. The RDM values are between 7.8% and 7.5%, and the MAG values are between 1.06 and 1.27, close to ideal values. The RDM values are non-negligible while MAG values are close to ideal values. Thus we understand that transverse conductivities are affected by inhomogeneity but not as strongly as longitudinal conductivities. For the skull elements, all the RDM and MAG values are very close to ideal values. For the combination of WM and skull elements, we find similar results to WM elements.

Table 5.16: RDM and MAG values produced by longitudinal conductivities.

	WM elements		Skull elements		WM + skull elements	
m	RDM	MAG	RDM	MAG	RDM	MAG
$0.1 \times \text{mean}$	7.5 %	1.4066	3.8%	0.9266	5.4%	1.2295
$0.2 \times \text{mean}$	7.5 %	1.6143	2.2 %	0.9483	5.6%	1.4809
$0.3 \times \text{mean}$	7.5 %	1.7452	0.0%	0.9993	7.5%	1.7436
$0.5 \times \text{mean}$	7.4 %	2.0089	0.0%	0.9999	7.4%	2.0089
$0.7 \times \text{mean}$	7.4%	2.1928	0.0%	1.0003	7.4%	2.1937
$1.0 \times \text{mean}$	7.4 %	2.4861	0.0%	1.0008	7.4%	2.4800

Table 5.17: RDM and MAG values produced by transverse conductivities.

	WM elements		Skull elements		WM + skull elements	
m	RDM	MAG	RDM	MAG	RDM	MAG
$0.1 \times \text{mean}$	7.8 %	1.0626	0.0%	0.9970	7.9%	1.0578
$0.2 \times \text{mean}$	7.5 %	1.1963	0.0%	0.9982	7.5%	1.1929
$0.3 \times \text{mean}$	7.7 %	1.2321	0.0%	1.0	7.9%	1.2331
$0.5 \times \text{mean}$	7.5 %	1.2652	0.0%	1.0	7.5%	1.2656
$0.7 \times \text{mean}$	7.5%	1.2688	0.0%	0.9999	7.5%	1.2667
$1.0 \times \text{mean}$	7.5 %	1.2580	0.0%	0.9998	7.5%	1.2576

5.3.6.4 Conclusion

This study demonstrates the effects of conductivity variations for the implementation of the WM and skull anisotropic inhomogeneity on EEG. This inhomogeneity within a tissue is based on the variations of mean conductivity values ranging from 10% to 100%. This study finds that there are 7.4% to 7.8% RDM and 0.92 to 2.48 MAG values for conductivity variations. This study also confirms that neglecting tissue anisotropic inhomogeneity and variations of mean conductivity would cause an inaccurate computation.

5.3.7 Implementation of inhomogeneous anisotropic conductivities using a stochastic FEM

5.3.7.1 Objective of the study

Computational EEG models include many input parameters, such as the geometric discretization of different head tissue layers or compartments, the conductivities of the tissues, and the representation of electric sources. In the case of the forward problem, tissue conductivity is an example of an input parameter which is very difficult to accurately obtain because of its inhomogeneous and anisotropic properties. Therefore, a full accounting of tissue inhomogeneity and anisotropy for all the tissues in the human head has yet to be performed.

This sub-section uses a spherical head model with stochastic FEM (SFEM) to investigate the magnitude of EEG for analyzing the effects of inhomogeneity and anisotropy of the head tissues. To implement SFEM, we employ a stochastic Galerkin method [Geneser *et al* 2008, Bashar *et al* 2010a] to solve polynomial chaos representation of the stochastic system. This method represents a stochastic process via orthogonal polynomials of random variables using Karhunen-Loeve expansion (Bashar *et al* 2010a). We apply the stochastic Galerkin method to the EEG forward

problem. This method has been successfully applied to tackle the uncertainty issue of the electrocardiographic forward problem [Geneser *et al* 2008] and other stochastic magnetic field problems [Enokizono *et al* 1987].

5.3.7.3 Simulation setup

Under the assumptions of Karhunen-Loeve expansion and stochastic Galerkin method, we define the conductivity values as [Bashar *et al* 2010a]:

$$\underline{\underline{\sigma}}(x; \vec{v}) = \underline{\underline{\hat{\sigma}}}_0(x) \lambda_0(\vec{v}) + \underline{\underline{\hat{\sigma}}}_1(x) \lambda_1(\vec{v}) + \underline{\underline{\hat{\sigma}}}_2(x) \lambda_2(\vec{v}) \dots \quad (5.8)$$

where $\underline{\underline{\sigma}}(x; \vec{v})$ is uniformly distributed on the interval $[a(x), b(x)]$ for each element.

Intervals for anisotropic tissue conductivities are selected to follow the Volume constraint and Wang's constraint. For example, the value of longitudinal conductivity for Volume constrained WM is 0.14 S/m for isotropic or 1:1 anisotropy ratio and 0.65 S/m for 1:10 anisotropy ratio. In this case, we select $a(x)$ and $b(x)$ in such a way that the obtained values are within the range of $[0.14 \ 0.65]$. We derive the scalp conductivity interval from the scalp inhomogeneous study, described in Section 3.5.4. We also assume the first term, middle term and last term of equation (5.8) for three inhomogeneous head tissue compartments, WM, skull and scalp, respectively. For analyzing individual tissue compartments, we use the corresponding conductivity term while putting zero value to other conductivity terms. For example, we use the first term ($\underline{\underline{\hat{\sigma}}}_0$) of equation (5.8) to analyze WM tissue compartment by putting $\underline{\underline{\hat{\sigma}}}_1 = \underline{\underline{\hat{\sigma}}}_2 = 0$.

We place six fixed dipoles at a starting point from 2mm outer of WM to 2mm below the cortex surface inside the GM with the elevation angles $\pi/5.22$, $\pi/4.67$, $\pi/4.0$, $\pi/3.86$, $\pi/3.83$ and $\pi/3.77$ radians with fixed azimuth angle $\pi/4$.

In the case of FEM or deterministic FEM, we employ homogeneous isotropic conductivity. However, in the case of SFEM, we use 50% uniform interval (0.5 times to 1.5 times of the mean conductivity value) conductivity values for inhomogeneous tissue compartment. Moreover, we employ constraints to restrict the conductivities for anisotropic tissue compartments.

Finally, we compute the potentials on the scalp (EEG). Based on the computed potentials, we select our EEG data from N points where EEG electrodes are located. We perform forward computation for six different models:

Model A: EEG using FEM (deterministic FEM).

Model B and C: EEG using SFEM for WM and skull tissue layers, respectively.

Model D: EEG using SFEM for both WM and skull tissue layers.

Model E: EEG using SFEM for inhomogeneous scalp conductivities.

Model F: EEG for a complete inhomogeneous anisotropic head model combining Model D and Model E together.

The EEG computed from model A is defined as a reference model. However, EEGs obtained from other models are considered as computed models. To quantify the differences between the reference and computed models, we use two measurements: relative error (ε) and correlation coefficient (η) defined in equations (5.3) and (5.4), respectively.

5.3.7.4 Simulation results

We compare the EEG obtained from the model A with other computed models for X, Y and Z orthogonal dipole orientations.

Model B: WM tissue conductivity

Figure 5.6 shows the resulting average ε and η for longitudinal and transversal conductivities on either Volume or Wang's constrained WM from six different dipoles. In Figure 5.6, *V* represents Volume constraint, *W* represents Wang's constraint, and *long* and *trans* represent longitudinal and transversal conductivities, respectively. For example, *Vlong* presents a computed head model based on the longitudinal conductivity for the Volume constrained WM. Due to the variations of conductivities, computed EEGs and the reference EEG are not identical, and as a consequence, we obtain different average values of ε and η for three X, Y and Z orientations. We observe that there are some effects of inhomogeneous anisotropic WM tissue properties on EEG. From the obtained results, we find that the average values of ε range from 31% to 72% and η values are between 0.47 and 0.98.

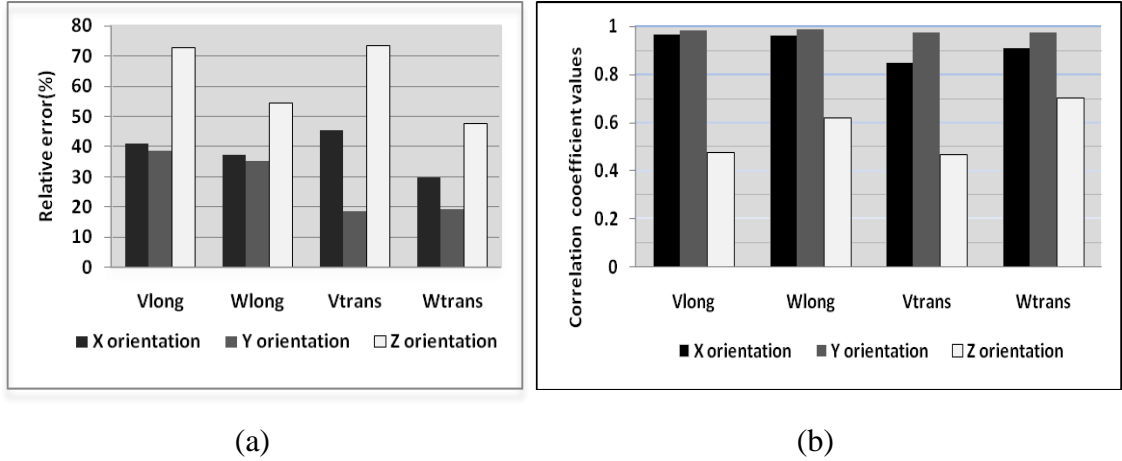


Figure 5.6: Effects of inhomogeneous anisotropic WM conductivity on EEG: (a) relative errors (ϵ) values (in percentage) and (b) correlation coefficient (η) values.

For Wang's constrained WM, it obtains 37% to 54% and between 0.96 and 0.63 average values for ϵ and η respectively. These average values for Wang's constraint are between 19% and 47% for ϵ and from 0.97 to 0.70 for η . Therefore, we conclude that constrained inhomogeneous anisotropic WM has both relative residual and coefficient correlation effects on EEG. To analyze dipole eccentricities, we model the dipoles from 2mm outer the WM surface to 2mm inner the cortex. As a result, dipole eccentricity starts from 0.76 and finishes to 0.87. Dipole eccentricity is the ratio between the dipole position from the centre of the sphere and the radius of outer surface [Marin *et al* 1998, Wang and He 1998]. We compared the scalp potentials generated by reference (V_{ref}) and computed (V_{comp}) head models varying the dipole eccentricities. We find that the results are virtually insensitive to dipole eccentricity.

Model C: skull tissue conductivity

For the case of inhomogeneous anisotropic skull conductivities analysis for both constraints, Figure 5.7 shows the resulting average ϵ and η errors where *rad* and *tan* represent the radial and the tangential conductivities, respectively. For example, *Vtan* represents a head model constructed by assigning tangential conductivity for the Volume constrained skull compartment. From the obtained results, we realize that inhomogeneous anisotropic conductivities on constrained skull have 19% to 96% average relative effects on EEG in our experimental cases. To analyze the dipole eccentricities for the skull compartment, we find the same results; namely, the results are virtually insensitive to dipole eccentricity.

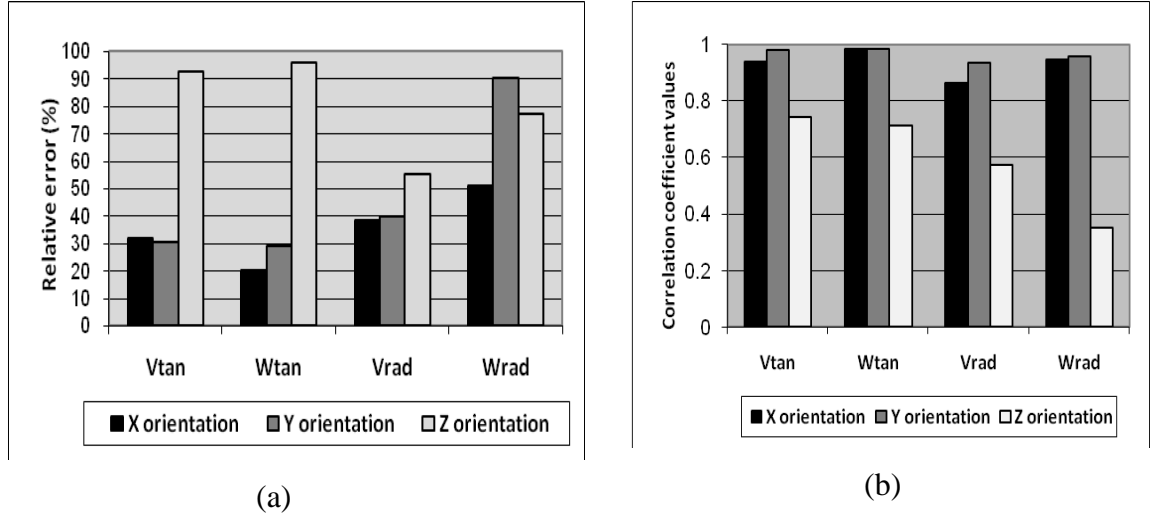


Figure 5.7: Effects of inhomogeneous anisotropic skull conductivity on EEG: (a) relative errors (ϵ) values (in percentage) and (b) correlation coefficient (η) values.

Model D: WM + skull tissue conductivity

Figure 5.8 shows the effects of including tissue properties for both the WM and the skull compartments applying either the Volume or the Wang's constraint where *par* and *per* represent the parallel and the perpendicular conductivities, respectively. Incorporating parallel conductivities (longitudinal for the WM and tangential for the skull) generates an average of 35% to 57% and 34% to 48% ϵ for Volume and Wang's constraints, respectively. The same conductivities generate an average of 0.98 to 0.59 and 0.98 to 0.69 values for ϵ values, for both compartments, respectively. Similarly, incorporating perpendicular conductivities (transversal for WM and radial for skull) generates 22% to 65% average ϵ and 0.97 to 0.57 average correlation coefficient values for Volume constrained compartments, 28% to 65% ϵ and 0.95 to 0.56 correlation coefficient values for Wang's constrained compartments. In most of the cases, Model D generates smaller differences than Model B or Model C, as Model B is more affected by parallel conductivity and Model C is more affected by perpendicular conductivity.

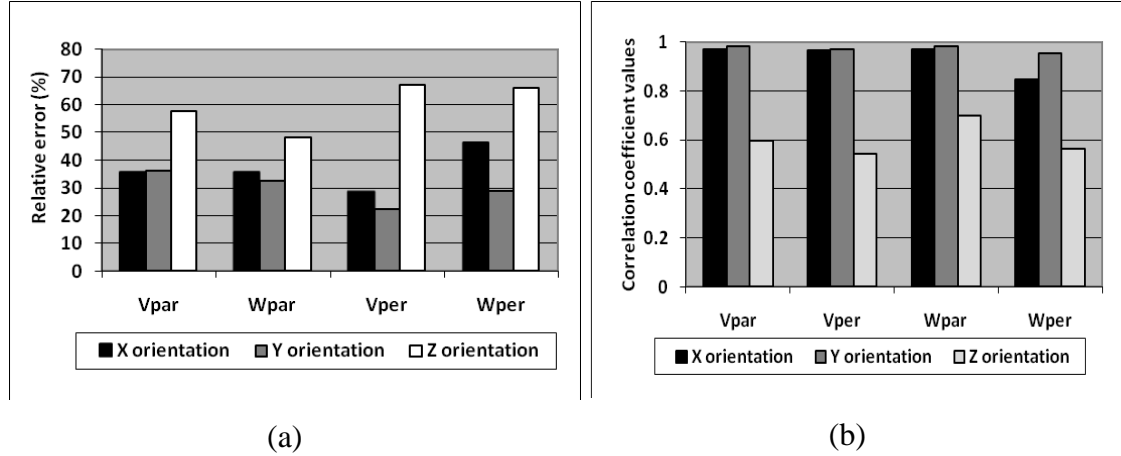


Figure 5.8: Effects of inhomogeneous anisotropic WM and skull conductivities together on EEG: (a) relative errors (ϵ) values (in percentage) and (b) correlation coefficient (η) values.

Model E: scalp tissue conductivity

Table 5.18 shows average effects of incorporating scalp inhomogeneous conductivity for different sources. The average relative errors are in the ranges from 21% to 37% and average correlation coefficient values are between 0.96 and 0.82. Therefore, we find that scalp tissue inhomogeneity affects EEG.

Table 5.18: Effects of inhomogeneous scalp tissue conductivity on EEG:

	X orientation	Y orientation	Z orientation
Relative error (ϵ)	27.21%	21.28%	37.57%
Correlation coefficient (η)	0.9312	0.9683	0.8274

Model F: Complete head tissue conductivity

Effects of including inhomogeneous and anisotropic head tissue properties are shown in Figure 5.9. Analyzing average ϵ and η values for different EEGs from six dipoles, we find that average ϵ ranges between 35% and 57% for the parallel conductivity using the Volume constraint, and its average values vary from 32% to 48% for the Wang's constraint. Similarly, the average values of η are between 0.59 and 0.98 for the Volume constraint, and those values are from 0.69 to 0.98 for the Wang's constraint conductivity.

Including tissue inhomogeneous and anisotropic properties into a complete head model construction, we observe that it results in an average of 45.5% relative errors and 0.78 for η values which are very close to model D. Analyzing the variations of conductivities for different tissue layers, it is observed that the

combined effect of conductivities is not additive, and thus cannot be predicted by the individual behaviour of each tissue layer.

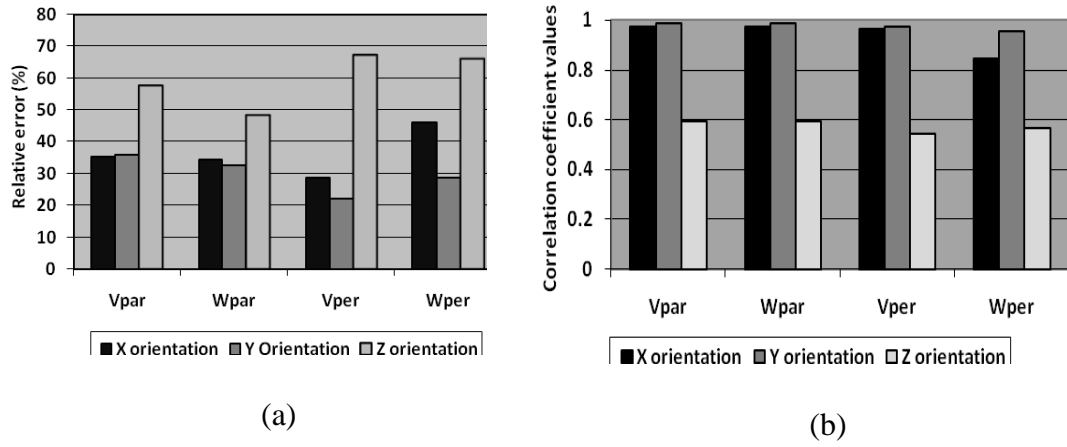


Figure 5.9: Effects of inhomogeneous anisotropic head model on EEG: (a) relative errors (ϵ) values (in percentage) and (b) correlation coefficient (η) values.

Figure 5.10 shows the topographic visualization of the obtained EEGs to observe the differences of the scalp potentials from different forward computations by varying the conductivities. We make visualization of the scalp potentials by adopting and feeding our obtained EEGs to the ASA. Figure 5.10 shows the obtained scalp potentials from the first dipole (elevation angles $\pi/5.22$ and azimuth angle $\pi/4$) in the back-front view of a head. To reduce the space, we only represent the scalp potentials from the head models (A) and (D). We observe that the potential distributions are different. This has happened due to the assigned conductivity. Different head models are constructed from different conductivity models which affect the forward computation and in turn, the scalp potentials. We easily understand that including inhomogeneous anisotropic tissue properties significantly affect the EEG. Figure 5.10(a) shows the scalp potentials generated by the reference Model A. Figures 5.10(b) to 5.10(e) show scalp potentials for different conductivities of Model (D). Visualizing other computed Figures (not included here), we observe that conductivity variations result in the variations of scalp potentials.

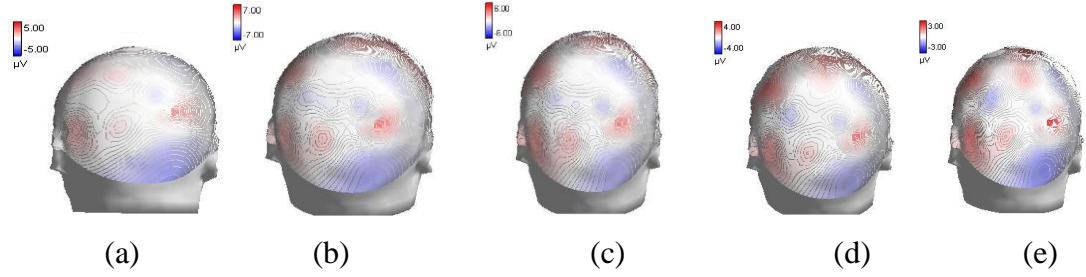


Figure 5.10: Topographic visualization of the scalp electrode potentials. (a) head model (A) and head model (D): (b) from the parallel Volume constraint, (c) from the parallel Wang's constraint, (d) from the perpendicular Volume constraint and (e) from the perpendicular Wang's constraint conductivity for the first dipole (elevation angles $\pi/5.22$ and azimuth angle $\pi/4$).

5.3.7.5 Conclusion

Comparing the stochastic model to the homogeneous isotropic model (Section 5.2) for WM, we find that these models generate fewer errors in most of the cases. We find that only limited errors, such as (70%) generated by the stochastic model is higher than the homogeneous isotropic model (64%), however, most errors are less. Apparently, this implemented stochastic method based conductivity model results in fewer errors than those most commonly used models in the literature.

The obtained EEG using the stochastic model is compared to homogeneous isotropic models (Section 5.2) for the skull and found that homogeneous isotropic model generates larger error. For instance, 49%, 58% and 53% for η and 0.76, 0.83 and 0.65 values of ε for X, Y and Z orientations, respectively, are results by this model for Volume constrained radial conductivity. However, the stochastic model generates 39%, 40% and 55% for η and 0.87, 0.94 and 0.60 ε values, respectively. The η values obtained from the stochastic computed model are closer to the ideal value 1. In one instance, stochastic model shows 2% higher error (55%) than this model (53%) while other errors are less. Therefore, we can envisage that our achievements on inhomogeneous anisotropic constrained skull tissue layer result in less errors compared to another anisotropic model.

5.4 Conclusion and Contribution

It is a prominent goal to construct an accurate head model which would include object specific head geometry from MRI and *in vivo* conductivity. However, it is impossible to obtain subject specific *in vivo* conductivity. For example, the skull

anisotropy also depends on skull bone thickness which is also variable and varies from person to person. As the thickness of the skull bone varies, the anisotropy ratio and conductivities also change. Considering all this information, we propose different conductivity models (CRA, SCA, FA based and the Monte Carlo method based conductivity model) to implement inhomogeneous and variable anisotropy ratio based head models.

Using CRA, we find 6.47% to 47% RDM and 0.71 to 1.49 MAG values. SCA produces 5.09% to 43.12% RDM and 0.71 to 1.53 MAG values. Similarly, FA shows 4.04% to 20.39% RDM and 0.84 to 1.11 MAG values, and the Monte Carlo method produces 38% to 171% RDM and 0.30 to 6.95 MAG values. On the other hand, the stochastic method based model shows 18% to 95% RE and 0.37 to 0.99 CC values. Conductivity variations also show 7.4% to 7.8% RDM and 0.92 to 2.48 MAG values. Analyzing these simulated results, we find that there are some non negligible effects of inhomogeneous anisotropic conductivities on EEG and the inhomogeneous conductivity variations also have an effect on EEG. We also compare the effects of inhomogeneous anisotropic conductivities from various anisotropy ratios, which produce fewer errors than the fixed or homogeneous anisotropic conductivity in most of the cases in our simulation. Therefore, this study concludes that the inclusion of inhomogeneous anisotropic conductivities is necessary to construct a more accurate head model for EEG forward computation.

CHAPTER 6

ADVANCED STUDY

Variations of conductivity in the intervening medium between the sources of the electric fields and the measurement points (electrodes positions) affect the behaviour of the electric fields; consequently, influencing the EEG and source localization. Therefore, local variations in the conductivity within tissues should be accounted for in head modelling. In the first part, we introduce local tissue conductivity and show its effects on EEG. In the second part of this Chapter, an application of head modelling is described by means of EEG analysis from normal and Alzheimer's disease (AD) sources.

6.1 Local Tissue Conductivity

6.1.1 Aims of this study

The aim of this Section is to investigate the effects of local tissue conductivity (LTC) on head modelling for the computation of EEG. We implement the LTC based head model by assigning the tissue conductivity based on their locations. We compare the EEG obtained from the LTC based head model, with the EEG from the homogeneous head model for the same sources. Finally, we analyze the results by means of two statistical measurements, RDM and MAG.

6.1.2 Introduction

Though most literature assumes the homogeneous conductivity for each head tissue layer, however, the conductivity of different parts of each head tissue layer is different in reality. For example, the presence of suture lines increases the skull conductivity and the absence of cancellous bone decreases the skull conductivity [Law 1993]. Similarly, the complex composition of GM, WM, blood, nerve, cerebellum in the brain [Ramon *et al* 2006a,b, Haueisen *et al* 1997] causes different

conductivities in a brain tissue layer and the presence of thick subcutaneous fat beneath the skin causes different conductivities in a scalp tissue layer [Petrofsky 2008]. Thus, the inclusion of accurate tissue conductivity in the appropriate location (local tissue conductivity) into a head model should be effective in obtaining a more accurate head model.

Awada *et al* (1998) studied conductivity uncertainties by assigning lower and higher conductivity values of GM, WM, CSF, skull, fat and muscle for analyzing source localizing errors in 1998. Their experiments resulted in a maximum 2cm source location error. In 2000, Ferree *et al* (2000) studied regional head tissue conductivities based on the conductivity of the brain, CSF, skull and scalp tissues. Vatta *et al* (2002a, b) accounted liquid and calcified brain lesion with various conductivities for source localization in 2002. They found 1.7cm source localization errors and conclude that brain lesions should be accounted for, for accurate head modelling. Ramon *et al* (2006a,b) investigated the influence of head models on EEG source localization using eleven different types of tissue. They emphasized mainly the scalp tissue layer (scalp, fat, muscle, eye socket and soft tissue) and the brain tissue layer (WM, GM and cerebellum). They used only skull hard and soft bone layers without concern for suture lines and other tissues. They concluded that the complexity of head models influences the scalp potentials and source localization. On the other hand, Ni *et al* (2008) studied only skull conductivity inhomogeneity considering compact bone, spongiform bone, lambdoid and coronal sutures without concern for the scalp and brain conductivity inhomogeneity. They found 45.38% maximum correlation errors for inhomogeneous skull conductivity. Therefore, it is obvious that a full accounting for all of the head tissues is required to be investigated, for accuracy in head modelling.

Several studies have been performed to investigate the effects of heterogeneous or non-uniform conductivity in the head on the EEG forward problem [Ary *et al* 1981, Ramon *et al* 2004a,b, Haueisen *et al* 2000, Haueisen *et al* 2002, Bashar *et al* 2008b] and inverse problem [Ramon *et al* 2006a,b, Awada *et al* 1998, Vatta *et al* 2002a, Ferree *et al* 2000, Ni *et al* 2008, Ollikainen *et al* 1999] using either spherical or realistic head models. The true fact of the improvement of the head model is the inclusion of more accurate conductivity of the head tissues. For this reason, the spherical head model improves from a single sphere to three-spheres, four-spheres, five-spheres and N-spheres. Therefore, a question arises; does this

phenomenon mean that the human head can be modeled using N-spheres with different conductivity? If the conductivity in the N-spheres model is wrongly assigned, then how would it affect an EEG? We attempt to answer these questions by means of local tissue conductivity.

6.1.3 Local tissue conductivity based head model I

6.1.3.1 Spherical head model construction

Three-layered spherical head model [Marin *et al* 1998, Bin He *et al* 1999] and four-layered spherical head model [Wen 2000, Wen and Li 2006] are considered with different radii for different tissue layers. We consider $r_1 = 8.7\text{cm}$, $r_2 = 9.2\text{cm}$ and $r_3 = 10.0\text{cm}$ for the outer radii of the brain, skull and scalp, respectively, for a three-layered model. For a four-layered model, we consider $r_1 = 7.9\text{cm}$, $r_2 = 8.1\text{cm}$, $r_3 = 8.5\text{cm}$ and $r_4 = 8.8\text{cm}$ for the radius of the brain, CSF, skull and scalp, respectively. For head modelling, we implement LTC in the following way.

The brain tissue layer consists of GM, WM, blood vessels, cerebellum, nerve and other tissues. These tissues comprise the brain. For example, the GM is found in left / right (L/R) accumbens, Amygdala, L/R amygdala anterior, L/R Caudate, L/R Cerebral cortex, L/R hippocampus, L/R pallidum, L/R putamen, L/R thalamus and L/R ventral [Makis *et al* 2008]. Haueisen *et al* (2002) and Ramon *et al* (2004a,b, 2006a,b) implemented the brain model using GM, WM, spinal cord and cerebellum. However, accurate head model construction requires accounting for brain lesion [Bruno *et al* 2001, Vatta *et al* 2002a,b], which is filled either with calcium or liquid. It is variable in shape and position. Based on the literature and anatomical structure we approximate the brain tissue layer into GM, WM, cerebellum, blood vessels, nerves or neurons, calcified brain lesion and liquid brain lesion. We consider GM and WM as the maximum tissues of the brain and the cerebellum with 4.0cm diameter. The area of the cerebellum is approximately 14cm^2 . We set a calcified and a liquid lesion in the brain. The area of these brain lesions are approximately 3.56cm^2 each.

For the creation of a skull layer, Ni *et al* (2008) accounted three bony layers and two suture lines (coronal and lambdoid). We approximate the skull tissue layer into three layers: upper cortical (hard), inner cancellous (soft) and lower cortical (hard) bone. The thickness of these bone layers is non uniform. For the sake of

simplicity during computer simulation, we consider only the non uniform skull with fixed thickness. For example, in the case of a three-layered head model, we consider 0.1cm thickness for the compact bone layers, 0.3cm thickness for the cancellous bone layer and the total thickness of the skull is 0.5cm (8.7cm to 9.2cm). We consider 18 sutures into the triple layer skull. Two cavities with 0.3cm diameter are also considered. These cavities are in variable shapes, filled with air and usually stay in random positions.

In the construction of the scalp tissue layer, Haueisen *et al* (2002) and Ramon *et al* (2004a,b, 2006a,b) implemented muscle, fat, eye socket, scalp and soft tissue. Muscle is contractile usually found in the forehead and neck regions. Soft tissue is beneath the lower jaw [Ramon *et al* 2006a]. In the approximation of the scalp tissue layer, we do not concern ourselves with muscle, eye socket and soft bone because we consider only the upper part of the head where most of the electrodes reside. In lieu of these tissues, we consider wet skin tissues because of using liquid gel to contact electrodes on the head surface during EEG recording. We assume 65 equally spaced electrodes with 20mm diameter each. The fat layer is beneath the skin or scalp layer. The scalp and fat layers are assumed equal in thickness. For example, each layer is 0.4cm thickness combining the total scalp thickness (0.8cm) for the three-layered model. Based on these assumptions, we approximate local tissue conductivity as shown in Figure 6.1 for the three-layered model.

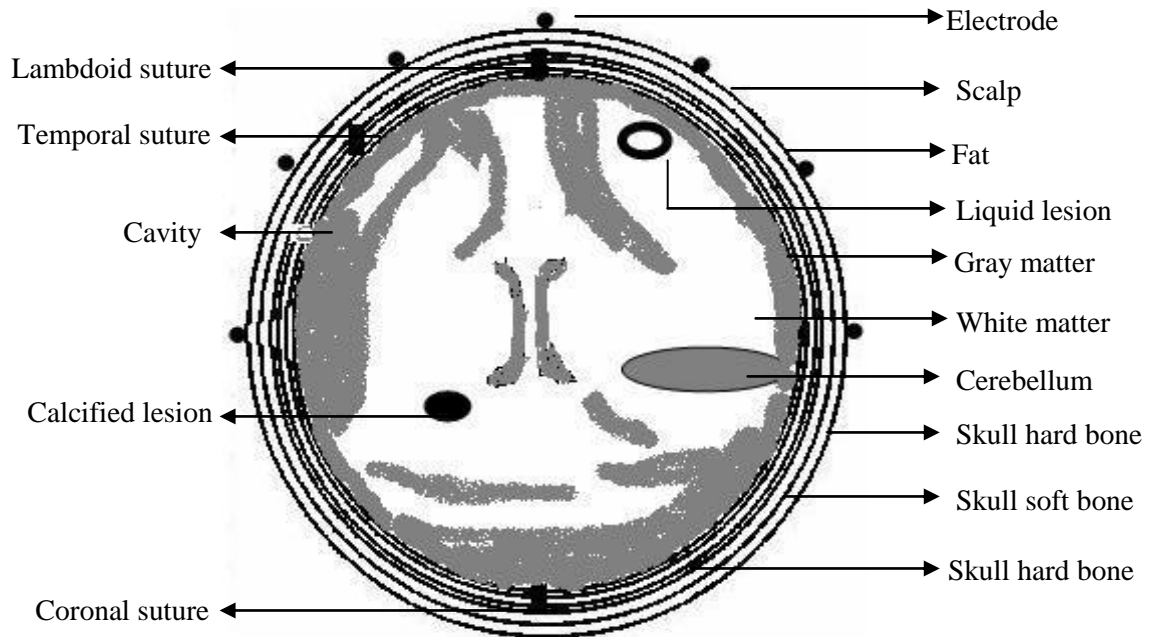


Figure 6.1: Simplified local tissue conductivity based three-layered spherical head model showing different tissues [Bashar *et al* 2010d].

Figure 6.2 shows an example of the local tissue conductivity approximation for the scalp tissue layer for the same model. X axis of Figure 6.2 represents 77535 scalp elements and Y axis represents scalp, wet skin and fat conductivities.

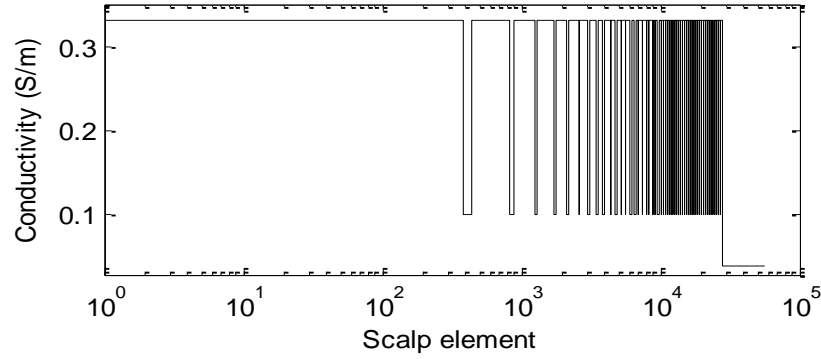


Figure 6.2: Local scalp tissue conductivity approximation. The conductivity for scalp (skin) is 0.33 S/m, wet skin (place of electrodes) is 0.1 S/m and fat is 0.04 S/m [Bashar *et al* 2010d].

To investigate how it would affect an EEG if the conductivity is wrongly specified, we perform $\pm 2\%$, $\pm 4\%$ and $\pm 6\%$ alterations of principal tissues. We are motivated for this study for two reasons. Positional variation of brain and CSF may have happened because of subject's position. MRI data is usually collected while the subject is in a supine position; however EEG data is collected while the subject is in sitting position [Ramon *et al* 2006a]. As a consequence, there might positional changes between the brain and CSF. The other reason is that if a tissue is damaged due to stroke, it will be filled eventually by CSF [Ramon *et al* 2006b]. We fill the altered brain tissues by CSF. For the skull and scalp's principal tissue variations, we fill these with other non principal tissues. To implement this, we alter the size of the principal tissue(s) restricting the size of the tissue layer. For example, we decrease the number of tissues of WM and GM by 2%, and fill by CSF. Therefore, the total size of the brain or total number of brain elements remains constant. It is to be noted that we only add one more CSF layer to construct the four-layered model. We consider CSF as a homogeneous tissue layer.

6.1.3.2 Realistic head model construction

A realistic head model construction is similar to the spherical head model construction except an inputted MRI and its segmentation. We follow the following

steps: (A) input an MRI; (B) segment the MRI and classify its tissues, and the other steps are identical to the (B) to (G) steps of the spherical head model construction described in Section 5.1.1. Figure 6.3 shows the block diagram of a realistic head model construction.

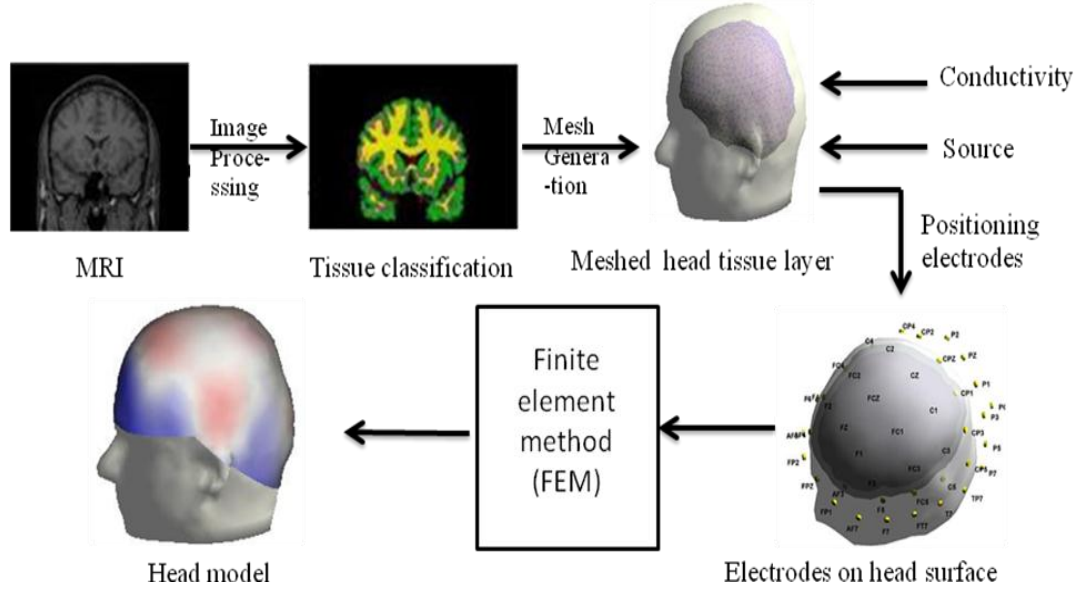


Figure 6.3 A realistic head model construction.

For the realistic head model construction, we use T1 weighted MRI image of $149 \times 188 \times 148$ (x, y, z) dimensions and $1.00 \times 1.00 \times 100$ (x, y, z) resolutions having 8MB in disk size from the World Wide Web of BrainSuite2. The head tissue segmentation is carried out using the tool BrainSuite2. Firstly, non-brain tissues are removed from the MRI using a combination of anisotropic diffusion filtering, Marr-Hildreth edge detection and mathematical morphology [Shattuck *et al* 2001, 2002, 2005, Dogdas *et al* 2005]. Secondly, each voxel is classified according to its tissue type by combining the partial volume tissue model with a Gibbs spatial prior to produce a classifier, which encourages continuous regions of similar tissue types [Shattuck *et al* 2001]. Finally, skull and scalp modelling is performed using threshold parameters. We then perform mesh generation and other head model construction procedures similar to the spherical head model construction. We manually further divided each of the tissue layers into different tissues to assign LTC with the same concept of the three-layered model construction.

In order to assign local conductivity, we approximate the tissues according to the description of the spherical head model sub-section. We also compute tissue

variations ($\pm 2\%$, $\pm 4\%$ and $\pm 6\%$) and construct head models in the similar method as stated above.

6.1.3.3 Conductivity assignment

Firstly, we assign a homogeneous constant conductivity for each tissue layer. We use $\sigma_{\text{brain}} = 0.33 \text{ S/m}$, $\sigma_{\text{skull}} = 0.0042 \text{ S/m}$ and $\sigma_{\text{scalp}} = 0.33 \text{ S/m}$ for a reference model of a three-layered spherical head model. We incorporate only $\sigma_{\text{CSF}} = 1.0 \text{ S/m}$ in addition to other tissue layers of the three-layered model for either a four-layered spherical head model or for a realistic head model. We address these models as reference models for the corresponding head geometry.

Secondly, we assign LTC to the brain, skull and scalp tissues. In some computations, we assign LTC to a single tissue layer, such as the brain, skull and scalp or sometimes, we assign to multiple tissue layers, for example brain + skull, brain + scalp, skull + scalp and brain + skull + scalp. We address these models as the LTC models. Any head models, except the reference model, are considered as computed models. Therefore, an LTC model is also a computed model. We assign the local conductivities obtaining from different studies listed in Table 3.4, Chapter 3.

Thirdly, we assign the LTC to each tissue for the brain, skull and scalp layers; however we vary the locations of tissues by implementing $\pm 2\%$, $\pm 4\%$ and $\pm 6\%$ principal tissue variations. We address these models as element variation models, which are also computed models.

6.1.3.4 Simulations

We construct finite element head mesh using the Tetgen® package as a bundle with FEM tool from BrainStorm2 online package. The FEM mesh of a three-layered model consists of 332K tetrahedral elements from 32K nodes. This head geometry is used to compute scalp potentials for a three-layered reference head model. We also implement LTC and element variation models with a constant number of total head elements in the three-layered model. Similarly, a four-layered spherical head model is meshed into 275K tetrahedral elements from 48K nodes. A four-layered reference head model is constructed where homogeneous conductivity to each tissue layer is assigned. For a realistic head model construction, an MRI is tessellated into 101K

brain tissues from 17K nodes by means of the same Tetgen® software. This head geometry is used for the realistic reference head model [Bashar *et al* 2010c,d,e].

We implement the forward computation using FEM based on an equivalent current dipole method with 1 μ A magnitude assuming the dipoles are in the somatosensory cortex (SC) and thalamus. To obtain scalp potentials, 65 electrodes (including the reference electrode) residing at different positions on the head surface are used. These obtained potentials are used for further analysis. The simulations are carried out as follows:

1. To study the effects of local conductivity on EEG forward computation, we compute scalp potentials by assigning the LTC to a head tissue layer or multiple tissue layers while conductivities in remaining tissue layers are constant.
2. To study how it would affect an EEG if conductivity is wrongly assigned, we compute scalp potentials by assigning the LTC using element variation models.

For comparison of the computed scalp potentials we use RDM and MAG errors.

6.1.3.5 Simulation results

Three-layered spherical head model

These simulations are conducted with the SC and thalamic dipoles. Figure 6.4 shows the RDM and MAG errors caused by local conductivity assignment to individual or collective head tissue layers for LTC based models. The experimental results demonstrate that assigning local conductivity results in higher changes in potentials which cause RDM and MAG errors. Individual scalp local conductivity results in fewer RDM (0.93 for the SC and 0.84 for the thalamic sources) errors and the brain local conductivity causes higher RDM errors (1.46 for the SC and close to 1.46 for the thalamic sources). The scalp local conductivity results in fewer MAG errors for both sources. Combining the brain and skull's local conductivities cause higher MAG errors. Though these errors do not present collective errors, but it shows significant changes on scalp potentials. It is also found that the thalamic sources generate less RDM and MAG errors than those of the SC sources.

Implementing element variation models by changing the number of principal elements for different head tissue layers and assigning the LTC, we also obtain significant scalp potentials differences. We compare these models with unvarying

head geometry and a homogeneous constant conductivity based model for both sources. The results of this comparison are shown in Table 6.1 in terms of RDM and MAG errors for different head tissue layers. The simulated results shown in Table 6.1 demonstrate that there are substantial effects of tissue element variations on scalp potentials. By implementing brain element variations (BEV) we obtain 1.09 average RDM and 2.64 average MAG errors. BEV produces the maximum 1.23 RDM and 4.07 MAG errors. With the changing of these principal elements, the conductivity of the entire brain layer is also changed. As a consequence, these changed conductivities affect the forward computation to compute scalp potentials, which result in RDM and MAG errors.

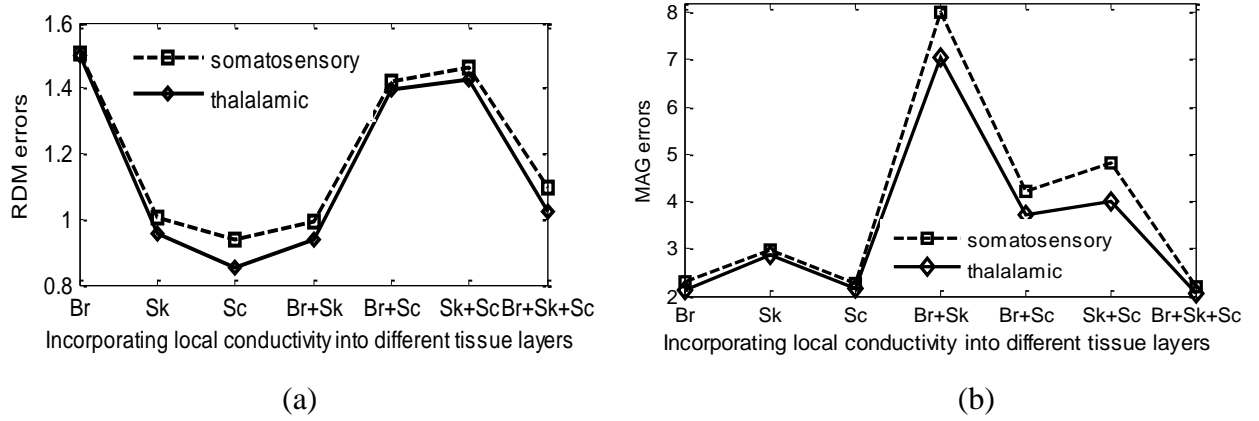


Figure 6.4: (a) RDM and (b) MAG from assigning local conductivity to different layers in a three-layered spherical head model using the SC and the thalamic dipoles. In the above figures, label *Br*, *Sk* and *Sc* represent brain, skull and scalp, respectively.

Table 6.1: Effects of conductivity variations in three-layered spherical head model.

Tissue layer	Source	Error	-6%	-4%	-2%	+2%	+4%	+6%
Brain	SC	RDM	1.12	1.2	1.16	1.23	1.13	0.82
		MAG	1.51	2.95	3.4	2.57	4.07	2.24
	Thalamic	RDM	0.95	1.18	1.14	1.22	1.09	0.77
		MAG	1.28	2.61	3.00	2.28	3.4	2.11
Skull	SC	RDM	1.06	0.97	0.91	1.05	1.04	1.06
		MAG	2.83	2.72	1.99	2.72	2.06	2.47
	Thalamic	RDM	1.02	0.93	0.84	1.0	0.97	1.02
		MAG	2.73	2.63	1.95	2.63	1.98	2.37
Scalp	SC	RDM	0.79	0.88	0.85	0.97	1.15	1.41
		MAG	2.39	2.98	2.83	2.45	2.55	2.95
	Thalamic	RDM	0.74	0.84	0.80	0.89	1.07	1.35
		MAG	2.19	2.68	2.58	2.33	2.41	2.51

In a similar way, we implement skull element variations (SEV) and scalp element variations (SCEV). In SEV, we obtain 0.99 and 2.43 average RDM and MAG errors, respectively. RDM errors lie between 0.84 and 1.06, and MAG errors range from 1.95 to 2.83. Mean RDM and MAG errors for SCEV are found as 0.98 and 2.58, respectively. The minimum RDM (0.74) is found in -6% variations for the thalamic source and the maximum value (1.41) is found in -4% variations for the somatosensory cortex source. Thalamic sourced -6% variations produce a minimum MAG while SC sourced +6% variations produce a maximum MAG value. In all of the element variations cases, it is apparent that the SC sourced scalp potentials generate higher RDM and MAG errors than those of the thalamic sources.

Four-layered spherical head model

Effects of including local conductivity in either a head tissue layer or collective head tissue layers are shown in Figure 6.5 in terms of RDM and MAG errors. These errors are from both the SC and thalamic sources. Models including single or multiple local conductivity layers incur significant changes in scalp potentials compared to those that incorporate homogeneous constant conductivity for the corresponding tissue layers. From these results, it is demonstrated that incorporating local conductivity into the brain and skull layers incurs maximum RDM and MAG errors for both sources.

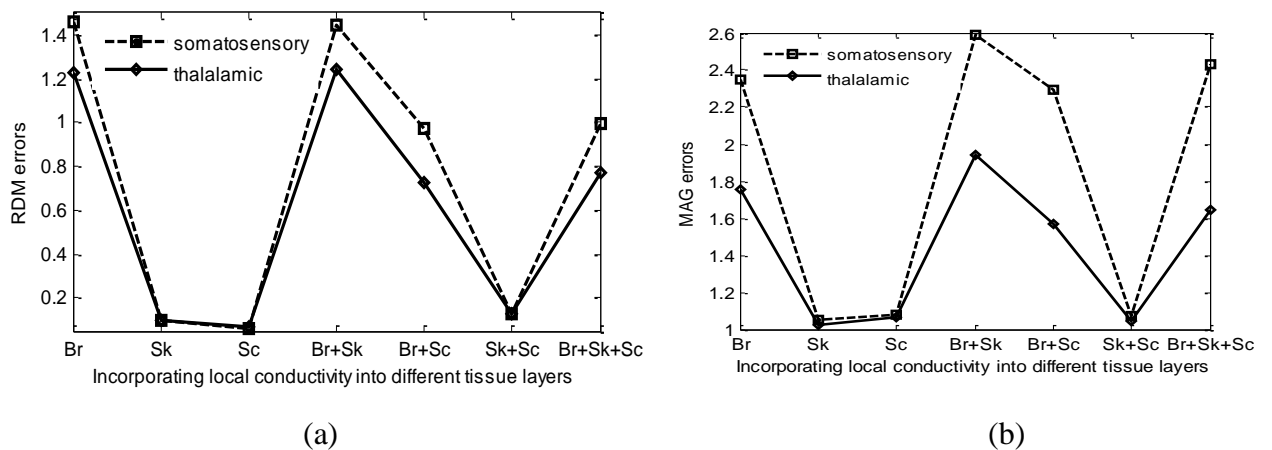


Figure 6.5: (a) RDM and (b) MAG from assigning local conductivity to different layers in a four-layered spherical head model using the somatosensory cortex and the thalamic dipoles.

In the above figures, label *Br*, *Sk* and *Sc* represent the brain, skull and scalp, respectively.

In order to compute the effects of element variations for the four-layered model, we consider only the brain, skull and scalp tissue layers. In this research, we consider CSF as a highly conductive homogeneous medium. Element variations in the four-layered model produce substantial changes in scalp potentials. Table 6.2 shows RDM and MAG errors incorporating element variations for both sources. BEV results in an average of 1.33 RDM and 2.51 MAG errors, SEV results in an average of 0.09 RDM and 1.03 MAG, and SCEV causes an average of 0.08 RDM and 1.06 MAG errors. In BEV, the minimum RDM is found in -2% variations for the thalamic source and the maximum RDM is found in +6% variations for the SC source. However, negative element variations (-2%, -4% and -6%) produce similar 1.71 MAG values for the thalamic source. The maximum MAG value (5.64) is found in +6% variations for the SC source. In SEV, we find the minimal changes in overall potentials resulting in low RDM and MAG errors. These errors are close to their ideal values of 0 and 1, respectively. It produces the maximum of 11% RDM and 1.06 MAG errors. The MAG values produced by the thalamic source are less sensitive than those of the SC source. In SCEV, the maximum RDM and MAG values are 0.10 and 1.08, respectively. Similar to BEV and SEV, SCEV is also more sensitive for the SC source than the thalamic source. Analyzing all element variations (BEV, SEV and SCEV), the simulation results demonstrate that the effect of element variations is non negligible and element variations in brain tissue layer cause a very high impact on EEG.

Table 6.2: Effects of conductivity variations in four-layered spherical head model.

Tissue layer	Source	Error	-6%	-4%	-2%	+2%	+4%	+6%
Brain	SC	RDM	1.45	1.45	1.45	1.45	1.35	1.49
		MAG	2.34	2.35	2.32	2.34	3.18	5.64
	Thalamic	RDM	1.22	1.23	1.21	1.22	1.22	1.23
		MAG	1.71	1.71	1.71	1.73	2.48	2.58
Skull	SC	RDM	0.10	0.10	0.11	0.09	0.9	0.08
		MAG	1.05	1.05	1.05	1.06	1.06	1.06
	Thalamic	RDM	0.10	0.10	0.10	0.09	0.09	0.08
		MAG	1.0	1.0	1.0	1.01	1.01	1.01
Scalp	SC	RDM	0.10	0.09	0.07	0.08	0.07	0.07
		MAG	1.07	1.07	1.08	1.08	1.08	1.08
	Thalamic	RDM	0.10	0.09	0.07	0.08	0.07	0.07
		MAG	1.03	1.03	1.04	1.04	1.05	1.05

Realistic head model

Figure 6.6 shows RDM and MAG errors for the realistic head model similar to those shown in Figures 6.4 and 6.5 for spherical head models. Simulation results demonstrate that assigning local conductivity incurs significant changes in the scalp potentials that cause RDM and MAG errors. Incorporating local conductivity into the brain tissue layer causes higher RDM errors. Associating local conductivity into multiple tissue layers results in similar RDM values. However, a single brain tissue layer incurs fewer MAG errors in comparison to other collective local conductivities assigned into multiple tissue layers, such as brain + skull (Br+Sk), brain + scalp (Br+sc) and brain + skull + scalp (Br+Sk+Sc). From Figure 6.6, it is apparent that the SC sourced scalp potential values are higher than those of the thalamic sources in most of the cases.

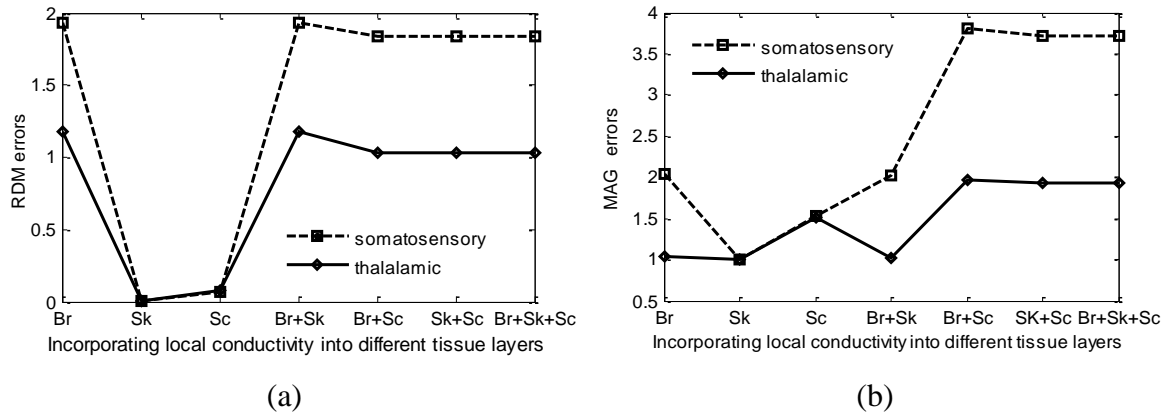


Figure 6.6: (a) RDM and (b) MAG from assigning the local conductivity to different layers in the realistic head model for both dipoles. Labels are similar to Figure 6.3.

Table 6.3 shows RDM and MAG values produced by element variations for realistic head models. BEV produces the mean RDM and MAG errors as 1.93 and 1.64, with the minimums of 1.92 and 0.76, and the maximums of 1.95 and 2.79, respectively. The minimum MAG error is found in -4% element variations for the thalamic source and the maximum RDM value is found in +6% element variations for the SC source. Zero percent mean RDM error and 0.99 mean MAG errors are found for SEV, which are almost the same as their ideal values of 0 and 1, respectively. The results demonstrate that there is no significant change using skull element variations. SCEV causes an average of 0.15 RDM and 1.25 MAG errors. The minimum RDM is found in +6% element variations for both sources and the

maximum value is found in +6% element variations for the SC source. The minimum MAG value (1.19) is found in -4% element variations for the thalamic source. Analyzing these results from the experiment, we find that BEV has a strong effect, SEV has less effect on scalp potentials and the SC source is more sensitive than the thalamic source.

Table 6.3: Effects of element variations assigning local conductivity in realistic head model.

Tissue layer	Source	Error	-6%	-4%	-2%	+2%	+4%	+6%
Brain	SC	RDM	1.93	1.93	1.93	1.92	1.93	1.93
		MAG	2.75	2.74	2.04	1.94	2.11	2.79
	Thalamic	RDM	1.95	1.95	1.94	1.94	1.94	1.95
		MAG	0.77	0.76	1.04	0.95	1.06	0.81
Skull	SC	RDM	0.0	0.00	0.00	0.01	0.01	0.01
		MAG	0.99	1.00	0.99	0.99	0.99	0.99
	Thalamic	RDM	0.00	0.00	0.00	0.00	0.01	0.00
		MAG	0.99	1.0	0.99	0.99	0.99	0.99
Scalp	SC	RDM	0.14	0.16	0.15	0.14	0.16	0.12
		MAG	1.21	1.2	1.22	1.30	1.28	1.34
	Thalamic	RDM	0.13	0.15	0.15	0.14	0.16	0.12
		MAG	1.2	1.19	1.21	1.29	1.27	1.33

6.1.4 Local tissue conductivity based head model II

6.1.4.1 Head models construction

In this head model construction, we assign the same local tissue conductivity as described above for the brain, but we further develop the conductivity assignment method to the skull and scalp.

For the assignment of the skull LTC, we consider the local tissues and their conductivity according to the literature [Law 1993]. Law estimated skull conductivity on twenty different positions using a 10-20 electrode system and reported that skull resistivity varies due to its anatomical structure, such as non-uniform thickness of hard and soft bones, presence of suture lines, etc. Table 6.4 shows the skull conductivity obtained from reported skull resistivity by Law. T3M, C3M, C4M and T4M are not found in the 10-20 electrode system. Therefore, we assume that these places are shown by T3, C3, C4 and T4, respectively in the 10-20 electrode system.

Table 6.4: Skull conductivity, width and features at different places [Law 1993].

Locations	Conductivity (S/m)	Width (cm)	Distinguishable
FPZ	0.01504	0.52	Frontal crest
F3	0.01779	0.62	
F1	0.01284	0.45	
FZ	0.01129	0.50	
F2	0.01475	0.47	Arachnoid pits
F8	0.01015	0.37	
T5	0.01196	0.44	
T3M	0.00467	0.47	Compact bone
C3M	0.01368	0.55	
CZ	0.02538	0.47	Suture line
C4M	0.01580	0.60	
C4	0.01764	0.62	
T4M	0.00787	0.46	Compact bone
T6	0.01282	0.49	
P3	0.01520	0.50	
PZ	0.02825	0.47	Suture line
P4	0.01109	0.50	
O1	0.02841	0.62	
OZ	0.07353	0.68	Suture line
O2	0.01215	0.50	Suture line

*The letter 'F' represents frontal, 'P' represents parietal, 'T' represents temporal, 'O' represents occipital lobes. 'C' represents for central and 'Z' stands for midline identification purposes. The even numbered digits represent right hemisphere and odd numbered are on left hemisphere.

There are 18 suture lines in the human head but five suture lines are mostly visible on the head surface [Gray 2002, Law 1993]. The suture lines on the skull surface are the lambdoid suture, medial sagittal suture, coronal suture, metopic suture and squamous or temporal suture [Gray 2002, Law 1993]. Law (1993) also reported the resistivity of four suture lines. Another medial sagittal suture line is on the central region Pz to Fz of the Inion and Nasion. Therefore, we do not consider the conductivity of suture lines individually. In the case of the scalp tissue layer, the skin and the fat are only considered.

6.1.4.2 Simulation and results

We also construct the head models as our previous study for different source positions. These positions are: (A) single dipole in somatosensory cortex, (B) 200 dipoles in the entire brain and (C) a cortical dipole layer [Wang and He 1998, Aoki *et al* 2006, Hori and He 2007].

For the dipole position A, we compare the scalp potentials between the reference and computed head models generated by the same dipole position in the somatosensory cortex. It is found that there are the value of 12% in RDM and 1.14 in MAG errors when we incorporate local tissue conductivity.

For dipole position B, the scalp potentials are computed by residing 200 dipoles in the entire brain region for both head models. We do not follow any order to place the dipoles. We place 50 dipoles in the cortex, 10 dipoles are in the vicinity of each calcified and liquid brain lesions, 50 are in the thalamus, and the remaining 80 dipoles are scattered between cortex and thalamus. The RDM and MAG errors for each dipole are computed and finally, the average RDM and MAG errors are calculated. From the simulated results, it is found that average RDM is 14% and average MAG is 0.2660. We separately compute an average of RDM and MAG errors produced by the dipoles in the vicinity of each lesion. It shows that the dipoles in the vicinity of calcified brain lesion results in an average of 19% RDM and 0.89 MAG errors. On the other hand, the dipoles in the vicinity of brain lesion results in an average of 9% RDM and 0.94 MAG errors.

For the simulation of dipole position C, we compute the scalp potentials generated by a cortical dipole layer (CDL) where 500 dipoles are placed at 4mm beneath the brain to CSF boundary. Similar to the simulation for dipole position B, we compute the RDM and MAG errors for each dipole and then make its average. We find that incorporation of LTC incurs an average of 50% RDM ranging between 13% and 78%. On the other hand, we find an average of 0.56 MAG errors with the minimum 0.7580 and maximum 1.14.

We also compute the RDM and MAG errors by making the dipole bunches (DB) from the dipoles of the CDL. To make the DB, we assume the dipoles in the corresponding lobe. For example, we make frontal DB by assuming all dipoles that are in the frontal lobe. Similarly, we make parietal DB, temporal DB and Occipital DB. Our simulation results show that parietal DB produces fewer RDM and MAG errors and Occipital DB generate higher RDM and MAG errors.

6.1.4.3 Discussion

Conductivity plays a vital role in the computation of EEG forward problem that have an effect on scalp potentials. For example, in the case of skull, the homogeneous conductivity is 0.0042 S/m in the reference model. However, the conductivity values

of the frontal, parietal, occipital and temporal regions of the skull are different (shown in Table 6.4) in the LTC based head model. Similarly, the brain and the scalp have different conductivities. The results in this study demonstrate that the effects of local tissue conductivity on the computation of scalp potentials are significant.

Dipole position also affects the scalp potentials. We find that the thalamic sources result in relatively fewer scalp potential variations than those by the cortical dipolar sources. The currents from a deeper source spread inside the brain and reach to the scalp electrodes through a larger portion of low conductive skull. However, a superficial source residing on the cortex beneath the skull layer allows close contact to scalp electrodes. As a result, a superficial source results in substantial variations in electrode potentials. Dipoles in the vicinity of the lesions cause significant changes in scalp potentials [Awada *et al* 1998, Bruno *et al* 2002]. Our LTC based head model also shows a result consistent with other literature.

The dipoles of the CDL are surrounded at 4mm below the brain boundary for all the brain regions. The gap between the dipoles and the scalp electrodes are filled by high conductive CSF, low conductive skull and scalp. The conductivity of the skull is highly dependent on the thickness of skull, presence of suture lines and absence of soft bone. Similarly, the scalp conductivity also depends on the muscle layer and subcutaneous fat layer. The muscle is usually found in the left and right temporal and occipital regions [Gray 2002]. There is a high resistance from subcutaneous fat. The thickness of fat layer is non uniform. With a thick subcutaneous fat layer in people who are overweight, this subcutaneous resistivity would be higher than that seen in thin people. The thicker the fat layer, the greater the resistance. The thickness of the subcutaneous fat layer is directly related to the loss on the scalp potentials [Petrofsky 2008]. As a result, dipoles of the CDL generate very different scalp potentials.

The conductivity in the parietal region of the skull is lower than the conductivity of occipital region (shown in Table 6.4). It is logical that the RDM and MAG errors generated by parietal DB would be higher than those of occipital DB. However, the presence of subcutaneous fat layer causes a great difference in scalp potentials. The conductivity of fat is eight times lower than the scalp conductivity. Another region is source and electrode distance. There are only limited electrodes on the occipital region and most dipoles are on the parietal and frontal regions of the scalp. The distance between the dipoles in the occipital DB and electrodes on frontal

region of the scalp are high. As a result, current from occipital DB spreads into the brain and passes a greater area of skull to the scalp electrodes. On the other hand, there is no thick fat layer in the parietal region and the sources are close to the electrodes. Therefore, the dipoles in the parietal DB cause less error.

6.2 EEG analysis on Alzheimer's disease sources

6.2.1 Aims of this study

In this study, we aim to show: (A) the feasibility to improve the neurological evaluation and study more precisely the EEGs from normal source (in somatosensory cortex) and Alzheimer's disease sources (in hippocampus), (B) a preliminary quantitative estimation of errors due to varying sources and (C) the variations of EEG due to different brain tissue distortion levels to address the effects of different levels of dementia.

6.2.2 Introduction

Alzheimer's disease (AD) [Kloppel *et al* 2008, Mosconi *et al* 2006, Chetelat *et al* 2008] is one of the challenging research areas for brain scientists for decades. AD is a neurodegenerative disorder which alters the structure and function of brain. Therefore, it is important to detect AD as early as possible because treatment may be most effective if introduced earlier. In practice, the diagnosis of AD is largely based on clinical history and different examinations supported by neuropsychological evidence of the pattern of cognitive impairments [Kloppel *et al* 2008]. However, in reality, only fifty percentage of probable AD is detected in the primary case.

The reason for, and progression of AD is not well understood so far. Primarily, some investigation indicates that the disease is associated with plaques and tangles in the brain. Plaques are extracellular deposits of amyloid in the GM of the brain. The plaques are flexible in shape and size, but are on the average of 50 μ m. The population of people with plaques almost linearly increases after the age of 60. Tangles are formed by a kind of protein known as tau causing it to aggregate in an insoluble form. Based on the aggregation of proteins into GM tissues of brain, dementia (caused by AD) is characterized into four classes: predementia, early

dementia, moderate dementia and advanced dementia. Predementia, the first symptoms of AD are often mistaken as related to aging or stress. Early dementia leads to difficulties with language, executive functions or movements and perception. These symptoms are more prominent than memory problems. Speech difficulties become evident due to an inability to recall vocabulary, which leads to frequent incorrect word substitutions in moderate dementia. Advanced dementia is the last step of this neurological disorder.

To develop prevention treatment for AD, it is necessary to identify early biological markers for AD prediction. The best recognized *in vivo* markers of AD are measures of brain structure and function as obtained with neuroimaging. Structural imaging with either CT or T1 weighted MRI allows brain atrophy to be assessed in *in vivo* [Baron *et al* 2001]. Different studies [Baron *et al* 2001, Smith and Jobst, 1996] in the early stages of AD have consistently reported that, the first brain region to be affected by atrophy is the medial temporal lobe, which comprises the hippocampus proper, the parahippocampal gyrus and the amygdala. The study by Chupi *et al* (2007) is also consistent regarding the sources of AD. They performed the segmentation of hippocampus and amygdala for constrained region deformation by AD. EEG has an important role in the evaluation of certain neurological disorders based on their criteria.

Most studies [Patel *et al* 2008, Polikar *et al* 2007] analyse event related potentials (ERPs) of EEG recorded from different candidates and controls, to diagnose early detection of AD. Topographic maps of the spectral power of EEG provide information that helps differentiating neurological disorders for various neurological cases. Other studies [Kloppel *et al* 2008, Chetelat *et al* 2008] perform MRI segmentation scanned from candidates and controls, to show the changes of GM inside the brain to diagnose AD and to understand its severity.

6.2.3 Methods

We use the same head model with same number of tessellated elements illustrated in the previous sections. However, we use different sources.

6.2.3.1 Finite element conductivity

The tetrahedra or elements of head tissues are labelled according to their compartment memberships. The following isotropic conductivities [Awada *et al* 1997, Haueisen *et al* 1997, Gullmar *et al* 2006] are assigned to brain (σ_{brain}) = 0.33S/m, CSF (σ_{CSF}) = 1.0 S/m, skull (σ_{skull}) = 0.0042 S/ and scalp (σ_{scalp}) = 0.33 S/m. AD is caused from the deposition of unsaturated tau protein in brain tissues. We assume that tau protein consumes fat resistivity. Haueisen *et al* (1997) measured resistivity of human head tissues and found 2500 Ωcm mean value with 1500 Ωcm lower bound and 5000 Ωcm upper bound values for fat tissues. Awada *et al* (1997) accounted 0.02 S/m and 0.05 S/m conductivity values for fat tissues. Therefore, we assign 0.04 S/m mean conductivity values for the AD regions (distorted brain tissues).

6.2.3.2 Source Modelling

The dipole located at SC in the parietal lobe is addressed as a normal source and AD sources are addressed by the dipole positioned in right amygdala (RA) and left amygdala (LA) in hippocampus of medial temporal lobe. Figure 6.7 shows different parts of brain.

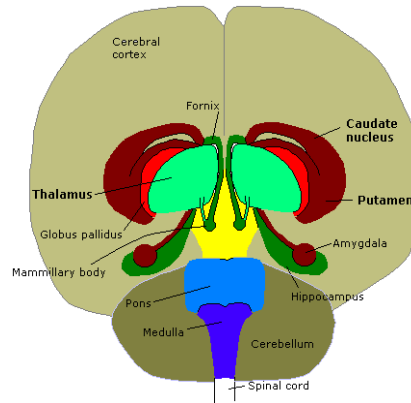


Figure 6.7: The brain is viewed from the outer side and front with the hippocampus and amygdala [Amygdala].

Figure 6.8 shows an example of dipole location for RA source in MRI. We choose the dipole situated in SC as a reference dipole. By surveying different studies [Baron *et al* 2001, Smith and Jobst, 1996] we find that the source of AD resides in the hippocampus. Therefore, we choose to set other sources either in RA or LA to investigate how it would affect an EEG. We consider the dipole located in axial,

coronal and sagittal planes with magnitude of 1 μA using equivalent current dipole method.

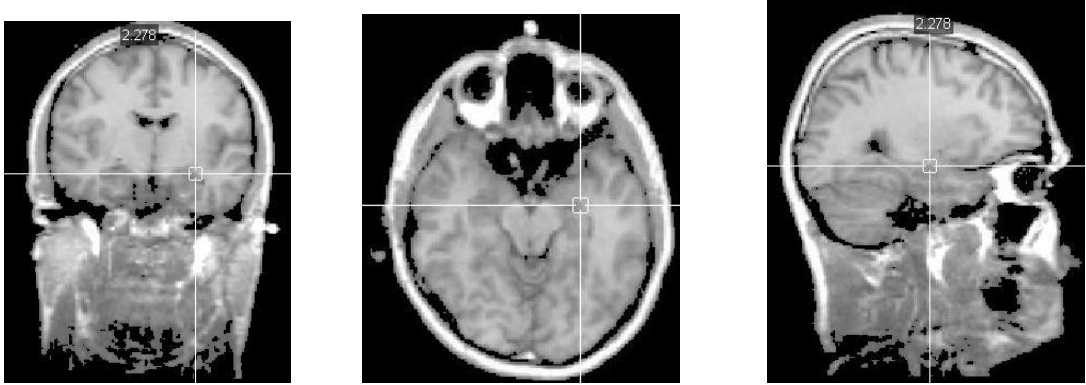


Figure 6.8: Location of one of the AD sources in RA by the cross hairs in different views.

6.2.3.3 Simulation and results

The realistic head model is from the same MRI and methods in our previous study with the sources in SC, RA and LA locations. We assign homogeneous isotropic conductivity to each tissue. We also developed other four realistic head models with 5%, 10%, 15% and 20% distorted brain elements, respectively. The head model from the homogeneous isotropic conductivity without distorted brain elements is defined as a reference head model while other models are computed models.

We first compare the scalp potentials obtained from two AD sources (RA and LA) to those of normal (SC) sourced EEG. We find that RA and LA sourced potentials result in 61.97% to 197.12% RDM errors, and 0.21 to 0.07 MAG errors, respectively. Analyzing these errors, we find that the scalp potentials originated from AD sources differ from the SC source and also exhibit less scalp potentials.

Figure 6.9 shows RDM and MAG errors where scalp potentials of computed head models are from different brain tissue distortion levels (BTDLs). These comparisons are made with the reference model from the same source of the computed models. For instance, we compare the EEGs obtained from 5% BTDL for the SC source as computed model to the EEGs obtained from the reference model for the same SC source. Similarly, we perform the same computations for other BTDLs. RDM errors are between 10% and 28% and MAG errors are in the range of 0.98 to 1.09. RA sourced BTDLs show higher RDM and SC sourced BTDLs show higher

MAG errors. We find that 10% distortion level is more sensitive than other BTDLs in both RDM and MAG respects.

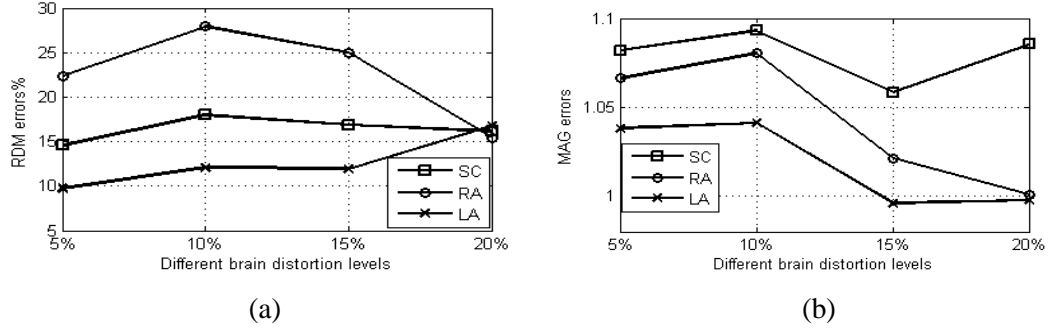


Figure 6.9: RDM (a) and MAG (b) errors from different brain tissue distortion levels on source to source basis.

Figure 6.10 shows RDM and MAG errors where the computed models are from the AD sources and reference model from the SC source. In Figure 6.10, normal represents a model without any brain tissue distortion. RA shows 59% to 61% RDM and 0.21 to 0.23 MAG errors, while 197% RDM and 0.076 to 0.08 MAG errors are shown by LA sourced EEG. We observe that RA generates less RDM and MAG errors than LA.

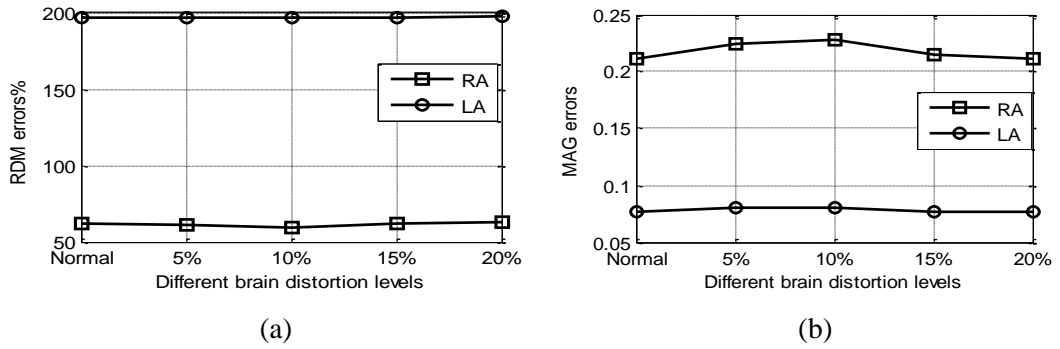


Figure 6.10: RDM (a) and MAG (b) errors from RA and LA sourced without and with different brain tissue distortion levels to SC sourced normal EEG.

Figure 6.11 shows the contour map of scalp potentials resulted from different realistic head models. Analyzing the contour maps, we find that the scalp potentials generated by various brain distortion levels are different from the reference model and vary from each other significantly.

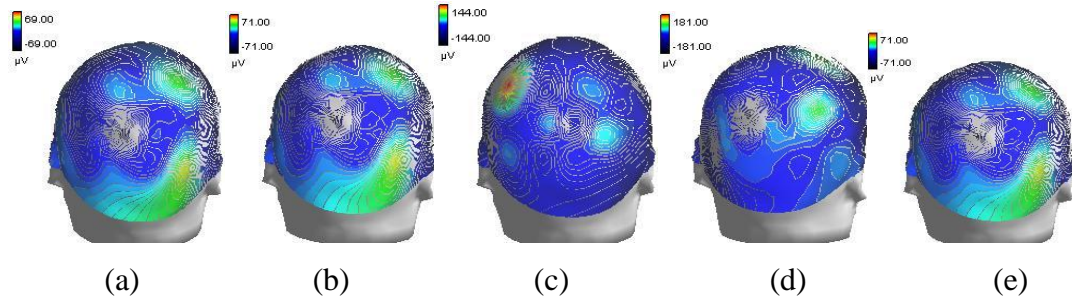


Figure 6.11: Contour view of scalp potentials obtained from somatosensory cortex (a) reference model, (b) five percent, (c) ten percent, (d) fifteen percent and (e) twenty percent brain tissue distortions.

6.2.3.4 Discussion

In this study, we observe the significant changes on scalp potentials by means of RDM and MAG in the forward computation for the sources in the AD region. We also implement 5%, 10%, 15% and 20% brain tissue distortions to address different stages of dementia, such as predementia, early dementia, moderate dementia and advanced dementia, respectively. We find the minimum of 10% RDM and 0.99 MAG values, and the maximum of 27% RDM and 1.09 MAG values for different brain tissue distortions.

Comparing the EEGs obtained from AD sourced to SC sourced EEG, we find the differences of scalp potentials due to the changing of the sources. Similarly, different levels of brain tissue distortion also cause substantial potential changes. In most of the cases, MAG errors generated by the SC source for different brain distortion levels show higher values than those of AD sourced EEG (Figure 6.9(b)). The reason is the position of sources. When a source is closer to the cortex, the distance between the source and the sensor is shorter. Therefore, more potential is measured on the sensor than the source at the deeper brain region. We also implement two different AD sources in the right amygdala and left amygdala to show the changing of EEGs in order to source position.

Visualization of scalp potentials (shown in Figure 6.11) is carried out based on our obtained results. A head model with electrodes is shown in Figure 6.12. Though all electrodes are not visible, electrodes are addressed by different names with 'F' for frontal lobe, 'P' for parietal lobe, 'O' for occipital lobe and 'T' for temporal lobe. Combining the concepts of electrode positions and scalp potentials, it is apparent that the electrodes in the source region are more sensitive to the

electrodes in other regions. When the source is placed in the somatosensory cortex, it spreads the potentials to its nearest electrodes positioned in the central parietal region. Therefore, the electrodes that are in parietal and temporal show more potential when the dipole is in the hippocampus.

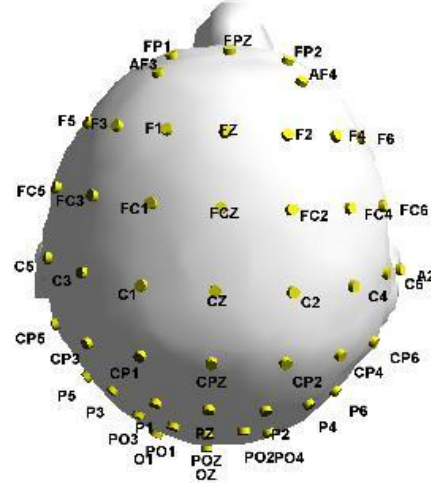


Figure 6.12: Electrode positions (left ear-Nasion – right ear). Odd numbers with electrode names indicate left hemisphere, even numbers with electrode names indicate right hemisphere.

In summary, we find that scalp potentials generated from AD sources differ and produce less values than a normal source. Different brain distortion levels also cause substantial potential changes. It is also found that the electrodes positioned in the source regions are more sensitive than other electrodes.

6.3 Conclusion

In this Chapter, we discuss the local tissue conductivity based head model and an application of head modelling on EEG analysis of Alzheimer's disease sources. In the first part, we construct LTC based head models where we assign the tissue conductivities based on their position or location. Analyzing several simulations, we find that it is important to assign LTC for an accurate head model. We find that the incorrect assignment of brain tissue conductivity causes substantial effects on scalp potentials while the skull produces negligible effects in this study. We also implement LTC based on different skull conductivities at different places. In both head models, we find substantial changes on EEG and the importance of using LTC.

Therefore, we conclude that accurate modelling requires LTC. In the second part of this Chapter, we discuss the EEGs originated from the normal source (somatosensory cortex) and the Alzheimer's disease sources (left and right amygdala). We also analyze different levels of dementia which causes storing atrophy in the brain cell, in turn, causes brain tissue distortion. We find that EEGs obtained from AD sources are different from normal sources, and the electrodes residing in parietal and temporal lobes are more sensitive than other electrodes for AD sourced EEG.

CHAPTER 7

SENSITIVITY ANALYSIS

This study is to investigate the effects of conductivity uncertainty on scalp potentials and to analyze its sensitivity, towards better understanding and representing a human head in EEG. In particular, we focus our attention on: how conductivity uncertainty in either tangential or radial direction affects an EEG and how much mean scalp potential varies by assigning these conductivities.

We implement a stochastic finite element method based on anisotropic and inhomogeneous conductivity properties for head model construction. We perturb the uncertain conductivity and compute the EEG. We analyze the conductivity uncertainty on output EEG by means of relative errors and correlation coefficients. Finally, we determine the sensitivity indexes by means of probabilistic sensitivity analysis.

7.1 Head Model Construction

We implement a five-layered spherical head model with 8.8cm, 8.5cm, 8.1cm, 7.9cm and 6.5cm radii for the scalp, skull, CSF, GM and WM, respectively. We also consider a realistic head model obtained from a T1 weighted MRI. Similar head models from our previous studies are used in this study. However, the conductivity approximations are different.

7.2 Uncertain Conductivity Approximation

Uncertainty analysis determines the uncertainty in outputs as a consequence of uncertain inputs. It is formed by means of the following Steps [Glavaski, 1998]: (A) identification of uncertain input parameters, (B) definition of the minimum and maximum uncertain ranges of the parameter, (C) specification of probability density function over these ranges and (D) generation of random data using the probability density function for input parameters to perform the simulation.

The output of an EEG forward problem is computed from known head geometry, electrical conductivity of the tissues and a current source. The input parameter, electrical conductivity, substantially affects the output of an EEG forward problem. It varies from person to person, and even spatially within a tissue. Therefore, it creates uncertainty in the EEG forward problem. We use conductivity as an uncertain input parameter (Step A of uncertainty analysis).

To define the minimum and the maximum uncertainty ranges (Step B of uncertainty analysis), we consider tissue anisotropy and inhomogeneous properties. Among the head tissues, the WM and the skull show anisotropic conductivity in longitudinal (tangential) and transversal (radial) directions. The anisotropy ratio (ar) between longitudinal and transversal directions varies from place to place between 1 and 10 [Marin *et al* 1998, Wolters 2003]. To construct an anisotropic model, we consider Volume and Wang's constraints.

The variations of ar cause the variation of conductivities. For example, when $ar = 1$ in the Volume constraint, longitudinal conductivity (σ_{long}^{Vol}) and transversal conductivity (σ_{trans}^{Vol}) values for the WM are both 0.14 S/m. When $ar = 10$, these values are 0.65 S/m and 0.065 S/m, respectively. These lower and upper conductivity values are assumed as the conductivity uncertainty ranges. Similarly, we determine the minimum and the maximum uncertainty values for the skull conductivity.

We also consider the scalp as an inhomogeneous conductor for its complicated anatomical structure. We assume the scalp conductivity uncertainty ranges between 0.16 S/m to 0.5 S/m (more details are found in Wen (2000)).

As the conductivity changes from place to place of a head, or even in a same tissue, a randomness or stochastic process is required to present such conductivities. We use a known PDF to determine the randomness. For specifying the PDF we consider Gaussian PDF with physically constrained to be non-negative and non-zero (Step C of uncertainty analysis). Table 7.1 shows the uncertain head tissue layers, their mean conductivities, uncertain conductivity ranges and PDF used in this study.

Table 7.1: The uncertain parameter (conductivity) and its ranges used in this study for the head model construction.

Tissue layer	Constant/mean conductivity	Conductivity uncertainty ranges (S/m)	Direction	Constraint	PDF
WM	0.14 (S/m)	0.14-0.65	longitudinal	Volume	Gaussian
		0.14-0.065	transversal		
		0.14-0.44	longitudinal	Wang	
		0.14-0.044	transversal		
skull	0.0042 (S/m)	0.0042-0.009	tangential	Volume	Gaussian
		0.0042-0.0009	radial		
		0.0042-0.013	tangential	Wang	
		0.0042-0.001	radial		
scalp	0.33 (S/m)	0.16-0.50	-	-	Gaussian

In the generation of random numbers as uncertain conductivities for an uncertain tissue layer (Step D of uncertainty analysis), we consider a stochastic conductivity tensor $\underline{\underline{\sigma}}(x; \vec{v})$, where $x \in Volume$ and \vec{v} presents polynomial random variables. A stochastic process [Geneser *et al* 2008, Bashar *et al* 2010c] for different head tissue layers is implemented by different random variable vectors. To represent the independent and uncorrelated random variables, we use Karhunen-Loeve expansion. According to this expansion, we define the random numbers for the conductivity values as:

$$\underline{\underline{\sigma}}(x; \vec{v}) = \underline{\underline{\hat{\sigma}}}_0(x) \lambda_0(\vec{v}) + \underline{\underline{\hat{\sigma}}}_i(x) \lambda_i(\vec{v}), \dots \dots \dots (7.1)$$

where $\underline{\underline{\sigma}}(x; \vec{v})$ is randomly distributed on the interval $[a(x), b(x)]$ for each point of the *Volume*, where $a(x)$ and $b(x)$ are the conductivity uncertainty ranges as shown in Table 7.1, and $\underline{\underline{\hat{\sigma}}}_0(x) = \underline{\underline{\hat{\sigma}}}_i(x) = (a(x) + b(x)) / 2$. We set $\underline{\underline{\hat{\sigma}}}_0(x)$ to the isotropic homogeneous or mean conductivity. We then set $\underline{\underline{\hat{\sigma}}}_i(x)$ to a nonzero value for the uncertain head tissue layers we are interested in, and set $\underline{\underline{\hat{\sigma}}}_i(x)$ to zero for each of the remaining layers.

7.3 Sensitivity Parameter Definition

The aim of sensitivity analysis of a model is to quantify how a model output depends on its input parameters. It assists in determining which input parameters affect the model output the most or the least. Sensitivity and uncertainty analysis procedure can be either local or global. Let us assume such a model as $y = f(\mathbf{x})$, where \mathbf{x} is a vector

of input variables $\mathbf{x} = (x_1, x_2, \dots, x_m)$ and y is the model output. We consider a baseline estimate \mathbf{x}_0 for \mathbf{x} to know how the true output y changes from the baseline output $y_0 = f(\mathbf{x}_0)$. We use homogeneous conductivity as the baseline or reference conductivity. The homogeneous conductivity values of WM, GM and scalp are 0.33 S/m, 0.14 S/m and 0.33 S/m, respectively. Two assumptions for the skull homogeneous conductivity are common. In the first assumption, the mean conductivity of the skull is 0.0042 S/m [Geddes and Baker 1967, Liang and Wang 2009, Aarabi *et al* 2009, Chauveau *et al* 2008, Roche-Labarbe *et al* 2008] according to $\sigma_{scalp} : \sigma_{skull} : \sigma_{brain} = 1 : (1/80) : 1$. In another assumption, the conductivity value is 0.0220 S/m [Oostendorp *et al* 2000, Lai *et al* 2005, Zhang *et al* 2006] with the ratio of $\sigma_{scalp} : \sigma_{skull} : \sigma_{brain} = 1 : (1/15) : 1$. We consider both of these assumptions in this study. Similarly, the mean conductivity of CSF is considered as 1.0 S/m [Geddes and Baker 1967]. Moreover, it is also assumed 1.79 S/m in room temperature [Windel *et al* 2008, Baumann *et al* 1997]. As a result, we consider two sets of base lines or reference conductivities as shown in Table 7.2.

Table 7.2: Homogeneous conductivity values for different tissue layers for the construction of the reference head models.

	Scalp (S/m)	Skull (S/m)	CSF (S/m)	GM (S/m)	WM (S/m)
Conductivity set A	0.33	0.0042	1.0	0.33	0.14
Conductivity set B	0.33	0.022	1.79	0.33	0.14

The local sensitivity is limited on input \mathbf{x} because one input is varied but other inputs are constant. On the other hand, global sensitivity analysis considers more substantial changes in the input \mathbf{x} and can be assumed as $Y = f(\mathbf{X})$, where \mathbf{X} is unknown inputs and Y is output. The probabilistic sensitivity analysis can be represented in terms of a decomposition of the function $f(\cdot)$ into main effects and interactions [Oakley and O'Hagan 2004]:

$$y = f(\mathbf{x}) = E(Y) + \sum_{i=1}^m z_i(x_i) + \sum_{i < j} z_{i,j}(\mathbf{x}_{i,j}) + \sum_{i < j < k} z_{i,j,k}(\mathbf{x}_{i,j,k}) + \dots + z_{1,2,\dots,m}(\mathbf{x}), \dots \quad (7.2)$$

where $z_i(x_i) = E(Y | x_i) - E(Y)$,

$$z_{i,j}(\mathbf{x}_{i,j}) = E(Y | \mathbf{x}_{i,j}) - z_i(x_i) - z_j(x_j) - E(Y),$$

$$z_{i,j,k}(\mathbf{x}_{i,j,k}) = E(Y | \mathbf{x}_{i,j,k}) - z_{i,j}(\mathbf{x}_{i,j}) - z_{i,k}(\mathbf{x}_{i,k}) - z_{j,k}(\mathbf{x}_{j,k}) - z_i(x_i) - z_j(x_j) - z_k(x_k) - E(Y),$$

and so on. We refer $z_i(x_i)$ as the main effect of x_i , to $z_{i,j}(\mathbf{x}_{i,j})$ as the first-order interaction between x_i and x_j .

7.4 Implementation and Experimentation

For both the spherical and realistic head models development, we use isotropic homogeneous, anisotropic inhomogeneous and uncertain conductivities. Scalar conductivity value is used to represent isotropic homogeneous conductivity. We assign isotropic and homogeneous conductivity for different tissue layers shown in Table 7.2 (Conductivity sets A and B) for the construction of baseline or reference head models. To represent anisotropic conductivity for the WM and skull conductivity tensor is used. Then we assign the uncertain conductivities to tissue layers for the construction of the conductivity perturbed model.

We use five-layered spherical and realistic models with the same tessellation and number of elements as used in the previous studies. We compute EEGs from 24 fixed dipoles at different places inside the GM assuming $1\mu\text{A}$ magnitude of each dipole. We implement two relative difference measurement techniques to analyze the relative changes between the reference and computed models. These measurements are relative error (ε) and correlation coefficient (η) values.

In order to quantify sensitivity indexes mentioned in equation (7.2), we consider $y = f(\mathbf{x}) = \varepsilon$ for different sources and $E(Y|x_i)$ as the obtained ε for assigning the uncertain (perturbed) conductivity for x_i tissue layers. We compute $E(Y)$ from the base line conductivities.

7.5 Experimental Results

7.5.1 Results in the spherical head model

Figure 7.1 shows the mean relative error ($m\varepsilon$) and mean correlation coefficient ($m\eta$) values from different dipole depths comparing with reference model A or B. In Figure 7.1, *long* represents the longitudinal and *trans* represents the transversal conductivities with *V* for Volume constraint and *W* for Wang's constraint. When comparing with reference model A (solid lines in Figures 7.1a and 7.1b), the $m\varepsilon$

ranges between 24% and 31% producing an average of 28%. The $m\eta$ ranges between 0.92 and 0.97 with an average of 0.95. The transversal conductivities generate higher $m\epsilon$ and $m\eta$ values than those of the longitudinal conductivities. Wang's constrained transversal conductivities produce higher $m\epsilon$ and longitudinal conductivities generate fewer $m\eta$ values.

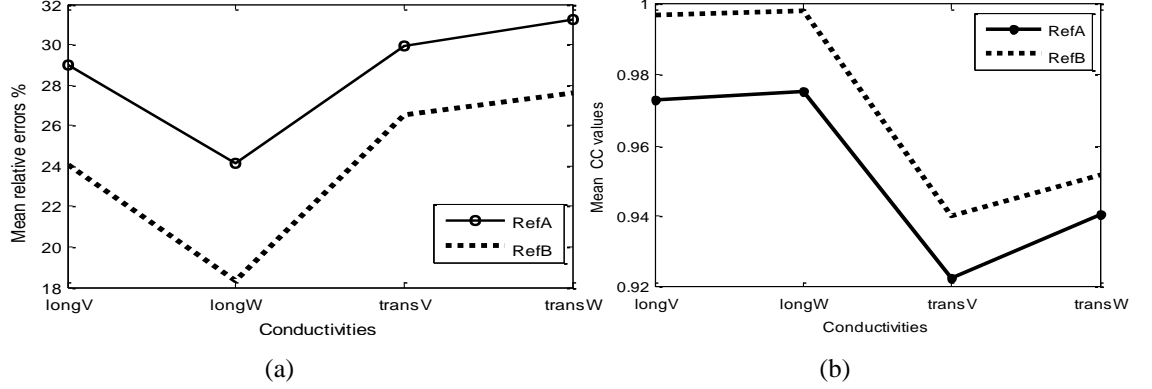


Figure 7.1: WM conductivity uncertainty: (a) mean relative errors ($m\epsilon$) and (b) mean correlation coefficient ($m\eta$) values generated by incorporating WM conductivity uncertainty.

RefA and *RefB* represent the Reference Models A and B, respectively. *long* represents the longitudinal and *trans* represents the transversal conductivities with *V* for Volume constraint and *W* for Wang's constraint.

When comparing with reference model B (dash lines in Figures 7.1a and 7.1b), the $m\epsilon$ ranges between 18% and 28% producing an average of 23% and $m\eta$ ranges between 0.94 and 1.0 with an average of 0.97. The results also show that Wang's constrained transversal and longitudinal conductivities generate higher $m\epsilon$ and fewer $m\eta$ values, respectively. Therefore, in analyzing the uncertainties for various constrained WM conductivities in different directions, it is found that the EEG forward modelling is more affected by the Volume constrained transversal conductivities in most of the cases in our study.

Table 7.3 shows the ϵ values generated by one dipolar source in the GM at various depths making different dipole eccentricities (Marin *et al* 1998, Wang and He 1998]. The results are obtained when comparing to reference model A. From the obtained results, it is found that the ϵ values are less when the dipole is closer to the origin. However, it produces more ϵ values when the dipole is close to the cortex. We also compute the ϵ values between the WM perturbed models and the reference model B for different dipole eccentricities and find the insensitive results.

Table 7.3: Relative error % (ε) values produced by the white matter conductivity perturbations for different dipole eccentricities.

Conduc -tivity	Dipole eccentricities										
	0.77	0.78	0.79	0.80	0.81	0.82	0.83	0.84	0.85	0.86	0.87
LongV	31.42	31.44	31.46	31.48	31.50	31.52	31.54	31.56	31.58	31.60	31.62
LongW	22.32	22.34	22.36	22.37	22.39	22.41	22.43	22.45	22.47	22.49	22.51
TransV	26.11	26.12	26.12	26.12	26.12	26.12	26.12	26.12	26.12	26.12	26.12
TransW	24.69	24.69	24.70	24.71	24.72	24.72	24.73	24.73	24.74	24.74	24.75

* *Long* represents the longitudinal and *Trans* represents the transversal conductivities with *V* for Volume constraint and *W* for Wang's constraint.

The $m\varepsilon$ and $m\eta$ values for the skull perturbed conductivity models in comparison with either reference model A or B are shown in Figure 7.2. *tan* represents the tangential and *rad* represents the radial conductivities while other symbols and notations used in Figure 7.2 are identical to Figure 7.1. Comparing with both of the reference head models, the Volume constrained radial conductivity model generates fewer and the Wang's constrained radial conductivity generates the larger $m\varepsilon$ errors. On the other hand, Wang's constrained tangential produces fewer and Wang's constrained radial produces the higher $m\eta$ errors. Therefore, we understand that incorporating the skull conductivity uncertainty generates substantial scalp potentials variation between the reference and computed models. Analyzing these results, we find that the radial conductivity affects the scalp potentials more than those of the tangential conductivities in most of the cases in our study.

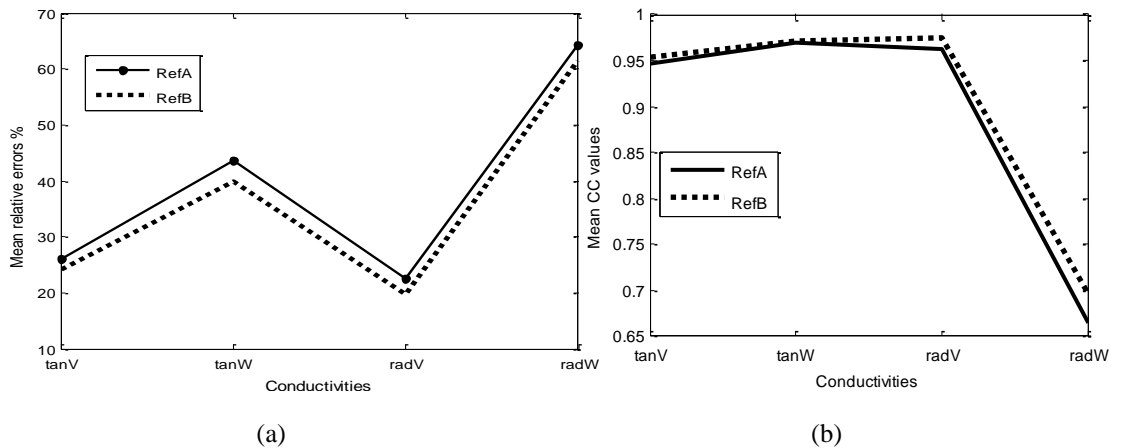


Figure 7.2: Skull conductivity uncertainty: (a) mean relative errors ($m\varepsilon$) and (b) mean correlation coefficient ($m\eta$) values generated by incorporating skull conductivity uncertainty. *RefA* or *RefB* stands for either reference model A or B. *tan* represents the tangential and *rad* represents the radial conductivities with *V* for Volume constraint and *W* for Wang's constraint.

Incorporating the scalp conductivity uncertainty, we find 25% $m\varepsilon$ and 0.95 $m\eta$ values when comparing with reference model A. If we compare with reference model B, we find 28% $m\varepsilon$ and 0.98 $m\eta$ values. Therefore, it is apparent that the scalp conductivity perturbation has non-negligible effects on the output of EEG forward computation.

The sensitivity indexes based on equation (7.2) are shown in Table 7.4 for the reference model A. In Table 7.4 x_1 , x_2 and x_3 represent the conductivities of the WM, the skull and the scalp, respectively. $x_{1,2}$ represents the combined conductivities of the WM and skull. Similarly, the other combination represents the corresponding tissue layer's combined conductivities. $z_i(x_i)$ represents the main effect of x_i . The parallel direction is assumed for the longitudinal direction of the WM conductivities and the tangential direction of the skull conductivities. On the other hand, the perpendicular direction stands for the transversal and radial directed conductivities for the WM and skull, respectively. In Table 7.4 it is observed that each inhomogeneous tissue layer causes the variation of the mean scalp potentials. Anisotropic and inhomogeneous WM conductivity generates an average of 30.5% mean scalp potentials, the skull generates an average of 37.5% mean scalp potentials and the scalp generates 28% variations. The combined conductivity produces relatively less mean scalp potentials as the output scalp potentials are not additive to more tissue layers. Wang's constrained WM and skull conductivities generate the highest mean scalp potential variations. Combined anisotropic and inhomogeneous tissue conductivity properties generate the maximum 42% mean potential variation. We also compute the sensitivity indexes by the comparison with the reference model B. We find similar results with a small amount of variation in values. To avoid a duplicate table, we do not report it.

Table 7.4: Sensitivity indexes for different conductivities in the spherical head model compared with the reference model A.

Direction	Constraints	$z_1(x_1)$	$z_2(x_2)$	$z_3(x_3)$	$z_{1,2}(x_{1,2})$	$z_{1,3}(x_{1,3})$	$z_{2,3}(x_{2,3})$	$z_{1,2,3}(x_{1,2,3})$
Parallel	Volume	0.33	0.26	0.28	-0.33	-0.33	-0.35	0.42
	Wang	0.29	0.35		-0.17	-0.28	-0.23	0.25
Perpendicular	Volume	0.30	0.25	0.28	-0.12	-0.29	-0.25	0.09
	Wang	0.29	0.64		-0.40	-0.29	-0.63	0.35

7.5.2 Results in the realistic head model

For the realistic head model, we use similar approaches and conductivity perturbed models to compute the scalp potentials for the reference and the computed models. We consider the brain tissue layer with homogeneous conductivity 0.33 S/m assuming the WM and GM are in the brain. We also consider the skull layer as anisotropic and inhomogeneous, and the scalp is inhomogeneous. Figure 7.3 shows the $m\epsilon$ and $m\eta$ values caused by the skull conductivity perturbation. We find that the $m\epsilon$ is 20% and 21.5% when comparing with the reference model A and model B, separately. Similarly, it shows identical $m\eta$ values when comparing to reference model A but it shows 0.94 $m\eta$ when comparing to the reference model B (Figure 7.3(b)). The relative errors and CC values are almost identical for different conductivity models because the conductivities assigned to the perturbed models are not sufficient to substantially change the output. By analyzing the results, it is apparent that the skull conductivity perturbation has significant effects on $m\epsilon$ values and smearing effects on $m\eta$ values. All the perturbed models show similar affects on the scalp potentials.

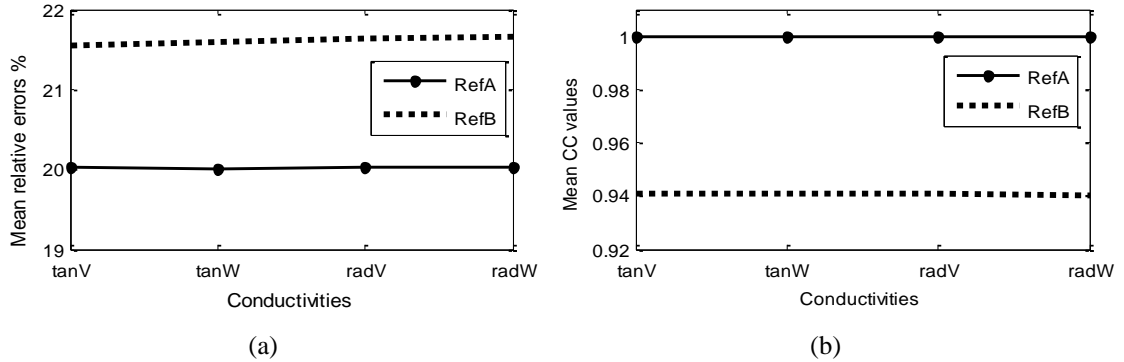


Figure 7.3: The scalp conductivity uncertainty: (a) mean relative errors ($m\epsilon$) and (b) mean correlation coefficient ($m\eta$) values. *RefA* or *RefB* stands for either reference model A or B. *tan* represents the tangential and *rad* represents the radial conductivities with *V* for Volume constraint and *W* for Wang's constraint.

For the scalp conductivity perturbation, we find 20% $m\epsilon$ and 0.98 $m\eta$ values comparing with reference model A. When compared with reference model B, we find 41% $m\epsilon$ and 0.85 $m\eta$ values. Therefore, it is obvious that the scalp conductivity uncertainty causes the differences in the output EEG.

Table 7.5 shows the sensitivity indexes generated by the realistic head model compared with the reference model A, where x_1 and x_2 represent the conductivities of the skull and the scalp. We find that the sensitivity of the skull has negligible effects on the output EEG; however the scalp has a strong effect on the output. We also find similar results with very small variations compared with the reference model B.

Table 7.5: Sensitivity indexes for different conductivities in realistic head model compared with the reference model A.

Direction	Constraints	$z_1(x_1)$	$z_2(x_2)$	$z_{1,2}(x_{1,2})$
Tangential	Volume	0.003	0.25	-0.003
	Wang	0.003		-0.003
Radial	Volume	0.003	0.25	-0.003
	Wang	0.004		-0.004

7.6 Discussion and Conclusion

The presented results show that the deeper dipolar source results in relatively fewer scalp potential variations than those from the superficial dipolar source. The currents from a deeper source spread inside the gray matter and reach to the scalp electrodes through a larger portion of low conductive skull. However, a superficial source residing on the cortex beneath the skull layer allows close contact to scalp electrodes. As a result, a superficial source results in substantial variations in electrode potentials. Therefore, it is important to represent skull conductivity accurately to get a better EEG. The results show that the skull conductivity uncertainty causes the maximum 63% mean relative differences for the spherical head model (shown in Figure 7.2a). The anatomical structure of the skull is more complex than other tissue layers. The hard and soft bone layers of the skull make it as an anisotropic conductor. In other parts, such as calvarium, suture lines make it an inhomogeneous tissue layer. The conductivities of these parts are also different. As a result, the computed scalp potentials are affected. Our experimental results find that the radial directional conductivity is more sensitive than the tangentially directed conductivity. Among the tissue layers, the scalp layer individually shows 28% mean potential differences in the spherical and 35% differences in the realistic head models. Similarly, for the WM

in the brain, our results demonstrate that WM has significant sensitivity indexes for anisotropic and inhomogeneous cases (Table 7.4).

We have investigated the uncertainty and sensitivity of spherical and realistic head models based on their tissue conductivity properties. We developed a conductivity model with respect to the tissue anisotropic and inhomogeneous properties. We analyze the effects of tissue conductivity uncertainty on EEG forward head computation by means of two relative statistical measurements. We quantify the sensitivity indexes for different tissue layers and their combined effects by means of probabilistic sensitivity analysis. The results demonstrate that the conductivity uncertainty causes significant potential changes on scalp electrodes. Among the tissues, white matter in the transversal direction, skull in the radial direction and the scalp are more sensitive. These tissue layers cause substantial mean potential changes on the output EEG.

CHAPTER 8

CONCLUSION

The electrical activity inside the brain is measured on the head surface by an EEG. The EEG becomes an important diagnostic tool for clinical purposes to analyze mental disorders or brain functions. The accuracy of the human head model partly depends on the head tissue conductivity. Tissue conductivity varies in different parts of the head, even in the same tissue layer. Some tissue layers are inhomogeneous and some are anisotropic. This dissertation studies human head modelling based on inhomogeneous and anisotropic head tissue conductivities and local tissue conductivity.

8.1 Main Contributions

The anatomical and physiological structure of a human head is too complex to be modelled exactly. Brain scientists have been devoted to developing an anatomically sound artificial or realistic head model for decades. This study is part of the modelling work. Head modelling depends mainly on head geometry and head tissue conductivity. Head geometry from magnetic resonance imaging is commonly used for the development of a subject specific head model. However the conductivity allocation to the head tissues is still the challenging problem to the brain researcher. This study focuses on the conductivity aspects of the head model. The major contributions of this study are: (A) we have successfully developed a series of inhomogeneous and anisotropic head models, (B) systematically studied the effects of inhomogeneous and anisotropic tissues on EEG computation, (C) investigated the local conductivity problem in realistic head modelling and (D) finally, sensitivities computations are studied based on tissue conductivity properties.

8.1.1 A series of head model construction on inhomogeneous and anisotropic tissue conductivities

In the homogeneous model, it is assumed that each tissue layer consists of the same tissue. However, it is realized that head tissues are not homogeneous. For example, the scalp tissue layer consists of subcutaneous fat and muscle tissues. Each tissue has its own conductivity. Therefore, head model development requires knowledge of the tissue inhomogeneity. When electric current passes through CSF to skull, the direction of current is obstructed due to lower conductive compact bone and the direction is changed to either radial or tangential. A similar situation happens when currents flows from GM to WM in the brain. These directional movements of current lead to anisotropy and it happens due to their anatomical structure.

Existing head models are based on fixed or constant anisotropy ratio. In reality, different parts of the WM and skull have different anisotropy ratios. We propose conductivity models on various anisotropy ratios to implement tissue inhomogeneity and anisotropy. The main focus of these conductivity models is to determine inhomogeneous and anisotropic conductivities. To implement these inhomogeneous and anisotropic conductivities, our proposed conductivity models are conductivity ratio approximation, statistical conductivity approximation, the Monte Carlo method based, and fractional anisotropy based conductivity models. These conductivity models implement separate statistical study. We propose conductivity ratio approximation and fractional anisotropy based conductivity models on various anisotropy ratios. The statistical conductivity approximation model is based on the Rayleigh distribution, and the Monte Carlo method based conductivity model is based on Normal distribution to determine the inhomogeneous and anisotropic conductivities. All proposed models are also on the Volume and Wang's constraints to restrict the conductivities between homogeneous isotropic, and inhomogeneous and anisotropic media. We develop a series of head models using our proposed conductivity models to investigate its effect on EEG. Analyzing a series of simulations, we find an average of 36.43% RDM and 1.12 MAG values for the conductivity ratio approximation model. An average of 21.49% RDM and 1.12 MAG values are found for the statistical conductivity approximation model. Similarly, an average of 7.61% RDM and 1.101 MAG values are found for the fractional anisotropy based conductivity models, and the Monte Carlo method based

conductivity models generate the 109% average RDM and 1.62 average MAG values.

8.1.2 Systematically studied the effects of inhomogeneous and anisotropic tissues on EEG computation

All molecules and ions in the body fluids are in random molecular motion due to thermal energy. A result of this motion is the process by which the matter is transported from one part of the system to another. Analogy, random motion of molecule is the reason for conductivity variation or inhomogeneous. Due to the variation of conductivity, it is difficult to obtain accurate conductivity for each subject. It also happens in an anisotropic medium. For example, anisotropy ratio is inhomogeneous in the entire brain, and the thickness of the spongiosum skull bone is non uniform through which liquid or blood passes.

We implement a stochastic method based head model for the randomness of conductivity properties. The purpose of this model is also to investigate the effects of inhomogeneous and anisotropic conductivities on EEG. We implement this model using stochastic FEM and determine the random numbers as the inhomogeneous and anisotropic conductivities using the Karhunen-Loeve expansion, and Volume and Wang's constraints. Analyzing simulation results, we find that incorporating inhomogeneous and anisotropic conductivities incurs 22% to 68% average relative differences, and 0.99 to 0.52 correlation coefficient values.

8.1.3 Local tissue conductivity on head modelling

The ultimate goal of the development of the realistic head model is to model a real head exactly. To make a more accurate head model, we propose a local tissue conductivity based head model. In this head model, we allocate conductivity to each head tissue based on their position in the head tissue layer. For example, the presence of suture lines increases the skull conductivity and the absence of cancellous bone decreases the skull conductivity. Similarly, the complex composition of GM, WM, blood and cerebellum in the brain causes different conductivities in a brain tissue layer, and the presence of thick subcutaneous fat beneath the skin causes different

conductivities in a scalp tissue layer. Therefore, we attempt to assign accurate conductivity to the head tissues based on the tissue location.

We model three- and four-layered spherical, and a realistic human head on local tissue conductivity where conductivities are allocated according to the tissue position. We compare the EEGs obtained from our local tissue conductivity based head model and homogeneous head model and find the maximum 1.4 RDM and 2.6 MAG values for the spherical head model, and the maximum 1.8 RDM and 3.85 MAG values for the realistic head model.

8.1.4 Computation of sensitivity indexes for inhomogeneous and anisotropic conductivity

Inhomogeneous and anisotropic conductivity properties are known. However, many studies neglect these properties. It is necessary to understand what effects would occur if these properties were neglected.

We analyze the sensitivity indexes on our stochastic method based spherical and realistic head models. We find that conductivity uncertainty produces 18% to 65% average relative errors, and 0.99 to 0.67 average correlation coefficient values for our five-layered spherical head model. In our realistic head model, these values are from 20% to 41% average relative errors, and 1 to 0.85 average correlation coefficient values. Analyzing the sensitivity indexes, we find the maximum 42% mean scalp potential variations for the spherical head, and maximum 25% mean scalp potential variations for the realistic head.

8.2 Future Work

Though the inhomogeneous and anisotropic or local tissue conductivity based head models developed in this dissertation would assist to create more realistic head models, there are still many things to explore to improve this approach and to enhance the models. We consider the following improvement would be of benefit in addition to this research.

8.2.1 The model improvement

The model can be improved in both ways for either geometry or conductivity. In this dissertation, we use common head models on the spherical and the realistic geometry. As the head geometry also plays an important role in the accuracy of the EEG forward and inverse problems, it is important to individually determine object-related head models.

To develop and implement different methods for the head modelling on inhomogeneous and anisotropic tissue conductivities, we use different methods to obtain random numbers either for the anisotropy ratio or conductivity value. However, it would be of great scientific benefit if it were possible to obtain an accurate anisotropy ratio. For example, the corpus callosum, anterior commissure have higher anisotropy ratios than other parts of the WM. The thickness of the hard and soft bone layers vary in different skull areas.

8.2.2 Segmentation

The anatomical boundaries represented in this study for structuring different tissues should be manageable for blood vessels and nerves. It may require extra care in segmentation if generic segmentation fails (if done manually) or a specific detection and segmentation technique (if done automatically). We anticipate that the rapid progress in MRI is very likely to provide better *in vivo* estimations of cell boundaries within a tissue layer. In this dissertation, we do not consider the lower part of the head because there are limited electrodes used in this region. This is the reason we do not include the eye socket, muscle and soft tissues in the scalp layer construction. However, if we collect data from forehead electrodes or the lower part of the head electrodes, we would consider including these tissues.

8.2.3 Conductivity

A major unknown parameter of a head model is the absolute value of the tissue conductivity. Great efforts have been taken in measuring, determining or computing the conductivity of different head tissues. However, a large inter-patient variability on tissue conductivity exists. Diffusion-weighted MRI are used to determine the

conductivity values for the WM assuming the diffusion of water is liner to the diffusion of electric particles. For the skull, Law (1993) measured conductivity in 20 different positions by filling the skull with saline water. The skull conductivity is dependent on the thickness of various skull bones, the amount of blood flow in the soft bone and the presence of the suture lines. The live skull conductivity values are between 0.00076 and 0.0115 S/m (0.76 mS/m to 11.5 mS/m) for four different skull samples. However, no complete *in vivo* skull conductivity values for different regions are found. Moreover, conductivity varies from person to person, or even for the same person at different ages, situation and conditions. Therefore, more investigations are required to determine the *in vivo* conductivity and the necessity of using object specific conductivity on head modelling.

This dissertation considers Rayleigh distribution for statistical conductivity approximation model and Normal distribution for Monte Carlo simulation models. Poisson distribution may also be able to generate random numbers which can also be treated as inhomogeneous and anisotropic conductivities.

8.3 Summary

This dissertation deals with human head modelling based on tissue conductivity using spherical and realistic geometries. Head tissue conductivity is modelled in two approaches: inhomogeneous and anisotropic tissue conductivities and local tissue conductivity. This dissertation covers the following major topics. Firstly, we introduce conductivity ratio approximation, statistical conductivity approximation, fractional anisotropy based and the Monte Carlo method based conductivity models to implement inhomogeneous and anisotropic tissue conductivities. Secondly, we show the effects of tissue inhomogeneity and anisotropy on scalp potentials using these conductivity models. We also investigate the effects of inhomogeneous and anisotropic conductivities on EEG using stochastic method. Thirdly, we introduce the local tissue conductivity based head model and investigate its effects on EEG. We also investigate the effects of tissue or element variations due to positional variations of local conductivity assignment or subject's supine position. Fourthly, we analyze normal sourced and Alzheimer's disease sourced EEGs with different levels of dementia and finally, we show the effects of conductivity uncertainty and sensitivity indexes.

REFERENCES

Aarabi, A., Kazemi, K., Grebe, R., Moghaddam, H. A. and Wallois, F., *Detection of EEG transients in neonates and older children using a system based on dynamic time-warping template matching and spatial dipole clustering*, NeuroImage, 48, 50-62, 2009.

Amygdala, Wikipedia, [<http://en.wikipedia.org/wiki/Amygdala>]

Anwandwer, A., Wolters, C. H., Dumpelmann, M. and Knosche, T., *Influence of realistic skull and white matter on the inverse problem in EEG/MEG- source localization*, Proceedings of International Conference on Biomagnetism, Germany, 679-681, 2002.

Aoki, N., Hori, J. and He, B., *Estimation of Cortical Dipole Sources by Equivalent Dipole Layer Imaging and Independent Component Analysis*, 28th IEEE EMBS Annual International Conference, New York, USA, 992-995, 2006.

Ary, J. P., Klein, S. A. and Fender D. H., *Location of sources of evoked scalp potentials: Corrections for skull and scalp thickness*, IEEE Trans. Biomed. Eng., 28(6), 447-452, 1981.

ASA *Advanced Source Analysis*, ANT Software, The Netherland. www.ant-neuro.com

Awada, K. A., Baumann, S. B. and Jackson, D. R., *Effect of conductivity uncertainties on EEG source localization using a 2D finite element model*, Proc. of 19th International Conference – IEEE/EMBS, 2124-2127, 1997.

Awada, K. A., Jackson, D. R., Baumann, S. B., Williams, J. T., Wilton, D. R., Fink, P. W. and Prasky, B. R., *Effect of conductivity uncertainties and Modeling errors on EEG source localization using a 2-D model*, IEEE Trans. Biomed. Eng., 45(9), 1135-1145, 1998.

Baillet, S., Mosher, J. C. and Leahy, R. M., *Electromagnetic Brain Mapping*, IEEE Signal Processing Magazine, 14-30, 2001.

Baillet, S., Mosher, J. C. and Leahy, R. M., *Electromagnetic Brain Imaging using Brainstorm*, IEEE International Symposium on Biomedical Engineering: Macro to Nano, 652-655, 2004.

References

- Baron, J. C., Chetelat, G., Desgranges, B., Perchey, G., Landeau, B., de la Sayette, V. and Eustache, F., *In vivo mapping of gray matter loss with voxel-based morphometry in mild Alzheimer's disease*, NeuroImage, 14, 298–309, 2001.
- Bannister, L. H., Berry, M. M., Collins, P., Dyson, M., Dussek, J. E. and Mark W. J. Ferguson, M. W. J., *Gray's Anatomy*, Churchill Livingstone, 38 Edition, Great Britain, 1995.
- Bashar, M. R., Li, Y. and Wen, P., *Tissue conductivity anisotropy inhomogeneity study in EEG head modelling*, International Conference on Bioinformatics and Computational Biology, Las Vegas, Nevada, USA, 862-867, 2008a,.
- Bashar, M. R., Li, Y. and Wen, P., *Effects of Local Tissue Conductivity on Spherical and Realistic Head Models*, Australas. Phys. Eng. Sci. in Med., 31(2), 122-130, 2008b.
- Bashar, M. R., Li, Y. and Wen, P., *Effects of white matter on EEG of multi-layered spherical head models*, IEEE International Conference on Electrical and Computer Engineering (ICECE 2008), Dhaka, Bangladesh, 59-64, 2008c.
- Bashar, M. R., Li, Y. and Wen, P., *A study of white matter and skull inhomogeneous anisotropic tissue conductivities on EEG forward head modelling*, IEEE International Conference on Computer and Information Technology (ICCIT 2008), Khulna, Bangladesh, 24-25 December, 7-13, 2008d,.
- Bashar, M. R., Li, Y. and Wen, P., *EEG analysis on skull conductivity perturbations using realistic head mode*, International Conference on Rough Set and Knowledge Technology (RSKT2009), Gold Coast, Australia, 208-215, 2009,.
- Bashar, M. R., Li, Y. and Wen, P., *A systematic study of head tissue inhomogeneity and anisotropy on EEG forward problem computing*, Australas. Phys. Eng. Sci. in Med., 33(1), 11-21, 2010a.
- Bashar, M. R., Li, Y. and Wen, P., *Study of EEGs from Somatosensory Cortex and Alzheimer's Disease Sources*, International Journal of Medicine and Medical Sciences, 1(2), 62-66, 2010b.
- Bashar, M. R., Li, Y. and Wen, P., *Uncertainty and sensitivity analysis for anisotropic inhomogeneous head tissue conductivity in human head modelling*, Australas. Phys. Eng. Sci. in Med., 33(2), 145-152, 2010c.
- Bashar, M. R., Li, Y. and Wen, P., *Effects of Local Tissue Conductivity on Spherical and Realistic Head Models*, Australas. Phys. Eng. Sci. in Med., 33(3), 333-342, 2010d.

References

- Bashar, M. R., Li, Y. and Wen, P., *Effects of the Local and Spongiosum Tissue Conductivities on Realistic Head Modelling*, International Conference on Complex Medical Engineering, (CME 2010), Gold Coast, Australia, 13 -15 July, 23-27, 2010e.
- Basser, P., Mattiello, J. and LeBihan, D., *MR diffusion tensor spectroscopy and imaging*, Biophysical Journal, 66, 259-267, 1994.
- Baumann, S. B., Wozny, D. R., Kelly, S. K. and Meno, F. M., *The Electrical Conductivity of Human Cerebrospinal Fluid at Body Temperature*, IEEE Trans. Biomed. Eng., 44, 220-223, 1997.
- Brainstorm2, [<http://neuroimage.usc.edu/brainstorm/>]
- Brain structure-online <http://www.arthursclipart.org/medical/nervous/coronal%20section.gif>].
- Brody, D. A., Terry, F. H. and Ideker, R. E., *Eccentric dipole in a spherical medium: Generalized expression for surface potentials*, IEEE Trans. Biomed. Eng. 20, 141-143, 1973.
- Bruno, P., Vatta, F. and Inchingolo, P., *Interaction between noise and lesion modeling errors on EEG source localization accuracy*, Proc of the 23rd Annual EMBS Int. Conf., 917-920, 2001.
- Bruno, P. , Hyttinen J., Inchingolo, P. , Magrofuoco, A. , Mininel, S. and Vatta, F. , *A FDM anisotropic formulation for EEG simulation*, IEEE EMBS Annual International Conference, New York, USA, 1121-1125, 2006.
- Berg, P. and Scherg, M., *A fast method for forward computation of multiple-shell spherical head models*, Electroenceph. Clin. Neurophysiol., 90, 58-64, 1994.
- Chauveau, N., Franceries, X., Doyon, B., Rigaud, B., Morucci, J. P. and Celsis, P., *Effects of skull thickness, anisotropy, and inhomogeneity on forward EEG/ERP computations using a spherical three-dimensional resistor mesh model*, Human Brain Mapping, 21(2), 86 – 97, 2003.
- Chetelat, G., Desgranges, B., Landeau, B., Mezenge, F., Poline, J. B. , de la Sayette, V., Viader, F., Eustache, F. and Baron, J. C., *Direct voxel-based comparison between grey matter hypometabolism and atrophy in Alzheimer's disease*, Brain, 131, 60-71, 2008.
- Chupi, M., Mukuna-Bantumbakulu, A. R., Hasboun, D., Bardinet, E., Baillet, S., Kinkingnehun, S., Lemieux, L., Dubois, B. and Garnero, L., *Anatomically constrained region deformation for the automated segmentation of the hippocampus and amygdala: Method and validation on controls and patients with Alzheimer disease*, NeuroImage, 34, 996-1019, 2007.

References

Cuffin, B. N., *Effects of local variations in skull and scalp thickness on EEG's and MEG's*, IEEE Trans. Biomed. Eng., 40, 42-48, 1993.

de Munck , J. C., *The potential distribution in a layered anisotropic spheroidal volume conductor*, J. App. Phys., 64(2), 464-470, 1988.

de Munck , J. C., and Peters, M. J., *A fast method to compute the potential in the multi sphere model* , IEEE Trans. Biomed. Eng., 40, 1166-1174, 1993.

Darvas, F., Pantazis D., Kucukaltum-Yildirim, E. and Leahy, R. M., *Mapping human brain function with MEG and EEG: methods and validation*, NeuroImage, 23, 289-299, 2004.

Dogdas, B., Shattuck, D. W. and Leahy, R. M., *Segmentation of Skull and Scalp in 3-D Human MRI using Mathematical Morphology*, Human Brain Mapping, 26, 273-285, 2005.

Enokizono, M. and Aoki, M., *Application of Stochastic Finite Element Method to the Analysis of Magnetic Field*, IEEE Trans. Journal on Magnetism in Japan (TJMJ), 2, 973-81, 1987.

Ferree, T. C., Eriksen, K. J. and Tucker, D. M., *Regional head tissue conductivity estimation for improved EEG analysis*, IEEE Trans. Biomed. Eng., 47(12), 1584-1591, 2000.

Four lobes-online [<http://www.braininjury.com/images/symptoms02.jpg>]

Gabriel, S., Lau, R. W. and Gabriel, C., *The dielectric properties of biological tissues: III. Parametric models for the dielectric spectrum of tissues*, Phy. Med. Bio., 41, 2271-2293, 1996.

Geneser, S. E., Kirby, R. M., and MacLeod, R. S., *Application of Stochastic Finite Element Methods to Study the Sensitivity of ECG Forward Modeling to Organ Conductivity*, IEEE Trans. Biome. Eng., 55, 31-40, 2008.

Glavaski, S., Marsden J. E., and Murray R. M., *Model Reduction, Centering, and the Karhunen-Loeve Expansion*, IEEE proceedings of the Conference on Decision & Control, 2071-2076, 1998.

Gray, F. J., *Anatomy for the Medical Clinician*, Shannon Books Pty Ltd, Victoria, Australia, First edition, December 2002.

Gullmar, D., Haueisen, J., Wiselt, M., Giebler, F., Flemming, L., Anwander, A. Thomas, R. K., Wolters, C. H., Dumpelmann, M., David, S. T. and Jurgen, R. R., *Influence of*

References

Anisotropic Conductivity on EEG source Reconstruction: Investigations in a Rabbit Model, IEEE Trans. Biomed. Eng., 53(9), 1841-1850, 2006.

Gullmar, D., Haueisen, J. and Reichenbach, J. R., *Influence of anisotropic electrical conductivity in white matter tissue on EEG/MEG forward and inverse solution, A high-resolution whole head simulation study*, NeuroImage, 51(1), 145-163, 2010.

Hallez, H., Hese, V., Vanrumste, B., Boon, P., Asseler, Y. D., Lemahieu, I. and Walle, R. V., *Dipole Localization Errors due to not Incorporating Layers with Anisotropic Conductivities: Simulation Study in a Spherical Head Model*, International Journal of Bioelectromagnetism (IJBEM), 7(1), 134-137, 2005a.

Hallez, H., Vanrumste, B., Hese, V., Asseler, Y. D., Lemahieu, I. and Walle, R. V., *A finite difference method with reciprocity used to incorporate anisotropy in electroencephalogram dipole source localization*, Phys. Med. Bio. 50, 3787-3806, 2005b.

Hallez, H., Vanrumste, B., Grech, R., Muscat, J., Clercq, W. D. et al., *Review on solving the forward problem in EEG source analysis*, NeuroEngineering and Rehabilitation, 4:46, 2007.

Hallez, H., Vanrumste, B., Hese, P. V., Delputte, S., and Lemahieu, I., *Dipole estimation errors due to differences in modelling anisotropic conductivities in realistic head models for EEG source analysis*, Phy. Med. Bio., 53, 1877-1894, 2008a.

Hallez, H., *Incorporation of Anisotropic Conductivities in EEG Source Analysis*, PhD dissertation, University of Gent, Belgium, 2008b.

Hallez, H., Staelens, S. and Lemahieu, I., *Dipole estimation errors due to not incorporating anisotropic conductivities in realistic head models for EEG source analysis*, Phys. Med. Bio. 54, 6079-6093, 2009.

Haueisen, J., Ramon, C., Eiselt, M., Brauer, H. and Nowak, H., *Influence of Tissue Resistivities on Neuromagnetic Fields and Electric Potentials studied with a Finite Element Model of the Head*, IEEE Trans. Biomed. Eng., 44(8), 727-735, 1997.

Haueisen, J., Tuch, D. S., Ramon, C., Schimpf, P. H., Wedeen, V. J., George, J. S. and Belliveau, J. W., *The Influence of Brain Tissue Anisotropy on Human EEG and MEG*, NeuroImage, 15, 159-166, 2002.

Haueisen, J., Ramon, C., Brauer, H. and Nowak, H., *The Influence of Local Tissue Conductivity Changes on the Magnetoencephalogram and the Electroencephalogram*, Biomed. Technik, 45, 211-214, 2000.

References

He, B., Wang, Y. and Wu, D., *Estimating Cortical Potentials from Scalp EEG's in a Realistically Shaped Inhomogeneous Head Model by Means of the Boundary Element Method*, IEEE Trans. Biomed. Eng., 46(10), 1264-1268, 1999.

Head muscles-online [http://www.medanimations.com/illustrations/illus_images/musclesHead.jpg].

Hori, J. and He, B., *3D Cortical Dipole Imaging of Brain Electrical Activity using Horizontal and Sagittal Dipole layers*, Proceedings of the 3rd IEEE EMBS Conference on Neural Engineering, USA, 221-224, 2007.

Huiskamp, G. J., Vroeijentijn, M., van Dijk R., Wieneke G. and van Huffelen A., *The need for correct realistic geometry in the inverse EEG problem*, IEEE Trans. Biomed. Eng., 46, 1281-1287, 1999.

Juan-Felipe, P. J. A., Arridge, S. R., Lionheart, W. R. B., Bayford, R. H. and Holder, D. S., *Validation of a finite-element solution for electrical impedance tomography in an isotropic medium*, Phys. Meas., 28, 129-140, 2007.

Klepfer, R. N., Johnson, C. R. and Robert, S. M., *The effects of Inhomogeneities and Anisotropies on Electrocardiographic Fields: A 3-D Finite –element Study*, IEEE Trans. Biomed. Eng., 44(8), 706-719, 1997.

Kloppel, S., Stonnington, C. M., Chu, C., Draganski, B., Scahill, R. I., Rohrer, J. D., Fox, N. C., Jack Jr, C. R., Ashburner J. and Frackowiak, R. S. J., *Automatic classification of MR scans in Alzheimer's disease*, Brain, 131, 681-689, 2008.

Lai, Y., Drongelen, W. V., Ding, L., Hecox, K. E., Towle, V. L., Frim D. M., He, B., *Estimation of in vivo human brain-to-skull conductivity ratio from simultaneous extra-and intra-cranial electrical potential recordings*, Clinical Neurophysiology, 116, 456-465, 2005.

Lanfer B., *Validation and Comparison of Realistic Head Modeling Techniques and Application to Somatosensory E/MEG Data*, Dissertation of Diplomarbeit in Physics, Univeristy of Munster, Germany, 2007.

Law, S. K., *Thickness and resistivity variations over the upper surface of the human skull*, Brain Topography, 6, 99-109, 1993.

Lee, W. H, Liu, Z., Mueller, B. A., Lim, K. and He, B., *Influence of white matter anisotropic conductivity on EEG source localization: Comparison to fMRI in human primary visual cortex*, Clinical Neurophysiology, 120, 2071-2081, 2009.

References

- Li, H., Liu, T., Young, G., Guo, L. and Wong, S. T., *Brain Tissue Segmentation based on DWI/DTI Data*, 3rd IEEE International Symposium on Biomedical Imaging: Nano to Macro, 57-60, 2006.
- Li, L., Wang, K., Zhu, S., Mueller, K., Lim, K., Liu, Z. and He, B., *A Study of White Matter Anisotropic conductivity on EEG Forward Solutions*, Proceedings of Noninvasive Functional Source Imaging of the Brain and Heart and the International Conference on Functional Biomedical Imaging (NFSI & ICFBI-IEEE explorer), 130-132, 2007.
- Liang, W. K. and Wang, M. S., *Source reconstruction of brain electromagnetic fields-Source iteration of minimum norm (SIMN)*, NeuroImage, 47, 1301-1311, 2009.
- Makis, N., Angelone, L., Tulloch, S., Sorg, S., Kaiser, J., Kennedy, D. and Bonmassar, G., *MRI-based anatomical model of the human head for specific absorption rate mapping*, Med. & Bio. Eng. & Com, 46, 1239-1251, 2008.
- Malmivuo, J. and Plonsey, R., *Bioelectromagnetism – Principles and Applications of Bioelectric and Biomagnetic Fields*, Oxford University Press, New York, 1995.
- Marin, G., Guerin, C., Baillet, S., Garnero, L. and Meunier, G., *Influence of Skull Anisotropy for the Forward and Inverse Problem in EEG: Simulation Studies using FEM on Realistic Head Models*, Journal of Brain Mappings, 6, 250-269, 1998.
- Meijis, J.W., Weier, O. W., Peters, M. J. and Oosterom, A. van, *On the numerical accuracy of the boundary element method*, IEEE Trans. Biomed. Eng., 36(10), 1038-1049, 1989.
- Mid sagittal view-online [<http://pages.slc.edu/~ebj/iminds04/L3-maps-phren/sagittal.html>]
- Mosconi, L., Sorbi, S., de Leon, M. J., Li, Y., Nacmias, B. and Myong, P. S., *Hypometabolism exceeds atrophy in presymptomatic early-onset familial Alzheimer's disease*, Journal of Nuclear Medicine, 47, 1778-1786, 2006.
- Mosher, J. C., Leahy, R. M. and Lewis, P. S., *EEG and MEG: Forward Solutions for Inverse Methods*, IEEE Trans. Biomed. Eng., 46(3), 245-259, 1999.
- Muravchik, C. and Nehorai, A., *EEG/MEG Error Bounds for a Static Dipole Source with a Realistic Head Model*, IEEE Trans. Biomed. Eng., 49(3), 470-483, 2001.
- Ni, A., Xiuzhen, D., Yang, G., Fu, F. and Tang, C., *Image reconstruction incorporated with the skull inhomogeneity for electrical impedance tomography*, Computerized Medical Imaging and Graphics, 32, 409-415, 2008.

References

- Nicolas, C., Xavier, F., Bernard, D., Bernard, R., Jean, P. M. and Pierre, C., *Effects of Skull Thickness, Anisotropy, and Inhomogeneity on Forward EEG/ERP Computations Using Spherical Three-Dimensional Resistor Mesh Model*, Journal of Human Brain Mapping, 21, 86-97, 2004.
- Nicolas, C., Xavier, F., Florent, A., Pierre, C. and Bernard, R., *Critical Imaging on Head Template: A Simulation Study Using Resistor Mesh Model (RMM)*, Brain Topo., 21, 52-60, 2008.
- Nunez, P. L. and Srinivasan, R., *ELECTRIC FIELDS OF THE BRAIN The Neurophysics of EEG*, 2nd Edition, Oxford University Press, Inc, USA, 2006.
- Oakley, J. E. and O'Hagan, A., *Probabilistic sensitivity analysis of complex models: a Bayesian Approach*, Journal of Royal Statistical Society, 63, 751-769, 2004.
- Ollikainen, J. O., Vauhkonen, M., Karjalainen, P. A. And Kaipio, J. P., *Effects of local skull inhomogeneities on EEG source estimation*, Med. Eng. Phy. 21, 143-154, 1999.
- Oostendorp, T. F., Delbeke, J. and Stegeman, *The Conductivity of the Human Skull: results of In Vivo and In Vitro Measurements*, IEEE Trans. Biomed. Eng., 47, 1487-92, 2000.
- Oostenveld, R. and Praamstra, P., *The five percent electrode system for high-resolution EEG and ERP measurements*, Clinical Neurophysiology, 112, 713-719, 2001.
- Pantazis, D., Nichols, T. E., Baillet, S. and Leahy, R. M., *A comparison of random field theory and permutation methods for statistical analysis of MEG data*, NeuroImage, 25, 383-394, 2005.
- Patel, T., Polikar, R., Davatzikos, C. and Clark, C. M., *EEG and MRI Data Fusion for Early Diagnosis of Alzheimer's Disease*, 30th Annual International IEEE EMBS Conference, Canada, 1757-1760, 2008.
- Petrofsky, J., *The effect of subcutaneous fat on the transfer of current through skin and into muscle*, Med. Eng. & Phy. 30, 1168-1176, 2008.
- Purves, D., Augustine, G. J., Fitzpatrick, D., Katz, L. C, Lamantia, A. S., McNamara, J.O., *NEUROSCIENCE*, Sinauer associates, Inc. Publishers, Sunderland, Massachusetts, USA. Third edition, 2004.
- Polikar, R., Green, R., Kounios, T. D., J. and Clark, C. M., *Comparative multiresolution wavelet analysis of ERP spectral bands using an ensemble of classifier approach for early diagnosis for Alzheimer's disease*, Computers in Biology and Medicine, 37(4), 542-558, 2007.

References

- Roche-Labarbe, N, Aarabi, A., Kongolo, G., Gondry-Jouet, C., Dupelmann, M., Grebe, R. and Wallois, F., *High-resolution Electroencephalography and Source Localization in Neonates*, Human Brain Mapping, 29, 167-176, 2008.
- Ramon, C., Schimpf, P. H. and Haueisen, J., *Effect of Model Complexity on EEG Source Localizations*, Neurology and Clinical Neurophysiology, 81, 1-3, 2004a.
- Ramon, C., Schimpf, P. H., Haueisen, J. and Ishimaru, A., *Role of Soft Bone, CSF, and Gray Matter in EEG Simulations*, Brain Topography, 16(4), 245-248, 2004b.
- Ramon, C., Schimpf, P. H. and Haueisen, J., *Influences of head models on EEG Simulations and inverse source localizations*, BioMedical Engineering Online, 5:10: 2006a.
- Ramon, C., Haueisen, J. and Schimpf, P. H., *Influences of head models on neuromagnetic fields and inverse source localizations*, BioMedical Engineering Online, 5:55: 2006b.
- Rayleigh distribution, Wikipedia, online [http://en.wikipedia.org/wiki/Rayleigh_distribution]
- Rodney, F. W., Gareth, J. J. and Kenneth, V. L., *Monte Carlo Simulation and Random Number Generation*, IEEE Journal on Selected Areas in Communications, 6(1), 58-66, 1988.
- Rush, S. and Driscoll, D., *Current distribution in the brain from surface electrodes*, Anesth. Analg, 47(6), 717-723, 1968.
- Sadleir, R. J. and Argibay, *A Modeling Skull Electric Properties*, Annals of Biomedical Engineering, 35, 1699-1712, 2007.
- Sanei S. and Chambers, J., *EEG Signal Processing*, John Wiley & Sons, Ltd, 2007.
- Shattuck, D. W., Sandor-Leahy, S. R., Schaper, K. A., Rottenberg, D. A. and Leahy, R. M., *Magnetic Resonance Image Tissue Classification Using a Partial Volume Model*, NeuroImage, 13, 856-876, 2001.
- Shattuck, D. W. and Leahy, R. M., *BrainSuite: An Automated Cortical Surface Identification Tool*, Medical Image Analysis, 8(2), 129-142, 2002.
- Shattuck, D. W., *BrainSuite 2 Tutorial*, online version, 2005. (<http://brainsuite.usc.edu>).
- Shimony, J. S., McKinstry, R., Akbudak, E., Aronovitz, J. A., Snyder, A. Z., Lori, N. F., Cull, T. S. and Conturo, T.E., *Quantitative diffusion-tensor anisotropy brain MR imaging: Normative human data and anatomical analysis*, Radiology, 212, 770-784, 1999.

References

Si, H., TetGen, 2004 (<http://tetgen.berlios.de>).

Skull parts-online

[http://www.face-and-emotion.com/dataface/anatomy/media/cranium_side.jpg].

Smith, A. D. and Jobst, K. A., *Use of structural imaging to study the progression of Alzheimer's diseases*, British Medical Bulletin, 52(3), 575-86, 1996.

Tuch, D. S., Wedeen, V. J., Dale, A. M., George, J. S. and Belliveau, J.W., *Conductivity tensor mapping of the human brain using diffusion tensor MRI*, Proceedings of the National Academy of Sciences, USA, 98(20), 11697–11701, 2001.

van Uiter, R., Johnson, C. and Zhukov, L., *Influence of Head Tissue Conductivity in Forward and Inverse Magnetoencephalographic Simulations Using Realistic Head Models*, IEEE Trans. Biomed. Eng., 51, 2129-2137, 2004.

Vanrumste, B., Van Hoey, G., Van de Walle, R., D'Have, M., Lemahieu, I. and Boon, P., *Dipole location errors in electroencephalogram source analysis due to volume conductor model errors*, Med. & Bio. Eng. & Com., 38, 528-534, 2000.

Vanrumste, B., *EEG dipole source analysis in a realistic head model*, PhD dissertation, University of Gent, Belgium, 2002.

Vatta, F., Bruno, P. and Inchingolo, P., *Improving Lesion Conductivity Estimate by Means of EEG Source Localization Sensitivity to Model Parameter*, Clinical Neurophysiology, 19(1), 1-15, 2002a.

Vatta, F., Bruno, P. and Inchingolo, P., *Accuracy of EEG source reconstruction in the presence of brain lesions: modelling errors and surface electrodes placement*, Biomed Sci Instrum, 38, 423-428, 2002b.

von Christine, R., *Source Analysis of Simultaneous sEEG and iEEG Measurements in Presurgical Epilepsy Diagnosis*, Dissertation of Diplomarbeit in Physics Univeristy of Munster, Germany 2008.

von Ellenrieder, N., Muravchik, C. H. and Nehorai, A., *Effects of Geometric Head Model Perturbations on the EEG Forward and Inverse Problems*, IEEE Trans. Biomed. Eng., 53(3), 421-429, 2006.

Wang, Y. and He, B., *A Computer Simulation Study of Cortical Imaging from Scalp Potentials*, IEEE Trans. Biomed. Eng., 45(6), 724-735, 1998.

References

Wang, D., Kirby, R. M. and Johnson, C. R., *Resolution Strategies for the Finite Element-Based Solution of the ECG Inverse Problem*, IEEE Trans. Biomed. Eng., 57(2), 220-237, 2010.

Wang, Y., David, R. H. and Kim, Y., *An Investigation of the Importance of Myocardial Anisotropy in Finite-Element Modeling of the Heart: Methodology and Application to the Estimation of Defibrillation Efficacy*, IEEE Trans. Biomed. Eng., 48(12), 1377-1389, 2001.

Wen, P., *Human Head Modelling and Computation for the EEG Forward Problem*, PhD dissertation, The Flinders University of South Australia, Australia, 2000.

Wen, P. and Li, Y., *EEG human head modelling based on heterogeneous tissue conductivity*, Australas. Phys. Eng. Sci. in Med., 29(3), 235-240, 2006.

Wendel, K., Narra, N. G., Hannula, M., Kauppinen, P. and Malmivuo, J., *The influence of CSF on EEG Sensitivity Distributions of Multilayered Head Models*, IEEE Trans. Biomed. Eng., 55, 1454-1456, 2008.

Wolters, C. H., *Influence of Tissue Conductivity Inhomogeneity and Anisotropy on EEG/MEG based Source Localization in the Human Brain*, PhD dissertation, University of Leipzig, Germany, 2003.

Wolters, C. H., Anwander, A., Tricoche, X., Weinstein, D., Koch, M. A. and MacLeod, R. S., *Influence of tissue conductivity anisotropy on EEG/MEG field and return current computation in a realistic head model: A simulation and visualization study using high-resolution finite element modelling*, NeuroImage, 30, 813-826, 2006.

Yan, Y., Nunez, P. L. and Hart, R. T., *Finite-element model of the human head: scalp potentials due to dipole sources*, Journal of Med. & Bio. Eng. & Com. 29, 475-481, 1991.

Zhao, X., Wang, M., Gao, W. and Liu, H., *White Matter Fiber Tracking Method by Vector Interpolation with Diffusion Tensor Imaging Data in Human Brain*, Proceedings of the IEEE Engineering in Medicine and Biology 27th Annual Conference, 5786-5789, 2005.

Zhang, Y., van Drongelen, W. and He, B., *Estimation of in vivo brain-to-skull conductivity ratio in humans*, Applied Physics Letter, 89(22), 223903-223903, 2006.

Zhang, Z., *A fast method to compute surface potentials generated by dipoles within multilayer anisotropic spheres*, Phys. Med. Bio. 40, 335-349, 1995.

References

Zhou, H. and van Oosterom, A., *Computation of the potential distribution in a four-layer anisotropic concentric spherical volume conductor*, IEEE Trans. Biomed. Eng., 39(2), 154-158, 1992.